FIELD AND LABORATORY MEASUREMENTS OF PMD USING INTERFEROMETRIC TECHNIQUES

MAPHUTI COMFORT MANKGA

FIELD AND LABORATORY MEASUREMENTS OF PMD USING INTERFEROMETRIC TECHNIQUES

MAPHUTI COMFORT MANKGA

Submitted in partial fulfilment of the
requirements for the degree of

MAGISTER SCIENTIAE

in the Faculty of Science at the
Nelson Mandela Metropolitan University

Supervisor: Professor A.W.R. Leitch
Co-Supervisor: Doctor A.B. Conibear

January 2007

To my mom, Regina Rankgomotha Raselomane

ACKNOWLEGEMENTS

I would like to express my sincere thanks to:

- My supervisor, Prof. Andrew Leitch, and co-supervisor Dr Ann Conibear for their excellent support, guidance and patience throughout my project

- Dr Lorinda Wu for the guidance, long discussions, assistance, proofreading this dissertation and her patience

- Mr Johann Visser, the former Telkom technician for his guidance and assistance with the Northern Cape field measurements

- Mr Chris Nel of Lambda Test and Equipment c.c for his guidance and assistance with the Pretoria field measurements

- Mr Tim Gibbon, Mr Nkosingiphile Sibaya, Mr Lawrance Viljoen, Mr Archie Pelaelo, and Mr Eric Mudau for their assistance with the field measurements

- Mr Len Compton for building the manual scramblers

- My family, for their support and encouragements throughout my studies

SUMMARY

In this study, the generalized and traditional interferometric techniques (GINTY and TINTY) are used to investigate some of the important aspects of Polarization Mode Dispersion (PMD) phenomenon in optical fibres.

Measurements of PMD and chromatic dispersion (CD) are performed on buried optical fibre cable in the Pretoria Telkom's metropolitan network. The upgradeability of this network was investigated, and it was observed that just over a half of the fibres are upgradeable to 10 $Gb.s^{-1}$ transmissions. Long-haul aerial network in the Northern Cape was also tested for upgradeability to 10 $Gb.s^{-1}$. It was found that 41 % of the fibres tested are upgradeable to 10 $Gb.s^{-1}$. Long-term monitoring showed that PMD varies rapidly in aerial fibres and, on the other hand, it is relatively stable in buried cables.

Investigations on the accuracy of the techniques showed that polarization scrambling is essential for the reduction of the measurements uncertainties. Furthermore, it was observed that TINTY underestimates the single scan PMD distributions.

The study on the effect of the change in mode coupling on various fibre configurations was performed, and fibres showed a reduction in PMD after the introduction of mode coupling. Measurements of PMD conducted in the laboratory on cabled fibre with low PMD showed the floor sensitivity of TINTY. Comparison between GINTY and Jones Matrix Eigeanalysis (JME) PMD measurements methods were performed on an emulator, and the results showed a good agreement in the measured PMD.

Keywords: Polarization mode dispersion, PMD, mode moupling, chromatic dispersion, GINTY, TINTY, Jones Matrix Eigenanalysis, JME

CONTENTS

CHAPTER 1

INTRODUCTION

The optical communications industry has been growing at a tremendous speed in the past few years. The growth has been caused mainly by more people using the internet. Network operators around the world require a large bandwidth to provide services such as internet protocol television (IPTV), video on demand, triple play (voice, data, video), etc. to their subscribers. This increase in demand of high speed service from subscribers has seen network operators wanting to increase their data transmission to even higher bit-rates (10, 40 and 80 Giga bits per second).

A major problem to the upgrade of the fibre optic systems to higher bit-rates, however, is polarization mode dispersion (PMD). PMD is caused by asymmetries of the fibre core resulting in fibre birefringence. The birefringent axes may have many different orientations along the length section of the fibre. This leads to coupling of light from the different orientations of the orthogonal axes called mode coupling. Birefringence and mode coupling vary with environmental fluctuations, and this leads to PMD values being statistically distributed. The different propagation speeds of the light signals due to birefringence and mode coupling will lead to a difference in their arrival time at the output of the fibre. The spreading of the light signals at the output can cause serious impairments at higher bit-rates.

There has been lot of research performed by many groups in trying to understand the PMD system impairments, mitigation and statistical variations. In order to understand the effects of PMD on the fibre optic systems, it is important that its measurements are performed with good accuracy. In this study the traditional and generalized interferometric techniques (TINTY and GINTY), the preferred field instruments, were used in the investigations of the upgradeability of the main South African network operator's (Telkom) metropolitan and long-haul optical fibres networks in Pretoria and

the Northern Cape. In this study, as part of the test for upgradeability of the Pretoria metropolitan optical fibre network, chromatic dispersion was also tested.

TINTY is a relatively old technique which has some limitations (e.g shape of the light source spectrum, mode coupling regions,etc.) in the calculation of PMD. GINTY, on the other hand, is a recent instrument developed by EXFO [1] that is said to be an improvement on TINTY and overcomes the limitations mentioned above. This study investigated the relative measurement accuracy of these techniques.

In the past or probably presently, network operators would try improving the accuracy of the interferometric measurements by continuously monitoring PMD on the deployed fibres over a relatively long period to time (long-term monitoring), unknowingly using the same state of polarization during the test. Since the two techniques are both polarization sensitive, PMD of the fibre in this case is averaged over single scans from one input and output state polarization and high measurement uncertainty is incurred. Polarization scrambling is essential for reducing the uncertainty of the measurements by averaging single scan PMD values for different states of polarization, as is shown in this study.

The dissertation is organized as follows:

Chapter 2 discusses some fundamental concepts of optical fibres, including states of polarization and their representation on the Poincaré sphere, attenuation and dispersion properties. The distance limitations imposed by the latter two are also discussed.

Chapter 3 introduces the definition of PMD and the different PMD measurement techniques. Chapter 4 focuses on operational principles of the traditional and generalized interferometric techniques (TINTY and GINTY) which were used in the study. Chapter 5 gives a literature review of the long-term monitoring of PMD that has been performed by other research groups. Moreover, measurements of PMD conducted with the interferometric technique in literature are also reviewed. Chapter 6 briefly discusses the instrumentation that was implemented in the investigations.

Measurements were conducted to determine the upgrade of the metropolitan and long-haul Telkom network in Pretoria and the Northern Cape. The results of this work are presented in Chapter 7. Long-term measurement results on the networks mentioned above to determine the variability of the PMD are also presented.

Chapter 8 reports on the effect of mode coupling on the PMD of the deployed optical fibres. The accuracy of GINTY and TINTY techniques is investigated using various buried and deployed fibre configurations. Chapter 9 provides concluding remarks regarding PMD measurement issues and possible future work.

References:

[1] **N Cyr** (2004), "Generalized Interferometric PMD Measurement Method: Exact Analysis and Traceable Result for any coupling regime", *J. Lightwave Technol.* **22**(3), pp 794-805

CHAPTER 2

SELECTED TOPICS IN THE THEORY OF OPTICAL FIBRES

In this Chapter, various topics of optical fibre technology are covered. The structures and types of optical fibres and polarization of light signals in space and fibre are discussed; attenuation or losses and dispersion of the light signals in the optical fibres are also presented. Furthermore, the maximum distance limitation brought about by attenuation and dispersion for different formats, Return to Zero (RZ) and Non-Return to Zero (NRZ), are also discussed.

2.1 Structure of Optical fibres

An optical fibre is a dielectric waveguide with cylindrical symmetry. A typical optical fibre design comprises the core, cladding and the jacket (see Figure 2.1). The core has a higher index of refraction than the cladding. The difference in the indices of refraction enables the light to be totally internally reflected at the core-cladding interface [1]. Fibres with a discontinuity in the index of refraction at the core-cladding interface are called step-index fibres as shown in Figure 2.1. Fibres with a continuously changing index of refraction from the core-cladding interface are called graded index fibres.

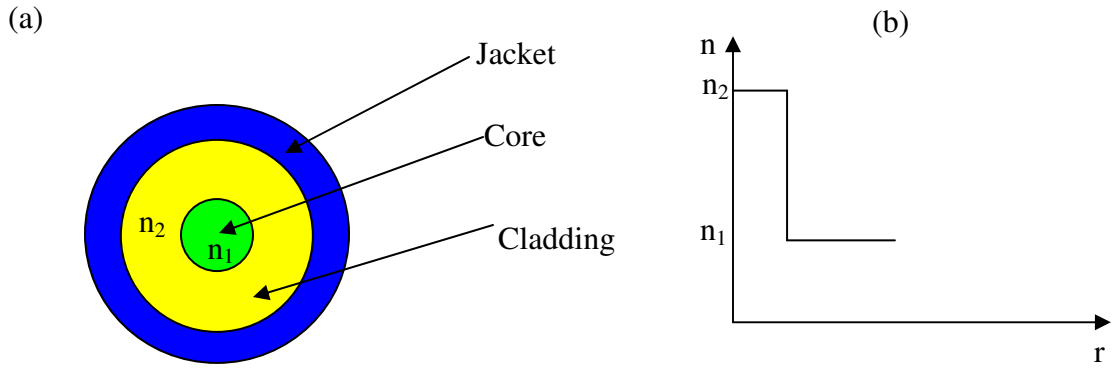

Figure 2.1: (a) Generic cross-section profile of an optical fibre; (b) the refractive index profile an optical fibre with radius r showing step index profile.

2.1.1 Types of Optical fibres

In some cases the geometrical optics can be used to describe the rays of the light signal that propagate in the optical fibre, but the actual propagation can be represented with guided waves optics. In the latter case, the Maxwell equations for the electric field and the boundary conditions at the core-cladding interface are used to find the solution to the radial part of the electric field in cylindrical coordinates [2, 3]. The radial part of the electric field are the Bessel functions called modes and are used to classify the fibres, i.e., multimode or single mode fibres [4].

a) Multimode fibres (MMF)

Multimode fibres allow more than one mode or bound solution for each light signal propagating through the fibre; each mode travels at its own speed in the fibre due to the dependence of the group velocity on the core refractive index. These fibres suffer a large amount of attenuation and dispersion, Section 2.3 and 2.4, and are normally used for transmission over short distances. Multimode fibres that are used for the short transmission distance have diameters within the range 50–100 μm.

b) Single mode fibres (SMF)

Single mode fibres allow only a single mode or bound solution through the core of the fibre. In this study, the experiments were performed on the single mode fibres. They have lower attenuation and dispersion relative to multimode fibres. A typical diameter of the single mode fibre core is about 9 μm. The attenuation and dispersion that affect the performance of multimode and single mode fibres are presented in Section 2.4 and 2.5, respectively.

c) Polarization maintaining fibres (PMF)

Polarization maintaining fibre (PMF) is a single mode fibre that keeps the state of polarization of the input signal constant throughout the length of the fibre. PMF are characterized by the stress member inserted in the silica cladding (see Figure 2.2). The material inserted, boronsilicate, have a thermal expansion coefficient higher than that of silica, and this arrangement causes stress induced difference in the refractive index of the fibre core for different geometrical orientations [5]. PMF have major applications in the fibre optic sensing and are not used for long haul transmission due to their high costs and loss.

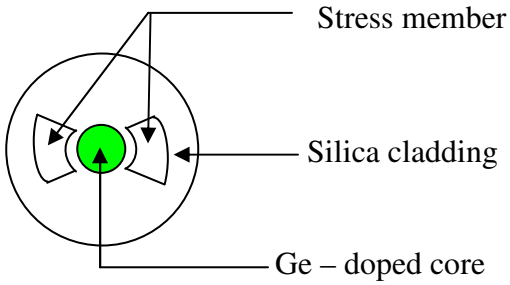

Figure 2.2: Panda or bow tie polarization maintaining fibre with a stressed member embedded in the cladding (after Ref. (1998) [5]).

2.2 Polarization

2.3.1 States of Polarization

The state of polarization of the light signal is normally defined in terms of the electric field; light is a transverse electromagnetic wave satisfying the general wave equation:

$$\nabla_x{}^2\mathbf{E} + \nabla_y{}^2\mathbf{E} + \nabla_z{}^2\mathbf{E} = \frac{1}{v^2}\nabla_t{}^2\mathbf{E}, \qquad 2.1$$

where **E** is the electric field vector and v is the speed of the light signal in the transmission medium. To simplify the mathematics, only the E_x, E_y and E_z components are considered. Light is considered as a plane electromagnetic wave propagating in the z-direction with angular frequency, ω. Since light is transverse, it can be divided into two orthogonal components given by,

$$\mathbf{E}_x(z,t) = \hat{\mathbf{x}}E_{0x}\cos(kz - \omega t + \delta_1) \text{ and} \qquad 2.2$$

$$\mathbf{E}_y(z,t) = \hat{\mathbf{y}}E_{0y}\cos(kz - \omega t + \delta_2), \qquad 2.3$$

where k and δ_1 (and δ_2) are the propagation constant and the phase of the wave, respectively. The resultant electric field vector from the two equations above is given by,

$$\mathbf{E}(z,t) = \mathbf{E}_x(z,t) + \mathbf{E}_y(z,t). \qquad 2.4$$

The type of polarization for the electromagnetic wave with the electric field **E**(z,t) is determined by the phase difference, $\delta=\delta_2-\delta_1$; if the phase difference, δ, is an integral multiple of π, then the wave or light signal is linearly polarized. Figure 2.3 shows the linearly polarized light with **E**(z,t) at 45^0 to the E_x-E_y axes. The general equation for the linearly polarized light can be derived by substitution of equation 2.2 and 2.3 into 2.4 as shown below:

$$\begin{aligned}\mathbf{E}(z,t) &= (\hat{\mathbf{x}}E_{0x} + \hat{\mathbf{y}}E_{0y})(\cos(kz - \omega t + \delta_1) + \cos(kz - \omega t + \delta_2)) \\ &= (\hat{\mathbf{x}}E_{0x} + \hat{\mathbf{y}}E_{0y})\cos(kz - \omega t + n\pi) \qquad 2.5 \\ &= (\hat{\mathbf{x}}E_{0x} + \hat{\mathbf{y}}E_{0y})\cos(kz - \omega t).\end{aligned}$$

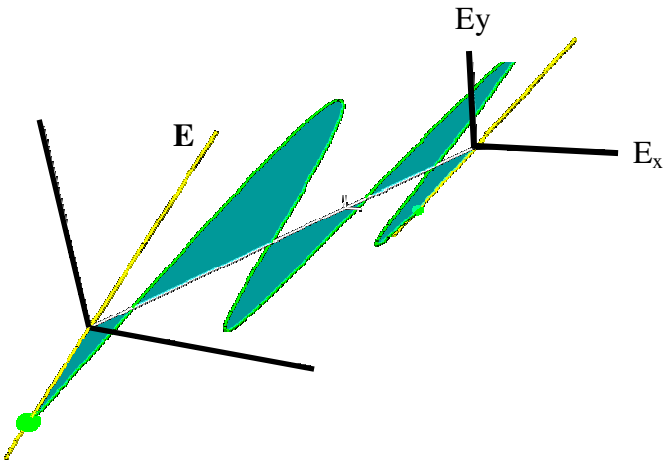

Figure 2.3: Linearly polarized light with the E-field at 45^0 to the E_y-E_x axes.

For circular polarization, the phase difference, δ, is defined by $\delta=\pm\pi/2+2n\pi$, where n is an integer. Assuming that the orthogonal components of the electric field have the same amplitude, $E_{0,}$ then the resultant electric field vector is given by,

$$\left.\begin{aligned}\mathbf{E}_x(z,t) &= \hat{\mathbf{x}}E_0\cos(kz-\omega t)\\ \mathbf{E}_y(z,t) &= \hat{\mathbf{y}}E_0\cos(kz-\omega t+(-\frac{\pi}{2}+2n\pi))\end{aligned}\right\}. \qquad 2.6$$

The amplitude of the electric field is constant, but the direction of the electric field varies with time. The electric field vector rotates either clockwise or anticlockwise about the z-axis depending on the phase difference. When the phase difference, δ, is given by $-\pi/2+2n\pi$, then the electric field rotates anticlockwise, and it defined to be left circularly polarized; for $\delta=\pi/2+2n\pi$ the electric field rotates clockwise and the electric field is termed right circularly polarized (see Figure 2.4).

For the general case where there is no restriction on the phase difference, the rotation and magnitude of the electric field. The equation that represents all the polarization states and independent of position and time, kz-ωt, is given by,

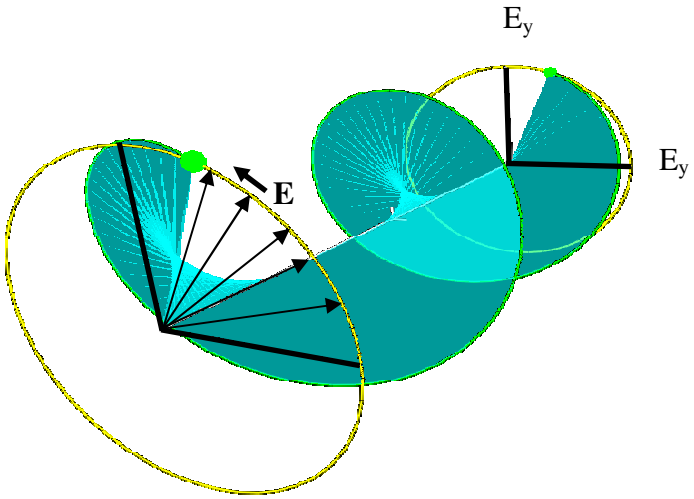

Figure 2.4: Left circularly polarized light with electric Field **E**.

$$(\frac{E_y}{E_{0y}})^2+(\frac{E_x}{E_{0x}})^2-2(\frac{E_y}{E_{0y}})(\frac{E_x}{E_{0x}})\cos\delta=\sin^2\delta\,. \qquad 2.7$$

The equation above is that of an ellipse, and it can be used to derive other special cases of polarization. In two dimensions, the ellipse makes an angle Ψ, $0\le\psi\le\pi$, with the coordinates system, E_x-E_y, such that,

$$\tan 2\Psi=\frac{2\times a\times b\times\cos\delta}{a^2-b^2}, \qquad 2.8$$

where a and b, $a\ge b$, are the lengths of the axes of the ellipse. In Figure 2.5, the values for a and b can be obtained by measuring the intensity of the light transmitted through a linear polarizer aligned with the E_x' and E_y' axes, respectively. The angle Ψ is measured by rotating the polarizer until the maximum intensity is measured, i.e., a point where the polarizer is aligned with Ψ; θ ($\theta=\arctan^{-1}(a/b)$) is called the ellipse angle, $0\le\theta\le\pi/2$. The geometry in Figure 2.5 shows an angle χ, $-\pi/4\le\chi\le\pi/4$, which can be used to determine the sense of direction for the elliptically polarized light.; Born *et al.*[7] showed that angle arctan χ = ± B/A, the signs indicate the direction of polarization. Figure 2.5

can be projected to 3D plot, and the result is a polarization representation called the Poincaré sphere (Section 2.2.3).

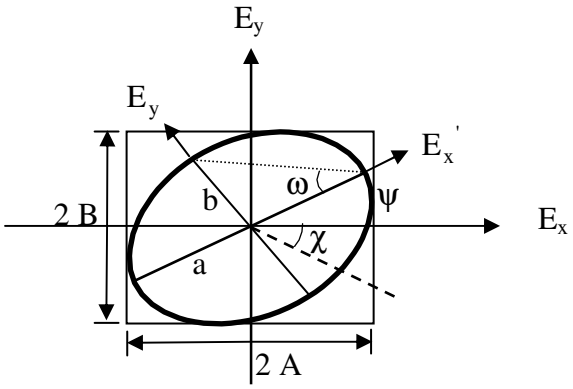

Figure 2.5: The elliptical states of polarization are characterized by the ellipse angle and ψ at the maximum intensity.

The special cases of polarization can be derived from equation 2.7 by choosing specific angles and making a certain assumption on the magnitude of the electric field. For example, the circular state of polarization has the phase difference $\delta = \pm \pi/2+m\pi$, and for this case equation 2.7 gives,

$$\frac{E_y^{\,2}}{E_{0y}^{\,2}}+\frac{E_x^{\,2}}{E_{0x}^{\,2}}=1. \qquad 2.9$$

and for $E_{0y}=E_{0x}=E_0$ the resulting equation is that of a circle, equation 2.10, in agreement with what was described above with the circular polarization,

$$E_y^{\,2}+E_x^{\,2}=E_0^{\,2}. \qquad 2.10$$

For linear polarization, the phase difference, δ, is the multiple of π. The general equation, equation 2.7, in the case of even multiples of π the following equation is obtained,

$$E_y = \frac{E_{0y}}{E_{0x}} E_x \qquad 2.11$$

and for the odd multiples of π equation 2.7 gives,

$$E_y = -\frac{E_{0y}}{E_{0x}} E_x . \qquad 2.12$$

Equation 2.11 and 2.12 are both equations of the straight lines with positive and negative slopes, respectively; this is in agreement with both the left and right linearly polarized light; the special cases of polarization from the assumptions made above are as presented in Figure 2.6.

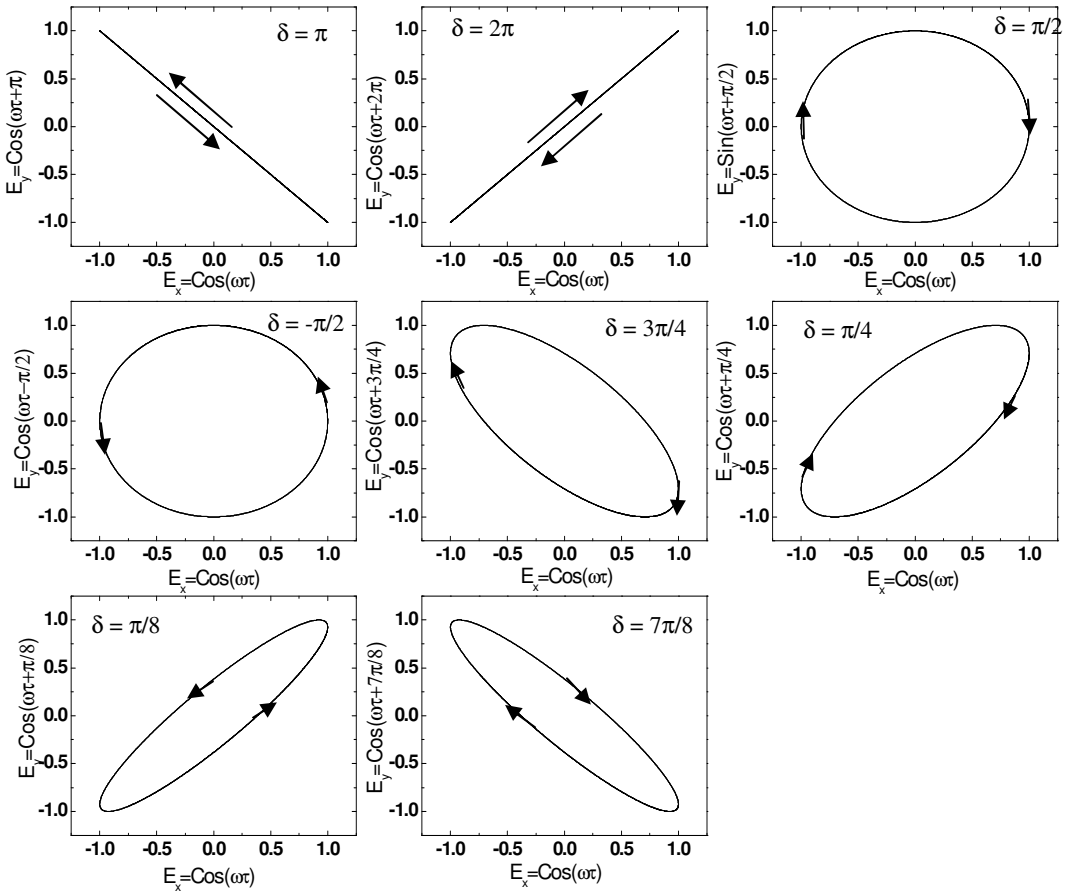

Figure 2.6: The special cases of polarization, i.e., linear polarization with δ = π and 2π, circular polarization with δ = ± π/2, and elliptical polarization with phases, namely, 3π/4, π/4, π/8 and 7π/8.

2.2.2 The Stokes parameters

The other method of representing the states of polarization is by using Stokes parameters. This can be achieved by measurement of the power for a partially and fully polarized light signal. The Stokes parameters, S_0, S_1, S_2 and S_3, are defined as follows:

$$\left.\begin{aligned} S_0 &= 2I_0 \\ S_1 &= 2I_1 - 2I_0 \\ S_2 &= 2I_2 - 2I_0 \\ S_3 &= 2I_3 - 2I_0 \end{aligned}\right\}, \qquad 2.13$$

where I_0 is the total irradiance for the incident light signal, I_1 is for the linearly polarized light signal, I_2 is for the linearly polarized light signal at 45^0 and I_3 is for the circularly polarized light signal. As can be seen in equations 2.13, the Stokes parameters can take both the negative and positive values. For example, $S_1>0$ corresponds with the linear horizontal polarization and $S_1<0$ with the linear vertical polarization; for $S_1=0$, the light signal is neither vertically nor horizontally polarized.

Similarly, $S_2>0$ means that the light signal is linearly polarized at 45^0, and the opposite is true for $S_2<0$. $S_3<0$ implies that the light is right circularly polarized, and left circularly polarized for $S_3<0$. Furthermore, for $S_1= S_2= S_3=0$, then the light signal is not polarized (unpolarized). The degree of polarization (DOP) of the light signal can be expressed in terms of the Stokes parameters [1],

$$\mathrm{DOP} = \frac{(S_1^{\,2} + S_2^{\,2} + S_3^{\,2})^{1/2}}{S_0}. \qquad 2.18$$

In free space, a light signal can maintain its DOP, but in an optical fibre it can change in relation to the spectral properties of the transmission path [6].

2.2.3 Poincaré Sphere

Figure 2.7 below shows the 3D projection of the ellipse in Figure 2.6. The projection is called the Poincaré sphere. The Poincaré sphere represents the states of polarization (SOP) in Stokes space [6, 7]. It allows the description of polarized signals and polarizations caused by propagation through the devices. All the states of polarization can be represented on the Poincaré sphere, i.e., partially polarized, unpolarized and polarized light signal.

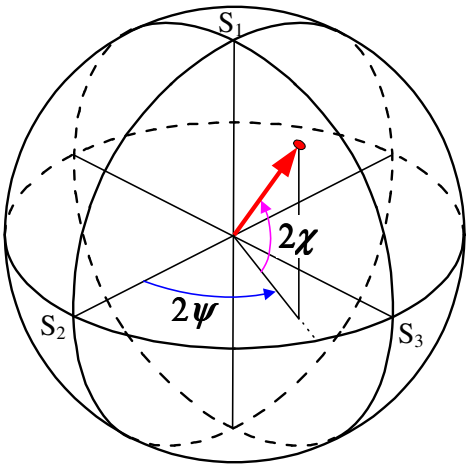

Figure 2.7: Poincaré sphere constructed from the projection 2D polarization ellipse with angle ψ and χ.

Polarized signal is represented by a point on the Poincaré sphere, and unpolarized light by a point at the centre of the sphere; for a partially polarized light signal, the state of polarization is represented by a point within the sphere. Circular polarizations are located at the poles, elliptical polarizations are located between the equator and the poles, and right-hand and left-hand elliptical states occupy the northern and southern hemispheres, respectively. The coordinates of the points on or within the sphere are for the normalized Stokes parameters. The distance from the centre of the sphere to its surface gives the DOP of the light signal (see Figure 2.8).

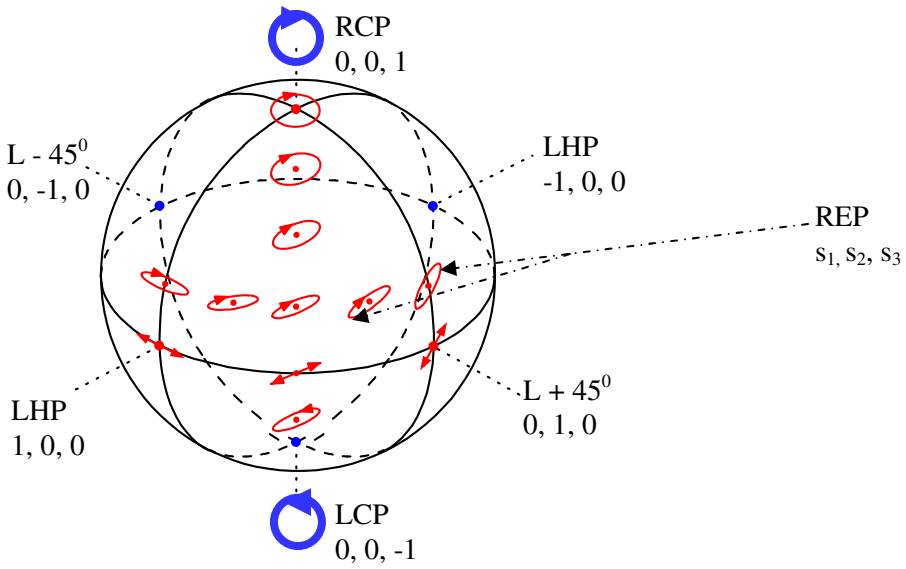

Figure 2.8: Poincaré sphere denoting various states of polarization of polarized light signal.

On the sphere, the SOP of the orthogonal polarization states is given by a point diametrically opposite each other. Points that have similar polarizations are close to each other on the sphere. For a birefringent device or polarization maintaining fibre (see Figure 2.9) the path of polarization followed on the sphere with the change in wavelength is a circle revolving around the principal states of polarization (PSP) of the device [6].

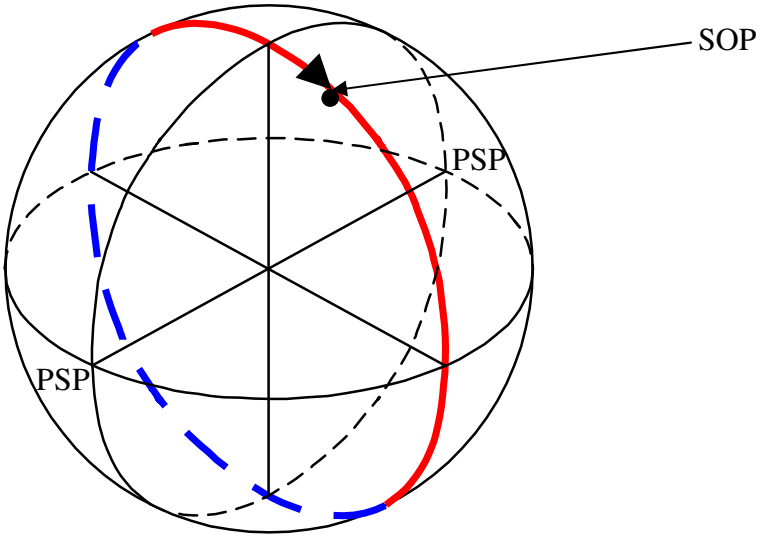

Figure 2.9: A trace of a circle on the Poincaré sphere showing the SOP evolution of a birefringent fibre, or polarization maintaining fibre, with a change in wavelength.

The size of the circle depends on the orientations of the PSPs to the input signal [6]. However, for a telecommunication single mode fibre the path of polarization followed on the sphere with a change in wavelength is random, as shown in Figure 2.10.

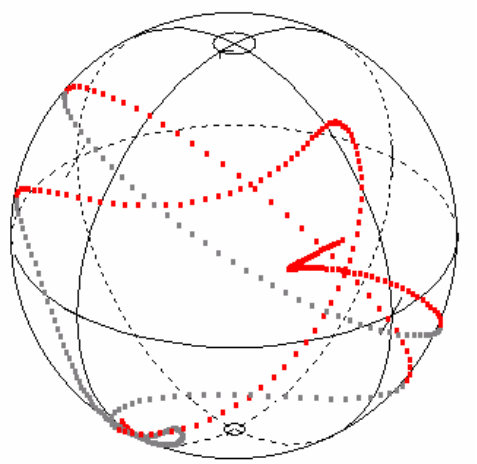

Figure 2.10: A random trace on the Poincaré sphere illustrating the SOP evolution for a single mode fibre with a small change in wavelength.

2.3 Attenuation

The attenuation in the optical fibre is, basically, the power loss in the fibre for every 1 km the signal travels in an optical fibre. Attenuation, $\alpha(z)$, of an optical fibre is normally defined as follows:

$$\alpha = \frac{1}{z} \mathrm{Log}_{10} \frac{P_1}{P_2}, \qquad 2.15$$

where P_1 and P_2 are the power at the input and at distance z of the optical fibre, respectively; the units of attenuation as can be from equation 2.15 are $dB.km^{-1}$. Since the mid-1960s, the attenuation of the optical fibres has improved from 1000 $dB.km^{-1}$ to ≤ 0.2 $dB.km^{-1}$; the latter attenuation for modern optical fibres implies that 95.5 % of light is transmitted after propagating through a 1 km length of optical fibre [3]. The sources of

loss or attenuation in the fibre are radiation and absorption which originate from the component material or the external environment of the optical fibre. Barnoski [8] showed that the component of the core of the fibre, silica, have electronic transitions from valence to conduction bands which cause absorption at short wavelengths, typically far ultraviolet, which decays exponentially with an increase in wavelength [8].

Glass optical fibres have metal ions which act as impurities; strong absorption from these ions occurs in the infrared, and also decays with increasing wavelength, as shown in Figure 2.11. The dominant factor in terms of the loss in the fibre, however, is the Rayleigh scattering caused by the variation in density of the fibre core. The magnitude of this loss is the largest at short wavelength, and decays as λ^{-4} [3, 8, 9]. For example, if the wavelength of the light signal is doubled the scattering losses would be decreased 16 times.

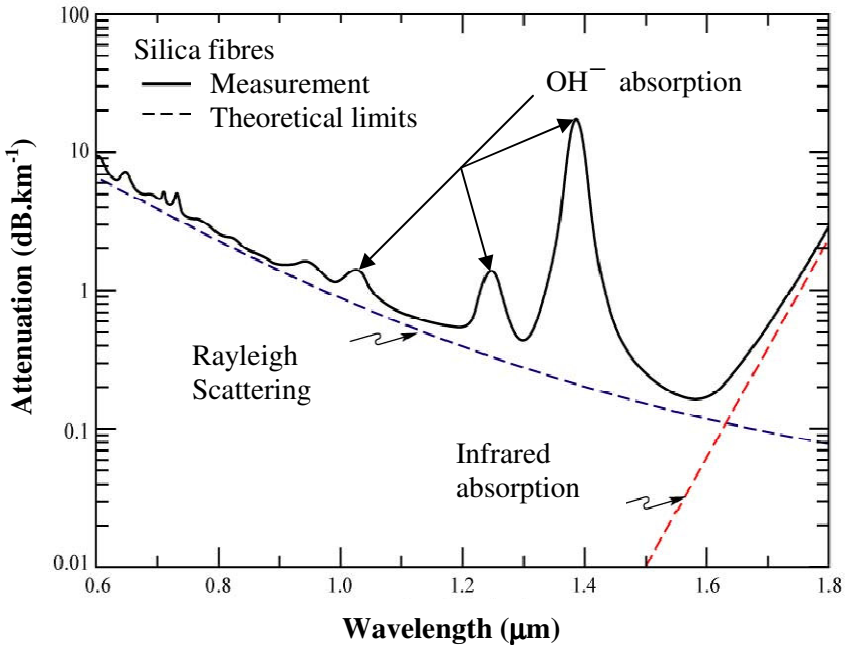

Figure 2.11: Optical fibre attenuation as a function wavelength for silica fibres; at 1300 and 1550nm transmission windows, the attenuation is 0.5 and 0.3dB/km. respectively.

The peaks at 725, 950, 1250 nm are for the absorption of the OH^- impurities. The absorption losses at 1380 nm are between 0.5 to 2 $dB.km^{-1}$ [5]. Macrobending and

microbending are some of the external factors that can result in losses in the optical fibre. These two bending methods introduce perturbations on the fibre axis which cause the light to radiate in the cladding. Losses due to microbending are dependent on the wavelength and vary a little at 1310 nm but vary greatly at 1550 nm as shown in Figure 2.12. On the other hand, macrobending losses of the fibre vary a little at short wavelengths but increase at longer wavelengths from 1550 nm and beyond.

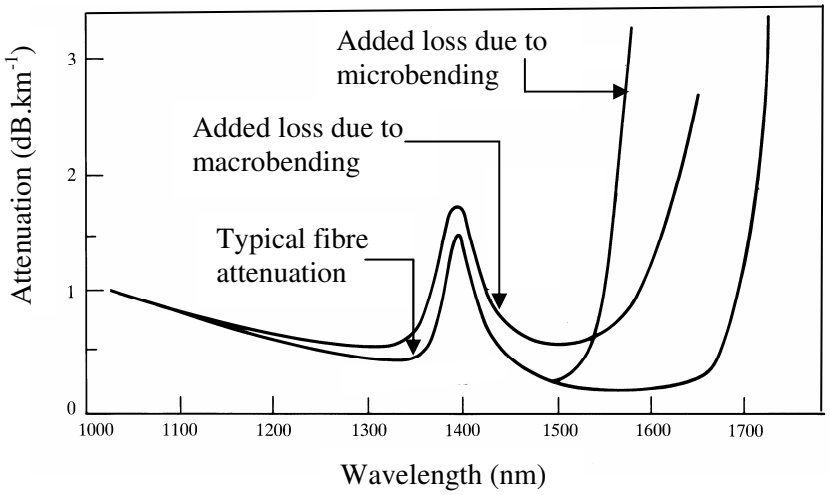

Figure 2.12: A typical single mode fibre attenuation spectrum showing the effect of macrobending and microbending (after Ref. [4]).

2.4 Dispersion

In the digital transmission, dispersion of the pulse transmitted through the optical fibre leads to its spreading. Pulse spreading imposes a limit on the maximum pulse rate that can be used with transmission systems. For a Gaussian pulse propagating in the optical fibre, the transmission bandwidth, B, is given by

$$B = \frac{0.44}{\delta\tau}, \qquad 2.16$$

where $\delta\tau$ is the full-width at half maximum power [10]. As can be seen from this equation, the bandwidth is inversely proportional to dispersion. There are two types of

dispersion that pose a problem in optical fibres, namely, the intermodal and intramodal dispersion.

2.4.1 Intramodal Dispersion

In single mode fibre, there is no intermodal dispersion but only intramodal dispersion. It results from the finite width of the light source, and the dependence of the group velocity on the wavelength of the light signal propagating in the optical fibre. Intramodal dispersion is defined as

$$\frac{\delta\tau}{L} = D\delta\lambda \text{ for } D \neq 0$$
$$= 0.2S_0(\delta\lambda)^2 \text{ for } D = 0, \qquad 2.17$$

where D is the dispersion factor, $\delta\lambda$ is the finite width of the light source, and S_0 is the dispersion slope,

$$S_0 = \frac{dD}{d\lambda} \quad \text{at } \lambda = \lambda_0, \text{where } D(\lambda_0) = 0\,. \qquad 2.18$$

It has been suggested for a typical digital system the dispersion in the optical fibre should be 1/2 the interpulse period T [2]. The maximum bandwidth will then be given by, 0.88/T from equation 2.16. The two main sources of intramodal dispersion are material and waveguide dispersion.

Material dispersion is the result of the refractive index of fibre core being function of wavelength, and waveguide dispersion is the result of the propagation constant of the core being wavelength dependent. The combination of waveguide dispersion and material dispersion is the chromatic dispersion (see Figure 2.13). For a fibre with core refractive index $n_1(\lambda)$, the material dispersion coefficient is given by,

$$D_{mat} = \frac{-L}{c}(\lambda^2 \frac{d^2 n_1}{d\lambda^2})\frac{\Delta\lambda}{\lambda}. \qquad 2.19$$

Waveguide dispersion also depends on the design of the optical fibres. For the step index single mode fibre used in this study, the waveguide dispersion, D_{wg}, is given by equation 2.20, where a is the fibre core radius and n_2 is the refractive index of the cladding [3, 8, 5].

$$D_{wg} = \frac{-0.0252\lambda}{a^2 c n_2} \qquad 2.20$$

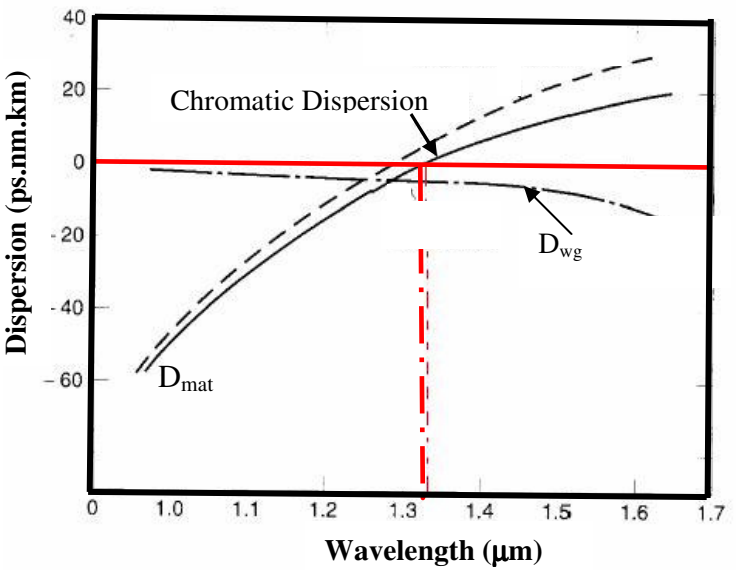

Figure 2.13: Material and waveguide dispersion in the optical fibres and their combined total (Chromatic dispersion).

From equation 2.20, D_{wg} can be made more negative by decreasing the fibre core radius, and this action can be used to shift the zero dispersion wavelength from 1310 nm to 1550 nm. A fibre with this property is called dispersion-shifted fibre, and will benefit transmission at the low loss 1550 nm window.

Another source of distance limitation in single mode fibres is polarization mode dispersion (PMD). PMD causes the broadening of the pulse propagating in the fibre and

subsequently leads to an increase in the bit-error rates in the transmission systems. PMD is the subject of this study and is discussed in more detail in Chapter 3.

2.5 Distance limitation in single mode fibres

As has been discussed above, attenuation or losses and dispersion limit the maximum transmission distance of the optical fibres. In single mode fibres, intramodal dispersion is the main cause of the distance limits, Section 2.5. Consider a SMF used with 2.5 $Gb.s^{-1}$ transmission system at a wavelength of 1550 nm. Suppose 0 dBm light is coupled into the optical fibre and the receiver has a sensitivity of -30.2 dBm. Allowing a loss of 8 dB for the margin, connectors and cabling losses, then from equation 2.21 the total loss allowed is 22.2 dB.

Taking the attenuation coefficient, α, as 0.3 $dB.km^{-1}$, the maximum transmission distance, L, is 74 km; if the attenuation coefficient of 0.25 $dB.km^{-1}$ the maximum distance of transmission is 88.8 km. This clearly indicates that the high attenuation or losses in the transmission system can hamper the maximum distance of transmission. Equation 2.21 below shows the calculation of the maximum transmission distance for a 2.5 $Gb.s^{-1}$ transmission system with loss allowance of 22.2 dB and attenuation coefficient of 0.3 $dB.km^{-1}$.

$$\begin{aligned} \text{Loss allowance} &= \text{Loss at the source} - \text{Loss at the receiver} \\ &= \alpha L \\ 22.2\text{dB} &= (0.3\text{dB.km}^{-1})\text{L} \\ \text{L} &= 74\text{km} \end{aligned} \qquad 2.21$$

For the transmission module formats, nonreturn to zero-NRZ and return to zero-RZ, the limit for transmission is given by, (Kaiser)

$$\begin{aligned} D\sigma_\lambda L &= 70\% \times \text{bit Period} \quad \text{(NRZ)} \\ D\sigma_\lambda L &= 35\% \times \text{bit Period} \quad \text{(RZ),} \end{aligned} \qquad 2.22$$

where σ_λ is the spectral width of the source and D is the total dispersion in the fibre. If the fibre has a dispersion D of 2.5 ps.(km.nm)$^{-1}$, a source spectral width σ_λ of 1 nm, and maximum allowed dispersion of the period of the pulse 400 ps, then the maximum distance from equation 2.22 is 112 km and 56 km for NRZ and RZ, respectively. It is seen that RZ is more sensitive to dispersion than NRZ modulation format.

Figure 2.14 shows the transmission limits as a function of data rate for the 1550 nm transmission for sources having spectral widths σ_λ of either 3.5 or 1.0 nm. The straight lines give the attenuation limit as function of data rate for InGaAs avalanche photodiode APD and InGaAs *Pin* detectors, for SMF with dispersion of 2.5 ps.(km.nm)$^{-1}$ and fibre attenuation of 0.3 dB.km^{-1}. InGaAs *Pin* photodiodes have longer transmission distance limits than InGaAs APD (avalanche photodiode). Sources with a spectral width of 1 nm will transmit further before a signal is degraded than a source with a broader spectral width of 3.5 nm.

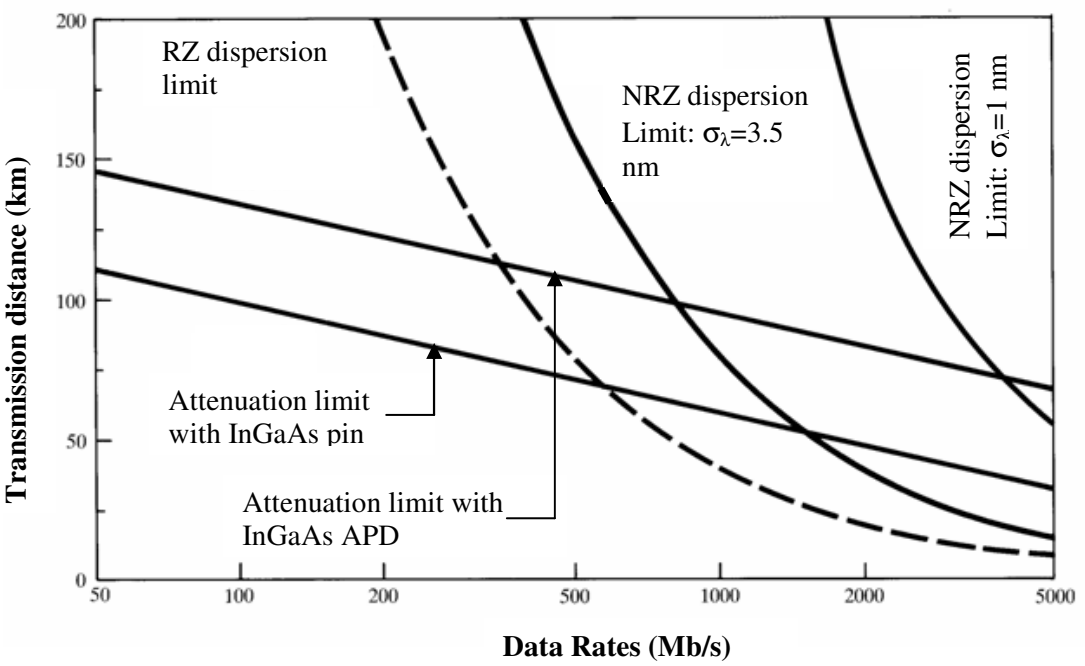

Figure 2.14: Transmission distance as a function of Data rates for a telecommunication single mode fibre in a system using Return to zero and Non-return to zero modulation formats, InGaAs Pin and APD photodetectors, and the source spectral width, σ_λ, of 3.5 and 1 nm; the dispersion coefficient is given by 0.3dB.km^{-1} (after Ref. [4]).

In this chapter we have looked at selected topics in optical fibre theory, as well as the impairments to data transmission. In the following chapter, we consider one system impairment in particular, namely Polarization Mode Dispersion which forms the main subject of this study.

2.6 References

[1] **E Hecht (1998)**, "Optics, 3rd Edition", Addison-Wesly, pp. 319 - 324

[2] **M Bass and E W Van Stryland** (2002), "Fiber Optics Handbook", McGraw-Hill, pp 1.6 – 1.7, 2.2 – 2.4

[3] **A Ghatak and K Thyagarajan** (1998), "Introduction to Fiber Optics", Cambridge University Press, pp.32, 132 – 149, 72 – 92, 325 - 334

[4] **G Keiser** (2000), "Optical Fiber Communications", McGraw-Hill International Editions, pp. 48 – 62

[5] **S E Miller and I P Kaminow** (1988), "Optical Fiber Telecommunications II", Academic Press Inc., pp 34 – 40

[6] **D Derickson** (1998), "Fiber Optic Test and Measurement", Prentice Hall, New Jersey, pp. 228 - 231

[7] **M Born and Wolf** (1999), "Principles of Optics", University Press, pp. 25 – 33

[8] **M Barnoski** (1976), "Fundamentals of Optical Fiber Communications", Academic Press inc, pp. 26 – 37

[9] **J Hayes** (2001), “Fiber Optics Technicians Manual 2nd Edition”, Delmar Thomson Learning, pp. 25

CHAPTER 3

POLARIZATION MODE DISPERSION

At high optical transmission rates (10, 40 and 80 $Gb.s^{-1}$) polarization mode dispersion (PMD) in the deployed single mode fibres can cause impairments at the receiver end of the fibre. Proper measurements of PMD and investigations of its dependence on the environmental conditions are very important for proper design of high-capacity optical communication systems. PMD is the result of asymmetry in the optical fibre core. This leads to a fibre supporting two orthogonal modes of polarization. The modes travel at different speeds in the fibre core because of the difference in the index of refraction (see Section 3.1). Section 3.2 discusses the statistical variation of PMD. A variety of techniques for measuring PMD are also briefly discussed in Section 3.3.

3.1 Fundamentals of PMD

This section focuses on the origins of polarization mode dispersion (PMD), namely, birefringence, mode coupling and the principal states of polarization.

3.1.1 Birefringence

When light propagates in a single mode fibre it may be analyzed in terms of two orthogonal states of polarization modes. In the ideal case where the core of the fibre is perfectly circular and symmetrical, these two orthogonal modes would travel through the fibre with identical velocities. In most cases however, many single mode fibres have a core which is noncircular and asymmetrical.

This leads to different orthogonal polarization modes of light travelling through different effective indices of refraction in the core. This difference in refractive indices of the fibre

core is called the birefringence. Optical fibre birefringence is caused by intrinsic and extrinsic perturbations (see Figure 3.1). Intrinsic birefringence occurs during the manufacturing process of the fibre. The intrinsic birefringence could be geometric due to non-circular core and stress applied on the fibre core by the cladding.

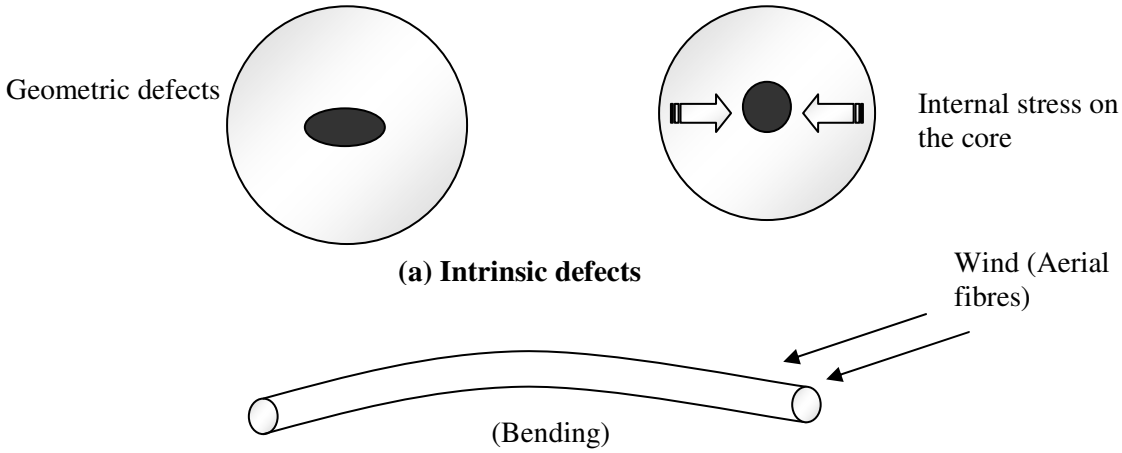

Figure 3.1: Fibre defects: (a) intrinsic fibre defects causing an elliptical fibre core and pressure being applied on the fibre. (b) Environmental changes, namely, temperature and wind also introduce extrinsic defects on the fibre.

When the fibre is spooled, cabled, or buried in the ground, birefringence can be induced from a number of extrinsic perturbations, including lateral stress, bending or twisting. These perturbations will change as the fibre's external environment changes. The perturbations listed above create a linear birefringence where there are two linearly polarized waveguide modes whose electric field vectors are aligned with the symmetry axes of the fibre [1]. Birefringence can be represented by the propagation constant β for orthogonal polarization modes,

$$\Delta\beta = \beta_s - \beta_f = \frac{\omega(n_s - n_f)}{c} = \frac{\omega\Delta n}{c} = \frac{2\pi}{\lambda}\Delta n, \qquad (3.1)$$

where ω is the angular frequency of the light, c is the speed of light in vacuum, λ is the wavelength of light propagating in a fibre and Δn is the refractive index difference between the slow and the fast axis (Figure 3.2).

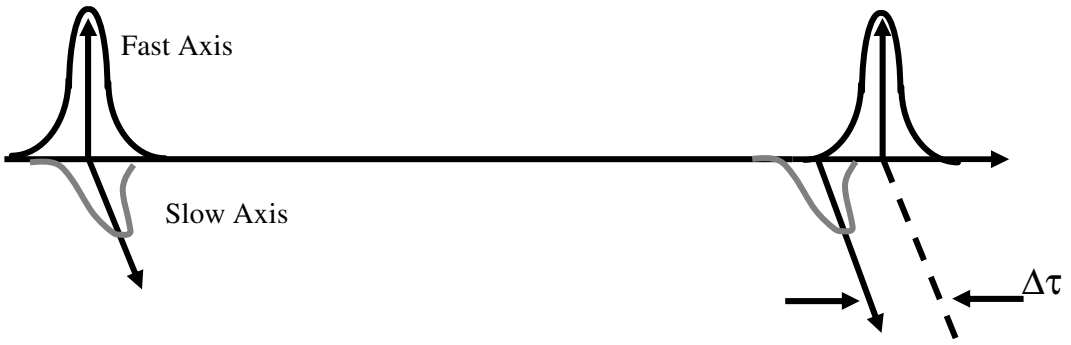

Figure 3.2: A typical birefringent optical fibre with light propagating in the fast and slow axes, resulting in differential group delay (DGD).

The difference in indices mentioned above leads to a difference in the group velocity of the orthogonal modes. The difference in group velocity gives rise to a differential group delay (DGD), $\Delta\tau$. In short length fibres in the time-domain, DGD can be obtained by taking the derivative of Equation 3.1 with respect to angular frequency,

$$\frac{\Delta\tau}{L} = \frac{1}{\Delta\upsilon_g}\left(\frac{\Delta n}{c} + \frac{\omega}{c}\frac{d\Delta n}{d\omega}\right), \tag{3.2}$$

where $\Delta\upsilon_g$ is the group velocity difference between the orthogonal modes and $\Delta\tau/L$ is the PMD coefficient in the short length regime measured in $ps.km^{-1}$ of the fibre length. The linear dependence of DGD occurs in a material or a fibre with a uniform birefringence and negligible mode coupling [1]. Section 3.2 discusses the behaviour of PMD in the long length regime and the effect of polarization mode coupling on PMD.

3.1.2 Polarization mode coupling

Terrestrial and submarine cables used by the telecommunication industries are of a very long length, so the short length conditions in the section above will not apply. The fibre can be considered to be a concatenation of short segments. The fast and the slow axes of the orthogonal modes from one segment of the fibre each divide into both the fast and the slow modes of the next segment, and this effect will continue throughout the fibre sections of the fibre. This process is called the polarization mode coupling. The coupling sites could be caused by localized stress during spooling, cabling, deployment, splices, variations in fibre drawing processes and fibre spinning during drawing [1].

To model the mode coupling effect in an optical fibre, the fibre could be assumed to be a concatenation of birefringent sections whose principal axes change randomly along the fibre as shown in Figure 3.3 [2]. The states propagating in the orthogonal axes are the principal states of polarization (PSP). The states are fixed for a fibre with a uniform birefringence and vary for a fibre with many birefringent sections.

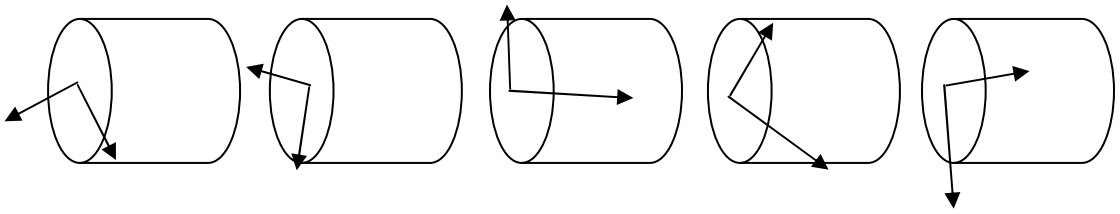

Figure 3.3: Concatenation Model of an optical fibre with the birefringent sections and the principal axes changing randomly.

The presence of mode coupling in the fibre makes the birefringence of the different sections add or subtract from the total birefringence of the fibre. In Section 3.1.1 (uniform birefringence), the DGD of the fibre varies linearly with the fibre length. In the presence of mode coupling the DGD of the fibre does not vary linearly with the length. It was shown by Poole *et al.* (1986) [3] that the DGD of the fibre with mode coupling accumulates as a three-dimensional random walk and on average increases with the square root of distance. As explained above, Mode coupling varies with the fibre's

environment, consequently the DGD also varies with the environment, time and wavelength. This variation implies that a statistical approach should be applied in the characterization of the fibres for PMD (Section 3.2).

Optical fibres are sometimes classified into two regimes, namely, the “short” and “long’ length regimes. The classification is done with respect to the parameter known as the coupling length. The coupling length, L_C, is the length at which the power in the orthogonal polarizations in the fibre has decayed as shown in Equation 3.3.

$$P_x - P_y = \frac{1}{e^2} \tag{3.3}$$

P_x and P_y are the power in the x and y polarizations, respectively. When the optical fibre transmission distance L satisfies $L<<L_C$, then the fibre is in the short length regime and the mean DGD of the fibre increases linearly with time. However, if L satisfies $L>>L_C$, the fibre is considered to be in the long length regime and the DGD increases with the square root of the distance [1].

3.2 Statistical variation of PMD

As was mentioned above, mode coupling sites of single mode fibres vary thermally and mechanically. This implies that the principal states of polarization (PSP) of the fibre change along the length of the fibre. The DGD of the fibre subsequently changes as a result of the changes in relative orientations of the PSPs. Figure 3.4 shows the light with the electric field $\mathbf{E}$ incident at the fibre input with angle θ to the x principal axis polarization of the fibre. The electric field in the first birefringent section divides into two orthogonal polarization modes, namely, E_x and E_y. In the next birefringent section, the polarization axes change and E_x and E_y divides into other components, E_{xx} , E_{xy}, E_{yy} and E_{yx}. The process continues until the last birefringent section of the fibre. As explained above, the orientations θ_i vary in response to the environmental fluctuations. The

fluctuations lead to the DGD and PSPs locations of the fibre varying with time [4]. If the PSPs of a device do not vary with environmental effects or time, then the device is said to be deterministic. The mean DGD of the device in this case is given by the difference in arrival times of the two PSPs. On the other hand, if the PSPs change in response to the environment, then the DGD is impacted by the environmental change. Since the DGD changes with time, statistics must be used to describe its variation.

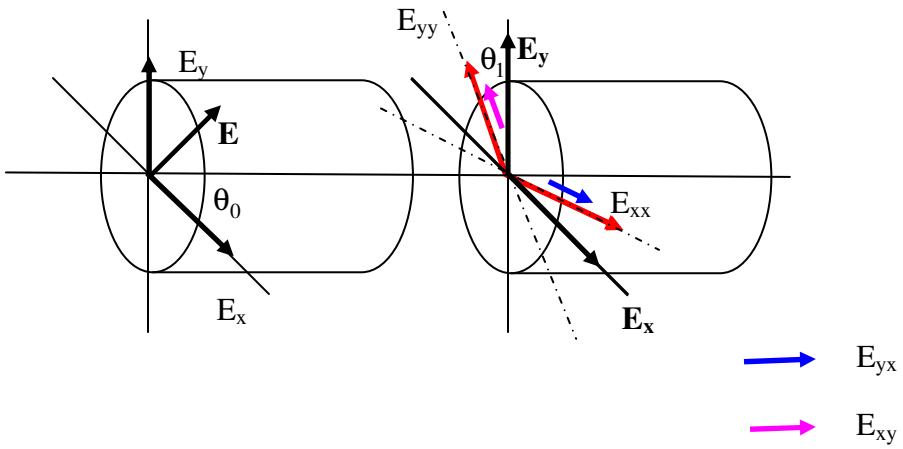

Figure 3.4: Light propagation through a birefringent fibre with the variation in PSP location.

It is important to start the statistical analysis with the instantaneous DGD. This is defined as the DGD of the fibre at a specific wavelength. Studies have shown that instantaneous DGD ($\Delta\tau(\lambda,t)$) of a fibre with a mode coupling is a random variable with a Maxwellian distribution given by Equation 3.4 [5, 6, 7]. In order to obtain a reliable average and distribution experimentally, a large sample of uncorrelated instantaneous DGDs must be taken. The Maxwellian distribution that describes the DGD distribution is given by,

$$\rho(\Delta\tau) = \sqrt{\frac{2}{\pi}}\frac{\Delta\tau^2}{\sigma^3}e^{(-\Delta\tau^2/2\sigma^2)} \tag{3.4}$$

where $\sigma = \langle\Delta\tau\rangle\sqrt{\frac{\pi}{8}}$ and $\langle\Delta\tau\rangle$ is the mean instantaneous DGD over a relatively longer period of time given by Equation 3.5.

$$\langle \Delta\tau \rangle_t = \frac{1}{N_t} \sum_{i=1}^{N_t} \Delta\tau(\lambda, t_i) . \qquad (3.5)$$

A typical distribution of DGD at a given wavelength is as shown in Figure 3.5.

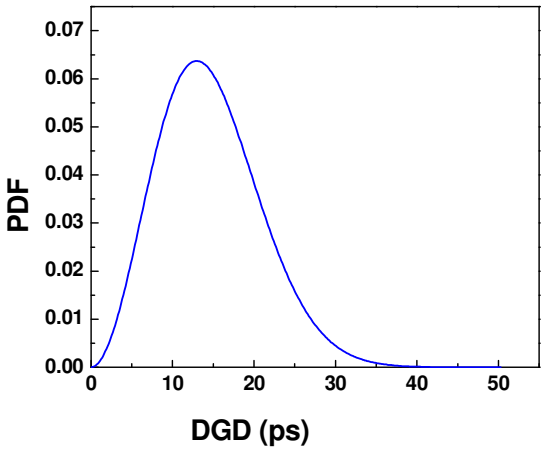

Figure 3.5: A typical Probability distribution function (PDF) of DGD for a mode coupled fibre with mean and rms PMD of 14.702 ps and 15.958 ps, respectively.

The distribution in Equation 3.4 can be used to find the probability of the DGD ($\Delta\tau$) exceeding a certain DGD (Cumulative probability) value.

$$P(\Delta\tau \geq \Delta\tau_i) = 1 - \rho(\Delta\tau) \qquad (3.6)$$

The cumulative probability of the DGD probability distribution function is plotted in Figure 3.6. From the Figure 3.6 the probability of exceeding the mean DGD (14.702 ps) is 46.4% and 40.1% for the rms DGD (15.958 ps) and 1.7×10^{-4} % for the 50.1 ps.

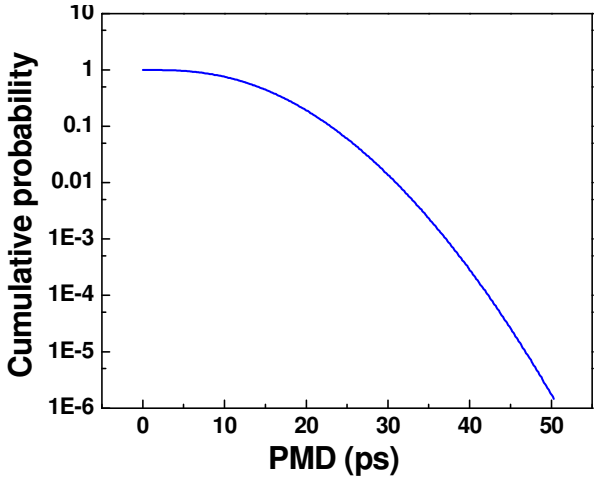

Figure 3.6: Cumulative probability distribution for a mode coupled fibre with the mean and rms PMD of 14.702 and 15.958 ps, respectively.

The information obtained from the plot of the cumulative probability distribution function is important for the design of an efficient long-haul fibre optic network. Allen *et al*. (2003) [5] have shown that for a network operating with non-return-to-zero (NRZ) format, the maximum tolerable DGD in the system is given by,

$$\text{Max. tolerable DGD} = 3.7\left\langle \Delta\tau \right\rangle . \tag{3.7}$$

In the NRZ system, the worst case scenario is observed when the DGD is 23% of the bit period resulting in a receiver sensitivity penalty of 1 dB. The tolerable DGD and mean PMD (calculated from Equation 3.7) for NRZ system for various bit-rates are given in Table 3.1.

Table 3.1: Tolerable DGD and PMD values for the NRZ systems.

Bit-rates (Gb.s^{-1})	***Max. tolerable DGD (ps)***	***Max. tolerable mean DGD (ps)***
2.5	*92*	*25*
10	*23*	*6.2*
40	*5.7*	*5.7*

3.3 Techniques for measuring PMD

PMD is measured by two different procedures, namely, the time and frequency domain methods. In the frequency domain, measurement is based on the evolution of SOPs as a function of frequency. The frequency domain measurement methods described in this chapter are the Jones Matrix Eigenanalysis, Poincaré Sphere and the Fixed Analyzer method. The time domain methods are based on the dispersion of the pulses or the interference of the states that have propagated through the fibre. The time domain technique used in this study is the Interferometric technique.

3.3.1 Frequency domain measurements

PMD measurement methods in the frequency domain involve a differential method where the difference in propagation delay between light travelling in the fast and slow PSP is measured by assessing its effect on the polarization state of light as it exits the test device [8]. The frequency domain methods use a polarimeter to measure the output state of polarization. The output state of polarization is necessary for the full interpretation of the DGD and PSPs as a function of the wavelength. In this section the Jones Matrix Analysis and the Poincaré sphere techniques are presented. Furthermore, the Fixed Analyzer technique which does not depend on all the components of the Stokes vector, is also presented.

3.3.1(a) Jones Matrix Eigenanalysis

The Jones matrix eigenanalysis (JME) setup comprises a tuneable laser source, polarization controller and a polarimeter to measure the output state of polarization from the fibre under test (FUT). The setup for the JME is as shown in Figure 3.7. The JME is used to measure the DGD of the fibre or device under test and the polarization dispersion vector $\boldsymbol{\Omega}$.

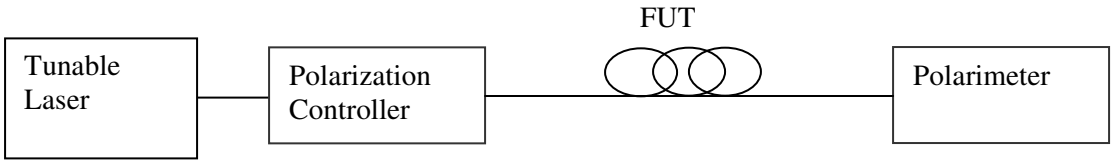

Figure 3.7: A typical set up of the Jones Matrix Eigenanalysis Technique with the fibre under test (FUT).

When starting the scans, the tuneable laser in the setup chooses an angular frequency ω_1, etc, at frequency ω_1 three non-collinear (0º, 45º and 90º) input polarization states are input into the fibre and the corresponding output polarizations are measured. The output states of polarization allow the calculation of the Jones Transfer Matrix $\mathbf{T}(\omega_i)$. This matrix describes the transformation of the input polarization states to the output states of polarization at angular frequency ω_i. The product of the transfer matrix $\mathbf{T}(\omega_{i+1})$ and the inverse transfer matrix $\mathbf{T^{-1}}(\omega_i)$ (product matrix $\mathbf{T}(\omega_{i+1})\mathbf{T^{-1}}(\omega_i)$) gives the matrix with the dispersion vector $\mathbf{\Omega}$ as the eigenvector, and the eigenvalues ρ_f and ρ_s which are related to the group delay between the principal states of polarization (PSPs). From the eigenvalues of the product matrix above, the DGD, $\Delta\tau$ for a wavelength increment $\Delta\omega$ is given by,

$$\Delta\tau = \left| \frac{\mathrm{Arg}(\rho_f / \rho_s)}{\omega_{i+1} - \omega_i} \right| \tag{3.8}$$

where Arg is the argument function $\mathrm{Arg}(\eta e^{i\theta}) = \theta$ [8-12]. A typical spectrum of the variation of the DGD with frequency measured with the JME technique is shown in Figure 3.8.

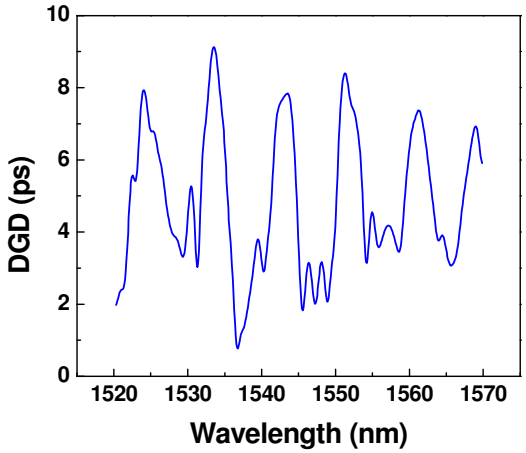

Figure 3.8: Typical spectrum of DGDs for a mode coupled fibred measured with the JME method collected at the NMMU fibre Optics Laboratory.

3.3.1(b) Poincaré Sphere Analysis

The setup for the Poincaré sphere (PSA) technique is the same as that for the JME shown in Figure 3.7 above. The difference between the PSA and JME is in the data analysis. The JME measures PMD with the Jones transfer matrix whilst the PSA uses Stokes parameters of the output SOPs to measure PMD. The technique makes use of three orthogonal output states polarization at angular frequency ω, namely, $\hat{h}$, $\hat{q}$ and $\hat{c}$. If the angular frequency is changed by an infinitesimal amount then the output SOPs in Stokes space at angular frequency $\omega + d\omega$ also change by an infinitesimal amount. For a finite change in the optical frequency $\Delta\omega$, Cyr *et al.* (1999) [10] showed geometrically in the Stokes space that the DGD for the mean frequency in the range $[\omega, \omega + \Delta\omega]$ is given by,

$$\Delta\tau = \left|\frac{\Delta\theta}{\Delta\omega}\right| = \frac{2}{\Delta\omega}\sin^{-1}\left(\frac{1}{2}\sqrt{\frac{1}{2}(\Delta\mathbf{h}^2 + \Delta\mathbf{q}^2 + \Delta\mathbf{c}^2)}\right)\sqrt{a^2 + b^2}\ . \qquad (3.9)$$

The Δh, Δq and Δc are finite changes in the orthogonal output states of SOPs. $\Delta\theta$ represents the angle of separation on the Poincaré sphere for the output SOPs at angular frequencies ω and $\omega + \Delta\omega$. The geometrical derivation was done for two linear

polarization states oriented at 90º to each other at the launch and their corresponding output states of polarization are also orthogonal on the Poincaré sphere [8, 10]. The PSP can also be measured with the PSA. As was explained in section 3.1 this is the axis around which the output SOPs rotates for a small change in angular frequency $\Delta\omega$. PSA uses the geometrical derivation in Equation 3.10 to determine the PSPs [8, 10, 11, 12].

$$\text{PSP} = \frac{\mathbf{u}}{|\mathbf{u}|} \tag{3.10}$$

$\mathbf{u}$ in Equation 3.10 is given by $\mathbf{u} = (\mathbf{c} \cdot \Delta\mathbf{q})\mathbf{h} + (\mathbf{h} \cdot \Delta\mathbf{c})\mathbf{q} + (\mathbf{q} \cdot \Delta\mathbf{h})\mathbf{c}$.

3.3.1(c) Fixed Analyzer technique

The simple setup for the Fixed Analyzer technique is as shown in Figure 3.9. Light from the light source is polarized at the input and output of the fibre. For the setup in our laboratory, the transmission through the fibre is detected with an optical spectrum analyzer (OSA). On the other hand, if a tuneable laser source is used, then a power meter would be used to detect the transmission through the polarizer.

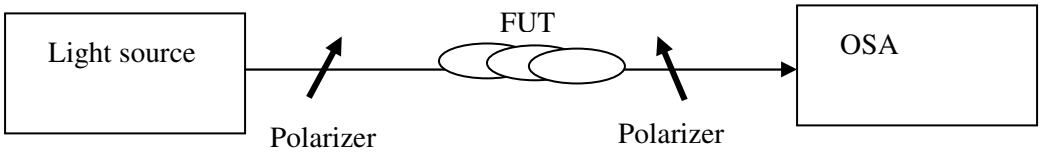

Figure 3.9: Typical setup for the fixed analyzer technique with the fibre under test (FUT) and the Optical spectrum analyzer (OSA) as the detector.

The variation in the power transmitted through the output polarizer is an indication of the variation of the states of polarization incident on the polarizer due to PMD in the test fibre [4]. Poole *et al.* (1986) [3] related the PMD of the fibre to the number of extrema (minima and maxima) in the transmission spectrum of the fibre under test over the

angular frequency range of the light source implemented in the tests. Equation 3.11 gives the relationship relating PMD of the fibre under test to the extrema in the transmission spectrum for a source operating in the angular frequency range $\Delta\omega$:

$$\langle \Delta\tau \rangle = \frac{k\pi N_e}{\Delta\omega} \tag{3.11}$$

N_e and k are the number of the extrema on the transmission spectrum and mode coupling factor, respectively. It has been shown that for a fibre with negligible mode coupling, k=1 and for highly mode coupled fibre k=0.805 [8]. In a fibre with negligible mode coupling, the transmitted power at the polarizer output varies sinusoidally. On the other hand, for a highly mode coupled fibre, transmitted output varies in a random manner [4, 8].

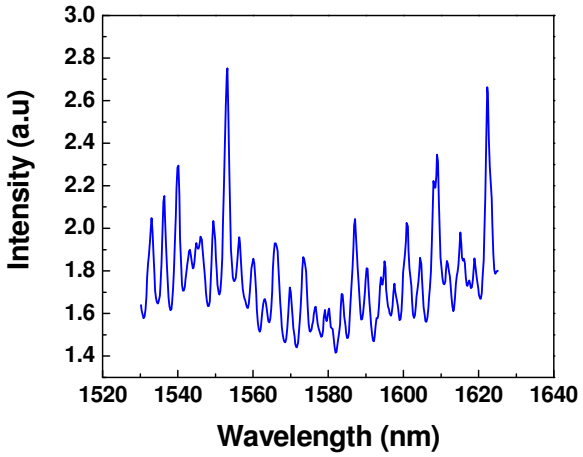

Figure 3.10: Transmission spectrum of an emulator obtained using the fixed analyzer method at the NMMU Optical Fibre laboratory.

3.3.2 Time Domain Measurements

When light travels through the fibre it can split into two orthogonal PSPs depending on how its polarization is oriented with respect to the principal axes of the fibre under test. If light is polarized in the fast or slow axes of the fibre, there will be no differential group delay experienced by light at the output end of the fibre. On the other hand, if the state of polarization of the input light signal will be at an angle to the principal axes, then light

will travel in both the fast and slow axes of the fibre. In the time domain PMD is measured from the arrival times of the light signals travelling in the fast and slow axes of the fibre. In this study, the traditional and the generalized interferometric techniques (TINTY and GINTY) were employed; Details of these techniques are the main focus of Chapter 4. The section below presents the summary of the operational principles of the techniques.

3.3.2.1 Interferometric technique

The time domain technique uses the Michelson interferometer to measure the PMD of an optical fibre. A typical setup of the interferometric technique is shown in Figure 3.11. The apparatus includes a broadband light source, interferometer and a detector. The light from the light source is input into the fibre and at the output it is depolarized and input into the Michelson interferometer. The light signal is split into the two interferometer arms of the interferometer by a beam-splitter.

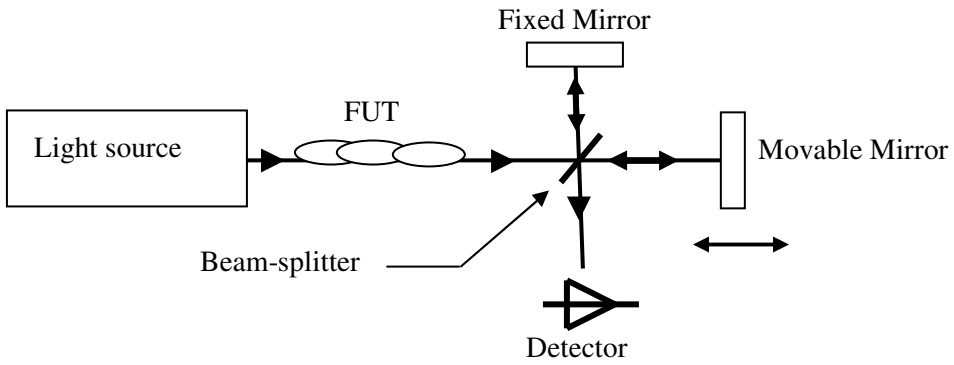

Figure 3.11: A typical set-up of an inteferometric PMD measurements method.

The light in one arm reflects at a fixed mirror and the other reflects at a movable mirror and introduces a relative delay in the two light signals. Light from the two arms of the interferometer recombine and interfere at the detector. Constructive interference is observed when the time delay between the two arms, matches the delay introduced in the fibre by PMD, to within the coherence time of the source [7]. The coherence time of the source is given by,

$$T_C = \frac{\lambda^2}{\Delta\lambda c} \tag{3.12}$$

where λ is the central wavelength of the light source, c is the speed of light and $\Delta\lambda$ is full-width at half-maximum (FWHM) of the light source spectrum. A broadband source is normally preferred for use with this technique as it has a short coherence time similar to the delay imposed by the PMD [11, 12]. Chapter 4 discusses TINTY and GINTY used our study.

3.4 Accuracy limitations on PMD Measurements

In mode coupled fibres, DGD varies with wavelength and environmental conditions [5]. PMD is defined as the mean or rms value of the DGDs. Since measurements of PMD involve averaging, then there is an intrinsic uncertainty associated with the PMD measurements. Gisin *et al.* (1996) [13] derived a formula of the accuracy limitation to the PMD measurement due to the statistical nature of DGD. The accuracy limitation is given by,

$$\sigma_{\text{statistical}} = \frac{\alpha\overline{\Delta\tau}}{\sqrt{\overline{\Delta\tau}\,\Delta\omega}} \tag{3.13}$$

where $\overline{\Delta\tau}$ and $\Delta\omega$ are the PMD and frequency bandwidth of the source used in the tests. All the PMD measurement techniques are affected by this uncertainty [13]. In addition to this intrinsic uncertainty, there are measurement uncertainties associated with the techniques. Section 4.2.4 (Chapter 4) discusses the measurement uncertainty associated with the interferometric techniques.

3.5 References

[1] **H Kolgenik** and R M Jopson (2002), "Polarization-Mode Dispersion", Chapter 15, *Optical Fiber Telecommunications*, vol. IV B, edited by I P Kaminow and T Li, Academic Press, San Diego, CA, pp 1

[2] **N Gisin,** R Passy, J C Bishoff and B Perny (1993), "Experimental Investigations of the Statistical Properties of Polarization Mode Dispersion in Single Mode Fibers", *IEEE Photon. Technol. Lett*. **5**(7), pp. 819-821

[3] **C D Poole** and R E Wagner (1986), "Phenomenological approach to the polarization dispersion in long single-mode fibers", *Electron. Lett*. **22**(6), pp. 1029-1030

[4] **S Shtaif** and A Mecozzi (2000), "Study of the Autocorrelation of the Differential Group Delay in Fibers with Polarization Mode Dispersion", *Opt. Lett*. **25**, pp. 707-709

[5] **C T Allen**, P K Kondamuri, D L Richards and D Hague (2003), "Measured Temporal and Spectral PMD Characteristics for Network-Level Mitigation Approaches", *J. LightwaveTechnol.* **21**(1), pp. 79-86

[6] **F Curti**, B Daino, and G de Marchis (1990), "Statistical Treatment of the Evolution of the Principal States of Polarization in Single-Mode Fibers", *J. Lightwave Technol.* **8**(8), pp. 1162-1165

[7] **N Gisin**, J P Von der Weid and J Pellaux (1991), "Polarization Mode Dispersion of Short and Long Single-Mode Fibers", *J.Lightwave Technol.* **9**(7), pp 821-827

[8] **P Williams** (2004), "PMD measurement techniques and how to avoid pitfalls", *J. Opt. Fiber. Commun*. Rep. 1, pp. 84-105

[9] **B L Heffner** and P R Hernday (1995), "Measurement of Polarization-Mode Dispersion", *Hewlett-Packard Journal*, pp. 27-33

[10] **N Cyr**, A Girard and G W Schinn (1999), "Stokes Parameter Analysis Method, The Consolidated Test Method for PMD Measurements", *NFOEC Proc.,* Tech. Digest*,* vol. II, pp 280

[11] Measurement methods and test procedures-Polarization mode dispersion (2005), *International Electrotechnical Commission (IEC)*, Part 1-48

[12] Definitions and test procedures for statistical and non-linear related attributes of single-mode fibre and cable (2005), *International Telecommunication Union*, ITU-T Recommendation G.650.2

[13] **N Gisin**, B Gisin, J P Von der Weid and R Passy (1996), "How Accurately Can One Measure a Statistical Quantity Like Polarization Mode Dispersion?", *IEEE Photon. Technol. Letters* **8**(12), pp1671-1673

CHAPTER 4

GINTY AND TINTY PMD MEASUREMENT TECHNIQUES

The EXFO FTB-5500 (TINTY) and FTB-5500B (GINTY) interferometry-based PMD analyzers were used in this study to measure PMD in the laboratory and in the field. The technique has a very fast scanning time and the equipment is portable, hence its suitability for the field characterisation of deployed fibres. In general, the Interferometry techniques are favoured for use as they give reliable results and are insensitive to fibre movement. The traditional interferometry technique or TINTY had some limitations which were recently addressed in the Generalized Interferometry Technique, or GINTY. In this Chapter the theory of interferometry, operation of the TINTY, GINTY and different components, assumptions and calculations making up the respective measurement setups are presented.

4.1 Traditional Interferometry Technique (TINTY)

4.1.1 Experimental set-up

The EXFO FTB 5500 used in this study is based on the Traditional Interferometry Technique, also known as TINTY. The generic set-up for the experimental implementation with TINTY is shown in Figure 4.1. The broadband light source used with TINTY should have a peak wavelength centred around 1310 or 1550 nm.

The output light from the source is polarized, while the light output from the fibre under test is polarized by the analyzer before it enters the interferometer. The light is then split by the beam splitter (BS) to the two arms of the Michelson interferometer containing the fixed mirror M_1 and the movable mirror M_2 (delay line). The light from the

interferometer arms which satisfies the conditions for interference is then detected and the interferogram envelopes used in the measurement of PMD [1].

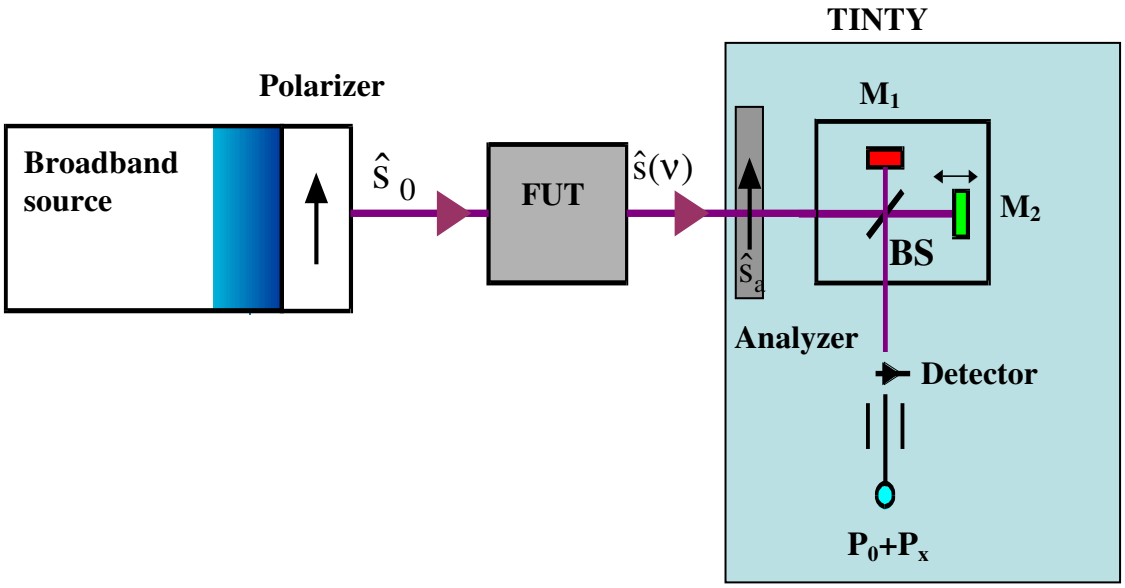

Figure 4.1: A typical measurement setup for TINTY consisting of broadband light source, fibre under test (FUT), analyzer, Michelson interferometer with the delay line, the detector for the auto- and cross-correlation interferogram envelopes (after Ref. [2]).

4.1.2 PMD calculations with TINTY

There are two methods that TINTY uses to calculate PMD depending on the mode coupling of the fibre under test. The methods are explained in Sections 4.1.2.1 and 4.1.2.2.

4.1.2.1 PMD calculation for negligible or no mode coupling

In the absence of mode coupling there are only two polarisation modes propagating in the fibre. The interferogram envelope for a deterministic device is characterised by an auto-correlation peak at the centre and two satellite peaks, one on each side of the auto-correlation peak as shown in Figure 4.2.

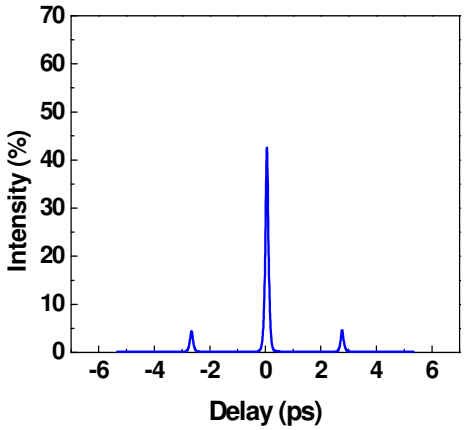

Figure 4.2: Interferogram envelope of a polarisation maintaining fibre containing a characteristic auto-correlation peak and two satellite peaks. PMD of this fibre is given by the time delay between the auto-correlation peak and either of the satellite peaks.

The auto-correlation peak occurs when the arms of the interferometer are of equal lengths. One satellite peak results from interference between the slow mode light travelling along the fixed mirror path and the fast mode light delayed by the extra distance travelled along the movable mirror path, and the other satellite peak is from the interference between the fast mode light travelling along the fixed mirror path and the slow mode light which advanced in the opposite direction to the former case by the shorter movable mirror path. The PMD in this case is measured as the time separation of the auto-correlation peak and either of the satellite peaks [2, 3, 4, 5,].

4.1.2.2 PMD calculation for a fibre or device with random mode coupling

Unlike in the previous case, a fibre containing a random distribution of mode coupling will in general have many birefringent sections, each with different principal axes of polarization (see Chapter 3). The method employed by TINTY in calculating PMD for the case of random mode coupling makes certain assumptions, which will be discussed in Section 4.1.3 below. The interferogram of a randomly mode coupled fibre has many peaks. Gisin *et al.* (1991) [1] showed theoretically that the broadness of light intensity distribution (interferogram), $I(\tau)$ (τ is the delay between interfering light signals), grows linearly with the fibre length for a device with low mode coupling, but for random mode

coupling it accumulates around the mean time of flight with a Gaussian-like distribution as shown in Figure 4.3.

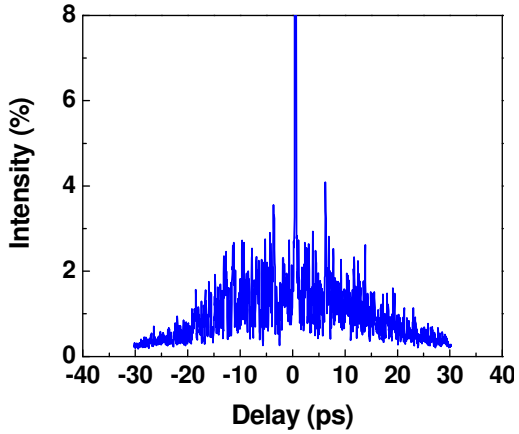

Figure 4.3: Typical Gaussian interferogram envelope obtained from TINTY for a fibre with strong mode coupling.

Furthermore, the spreading of the distribution also grows with the square root of the fibre length L [1, 4]. PMD can then be calculated as the mean square deviation of intensity distribution $I(\tau)$ in terms of the fibre length L, the mean coupling length h, and the average birefringence D, given by [1],

$$(\Delta\tau)^2 = \frac{D^2h^2}{2}\left[\left(\frac{2L}{h}\right) - 1 + e^{-2\frac{L}{h}}\right] \tag{4.1}$$

Equation 4.1 shows that for short lengths of low mode coupling fibre (L<<h),

$$(\Delta\tau) \cong DL\,, \tag{4.2}$$

while for long length fibre with strong mode coupling (L>>h),

$$(\Delta\tau) \cong D\sqrt{hL}\,. \tag{4.3}$$

Experimentally, TINTY measures the intensity ($I(\tau) = E^2{}_x(\tau)$) of the different interfering modes as a function of the time of flight (τ) of these modes. The interferogram envelopes for the randomly mode coupled fibres are relatively Gaussian. PMD is then determined from an algorithm based on the calculation of the second moment or rms width of the cross-correlation interferogram envelope as [2],

$$\sigma_x = \frac{1}{2}\left(\sqrt{\frac{\int_{j_1}^{j_n} E^2{}_x(\tau).\tau^2 d\tau}{\int_{j_1}^{j_n} E^2{}_x(\tau) d\tau}} + \sqrt{\frac{\int_{i_1}^{i_n} E^2{}_x(\tau).\tau^2 d\tau}{\int_{i_1}^{i_n} E^2{}_x(\tau) d\tau}}\right), \tag{4.4}$$

where the integration is over the limits j_1 to j_n and i_1 to i_n. The limit j_1 to j_n is for one half of the interferogram while i_1 to i_n is for the other half. The regions covered are for the delays smaller than the coherence time of the source. The algorithm used with Equation 4.4 involves the computation of the zero intensity, filtering out of the noise, removal of the central auto-correlation peak, computation of the second moment of the truncated interferogram envelope and determination of the standard deviation fitted to the truncated interferogram [6, 3]. The PMD value is defined as the root mean square DGD and is determined from the half width, σ_x, of the Gaussian curve fitting applied to the interferogram envelope [2]. The PMD of the fibre is then given by,

$$\sqrt{\langle \Delta\tau^2 \rangle} = \left(\sqrt{\frac{3}{4}}\right)\sigma_x \tag{4.5}$$

4.1.3 Assumptions made with TINTY calculations

In the computation of PMD from the widths of the cross-correlation interferogram envelopes measured with TINTY, several assumptions are made. These make the technique applicable in only a certain number of cases [2, 7]:

- Ideal random coupling (Gaussian interferogram envelope)
- PMD>>σ_A (where σ_A is the auto-correlation width of the broadband light source)
- Smooth source spectrum with no ripples
- Measured PMD is equal to the statistical root mean square (rms) DGD
- Analyzed envelope is equal to unrealisable average

When the conditions listed above are met or almost met, TINTY gives an accurate PMD value. On the contrary, when these conditions are not met, the results that TINTY gives may be misleading. Some of these assumptions and their validity are briefly explained in detail in the following sections. The reader is referred Cyr (2004) [7] and FOTP-124 (TIA/EIA standards (2004)) [2] for details.

4.1.3.1 Ideal random coupling

The birefringence of a single mode fibre varies along the length of the fibre. A long single mode fibre can be represented as a series of random length, birefringent sections of random rotation [6]. In the calculation it is assumed that the birefringence axes are uniformly distributed and the ratio of the fibre length to mode coupling length of the fibre approaches infinity ($L/h \to \infty$). This assumption is the basis of the theory presented in Section 4.1.2.2 for a highly mode coupled fibre, and implies that the interferogram envelope that is analyzed is in fact Gaussian in shape. This is not always the case as some interferogram envelopes in the presence of mixed mode coupling take other shapes such as rectangular, flattened, etc. In the presence of these forms, this assumption would not be valid.

4.1.3.2 Source Spectrum with no ripples

In the determination of PMD for a device or fibre with random mode coupling, the auto-correlation peak of the light source is removed (see Section 4.1.2.2) from the interferogram before PMD calculations. For a broad Gaussian source spectrum, its auto-

correlation (Fourier transform) is narrow (Figure 4.4 (a)) and can be easily identified and removed from the interferogram envelope.

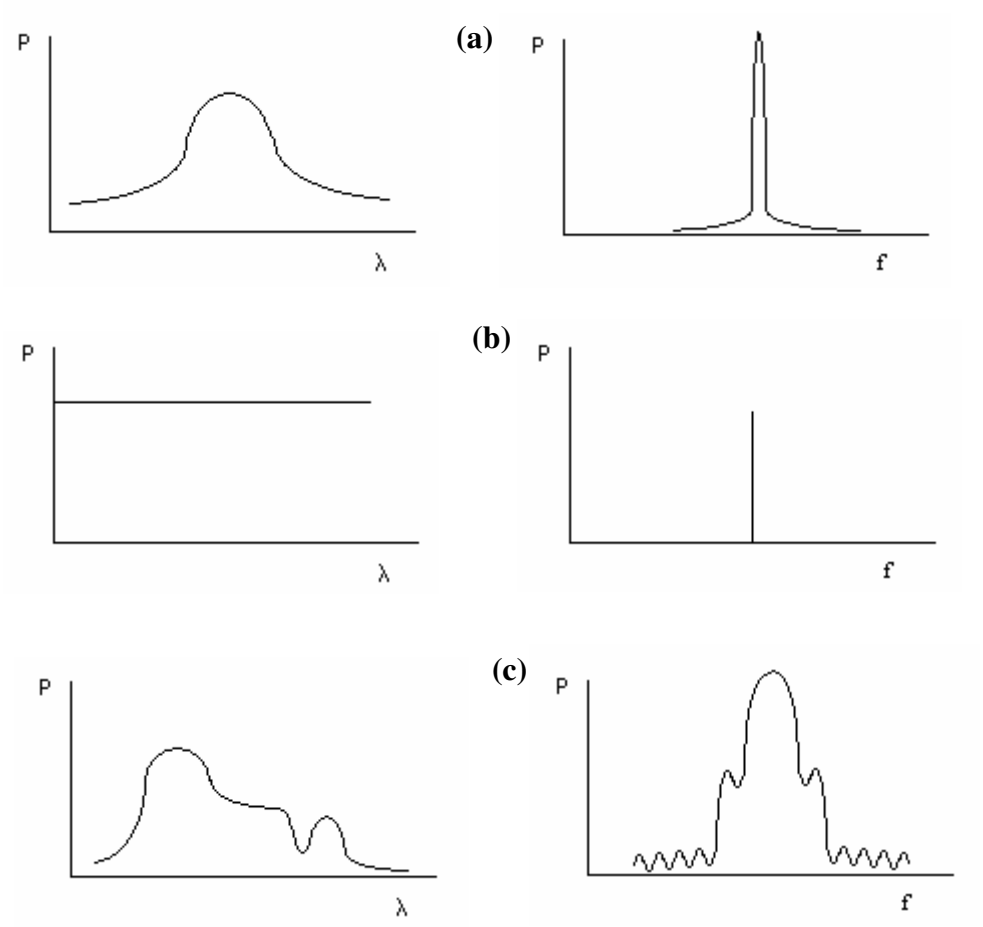

Figure 4.4: The auto-correlation functions of various spectra. The auto-correlation (Fourier transform) of the broad Gaussian source is narrow in **(a)** and can be easily removed from the Interferogram envelope, **(b)** infinite spectrum yields infinitely long line and **(c)** spectrum with ripples yields broad peaks with humps, ripples, etc.

As shown in Figure 4.4, a spectrum with ripples will yield an auto-correlation with humps, ripples, etc. and the interferogram envelope would need to involve complex mathematics to remove the auto-correlation part of the interferogram envelope. The requirement that TINTY use only a source with a smooth Gaussian spectrum is a serious limitation as the spectra of many light sources are not Gaussian.

4.1.3.3 PMD >> σ_A

The PMD of the fibre under test should be greater than the coherence time of the light source (Chapter 3). The light output will interfere if PMD is less than the coherence time of the source, and such condition is not conducive for measuring PMD [2, 3, 7].

4.1.3.4 Statistical rms DGD

The DGDs are assumed to be averaged over all the possible occurrences of the conceptual random variables and not over wavelengths. Further assumptions are made to make the measurements practical. That is, the mean, variance and probability density function of the locally random DGDs are wavelength independent, and wavelength and time averages are equal to the wavelength independent local averages [2, 7].

4.1.3.5 Analyzed envelope is equal to unrealisable average

In the PMD calculations it is known that the DGD values outside the source spectrum do not contribute to the average root-mean-square DGD (PMD). In this technique it is not specified as to how the rms DGD obtained from the interference envelope is weighted by the source spectrum [2, 7].

4.2 Generalized Interferometry Technique

An improved interferometry technique, first devised by N Cyr (2004) [7], named the generalized interferometric technique (GINTY) eliminates all the limitations mentioned in Section 4.1 above. The technique also uses the interferogram envelope to determine the PMD of the device under test. In contrast to TINTY however, the formula that links PMD to the interferogram envelope for GINTY is valid for all devices with any mode coupling ratio. PMD is measured within a specified wavelength range and the results can be traced to the frequency domain PMD measurement methods like the Poincaré Sphere Analysis and Jones Matrix Eigenanalysis method. Furthermore, the method eliminates the

offset generated by an irregularly shaped spectrum by separating the auto-correlation and cross-correlation interferogram envelopes. This section presents the operation of GINTY and the mathematical analysis used by the technique to overcome the limitations of the standard or traditional interferometry technique. EXFO FTB 5500B or GINTY is fairly a fairly new technique which at the moment few researchers have worked with. Most of the theory presented in this section was developed by Cyr [7].

4.2.1 Experimental set-up

The typical GINTY measurement setup comprises a polarized light source, fibre under test (FUT) and polarization scramblers (see Chapter 6 for description) at the input and output of the FUT. The GINTY instrument consists of the Michelson interferometer, polarization beam splitter and two photodetectors as shown in Figure 4.5.

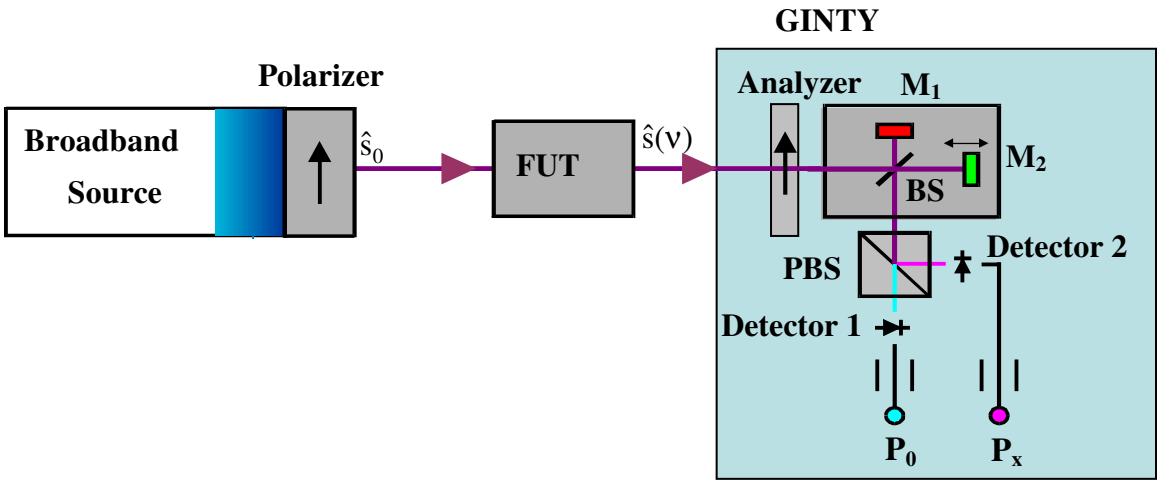

Figure 4.5: A typical GINTY measurement test setup indicating the input state of polarisation ($\hat{s}_0$), output state of polarization ($\hat{s}(\nu)$), Michelson interferometer, polarisation beam-splitter (PBS) and the two detectors (after Ref. [2]).

The photodetectors used by GINTY are sensitive in the O (1260-1360 nm), C (1530-1565 nm), and L (1565-1625 nm) bands. The polarization beam-splitter shown in Figure 4.5 is used to split the output light into two orthogonal polarization states and is collected by the two photodetectors. The splitting of the light signal from the interferometer enables the separation of the auto- and cross-correlation interferogram envelopes (Section 4.2.2).

4.2.2 Calculation of PMD with GINTY

GINTY calculates PMD from the raw interferogram envelopes obtained from an interferometry scan with the setup shown in Figure 4.5. The raw interferogram envelope as a function of the delay τ induced by the movable mirror is given by,

$$I(\tau) = P_0 + \mathrm{Re}[P_1(\tau)] \tag{4.6}$$

where P_0 (constant) is the delay independent part, and P_1 is dependent on τ. P_1 is given by the Fourier transform of the spectral density of the source $S(\nu)$,

$$P_1(\tau) = F(S(\nu)) \tag{4.7}$$

The spectral density at the analyser output is given by,

$$S(\nu) = \frac{1}{2}(S_0(\nu) + S_x(\nu)), \tag{4.8}$$

where $S_0(\nu)$ and $S_x(\nu)$ are the input spectrum and analyzer output spectrum, respectively. Therefore, the interferogram envelope is given by [7],

$$E(\tau) = \left|R_0(\tau) + R_x(\tau)\right|, \tag{4.9}$$

where $R_0(\tau)$ and $R_x(\tau)$ are the Fourier transforms of the input spectrum and analyzer output spectrum mentioned above, respectively. Hence the auto-correlation and cross-correlation interferogram envelopes are given by,

$$E_0 = \left|R_0(\tau)\right| \text{ and} \tag{4.10}$$

$$E_x = \left| R_x(\tau) \right| . \tag{4.11}$$

GINTY uses rms widths of the squared envelopes ($< E^2{}_x >$) of the auto-correlation and cross-correlation ($< E^2{}_0 >$) interferogram envelopes to calculate PMD. The expression for the PMD is then given by [2, 7]:

$$\sqrt{\langle \Delta\tau^2 \rangle} = \sqrt{\frac{3}{2}(\sigma^2{}_x - \sigma^2{}_0)} \tag{4.12}$$

where σ_0 and σ_x are the rms widths of the squared envelopes of the auto- and cross-correlation interferograms, and are computed from an algorithm using the equations for the second moment shown below [2],

$$\sigma_x = \sqrt{\frac{\sum(\tau^2 . < E^2{}_x(\tau) >)}{\sum < E^2{}_x(\tau) >}} \text{ and} \tag{4.13}$$

$$\sigma_0 = \sqrt{\frac{\sum(\tau^2 . < E^2{}_0(\tau) >)}{\sum < E^2{}_0(\tau) >}} . \tag{4.14}$$

4.2.3 Separation of the auto-correlation and cross-correlation interferograms

The auto-correlation and cross-correlation interferogram envelopes can be separated by using two opposite orientations of the analyzer axis, namely, $\hat{s}_a$ and $-\hat{s}_a$ in the Stokes space (Poincaré sphere). The delay dependent interferogram envelopes for these orientations are given by,

$$P_1 = R_0(\tau) + R_x(\tau) \tag{4.15}$$

and

$$P_2 = R_0(\tau) - R_x(\tau) \tag{4.16}$$

where $R_0(\tau)$ and $R_x(\tau)$ are as described in Section 4.2.2 above. The auto-correlation and cross-correlation can then be obtained by taking the real part of the sum and difference of Equation 4.15 and 4.16 as shown below [7]:

$$|P_1 + P_2| = |R_0(\tau)| \tag{4.17}$$

$$|P_1 - P_2| = |R_x(\tau)| \tag{4.18}$$

The equations above are identical to Equations 4.10 and 4.11 for the auto-correlation and cross-correlation interferogram envelopes, respectively. The example in Figure 4.6 shows the interferograms obtained for a spooled fibre in the laboratory. A PMD of 0.149 ps was obtained with the application of Equation 4.12.

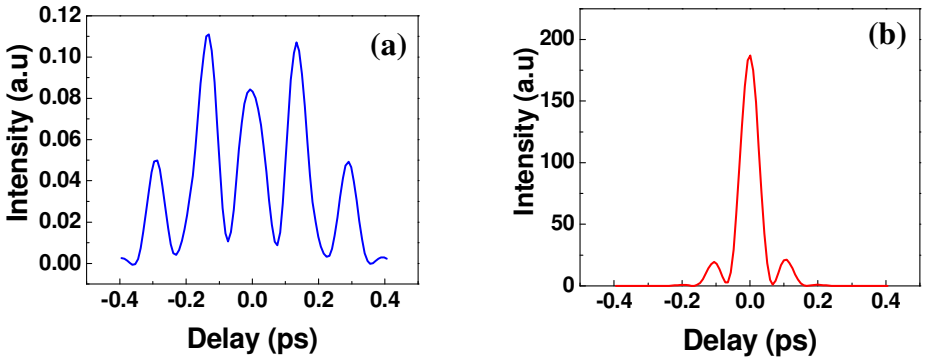

Figure 4.6: Typical squared interferograms separated by the addition and subtraction of the intensities of the two detectors used in the GINTY setup: **(a)** squared cross-correlation and **(b)** squared auto-correlation interferograms.

4.2.4 Scrambling of the light signal

The most important factor that GINTY and TINTY have in common is their dependence on the state of polarization. When measuring PMD with the interferometric techniques it is important to change the SOPs at the input and output of the fibre. PMD is then measured for every state of polarization change, and the mean PMD will approach the true PMD of the fibre. A higher uncertainty is incurred if no polarization scrambling takes place during the measurements with the intereferometric techniques. This uncertainty is procedural, and it arises because the single input and output SOP does not cover most of the regions of the Poincaré sphere. The uncertainty for single scan measurements ($\sigma_{\text{single scan}}$) can be predicted by Equation 4.19,

$$\sigma_{\text{single scan}} = \sqrt{(1-\frac{8}{3\pi})\frac{1}{\sqrt{1+\frac{1}{4}(\frac{\text{PMD}_{\text{mean}}}{\sigma_A})^2}}}, \qquad (4.19)$$

where σ_A is the rms width or the auto-correlation of the light source and PMD_{mean}, the mean PMD from the ensemble of PMD values measured for various SOPs. Polarization scrambling is performed to sample PMD values over an ensemble of random polarisation states [8]. In this study, scrambling was performed with the manual scramblers and the automated Adaptif polarisation controllers (see Section 6.3). The various ways of implementing polarization scrambling during the measurements are outlined below:

Random scrambling method is divided into three different types:

(a) Scan-to- scan

For each interferometer scan the scramblers are independently set differently to produce different states of polarisation. The input/output (I/O) measurement uncertainty (σ) in this case is given by

$$\sigma = \frac{\sigma_{\text{single scan}}}{\sqrt{N}} \tag{4.20}$$

where N is the number of random I/O-SOP pairs [2, 9, 10].

(b) Continuous scrambling

This occurs whilst the interferometer is scanning and is taken into consideration in PMD calculations when the averaging of the square envelope is activated on GINTY. The uncertainty associated with this type of scrambling is calculated with Equation 4.20. This could also be applied with TINTY for single interferometer scans; however, the averaging that occurs of the squared envelopes cannot be implemented with the particular EXFO TINTY instruments used in this study because it measures PMD from the cross-correlation envelope and not the square cross-correlation envelope.

(c) Fast scrambling with a single scan

This can be achieved with the automated scrambler scanning very fast, such that a well scrambled envelope can be observed with only a single scan. In the case of fast scrambling, the uncertainty can be calculated by Equation 4.20 but by substituting σ_A with the equivalent root mean square (rms) σ_{Aeq}, which is calculated as follows,

$$\sigma_{Aeq} \approx \frac{\sigma_A^{\,2}}{1+(\frac{3\sigma}{\sigma_B})^2}, \text{with } \sigma_B = \frac{v}{c}\tau_B \tag{4.21}$$

where v and c are the speeds of the scramblers and light, respectively. The term τ_B is the correlation time of the scramblers, which can be experimentally determined [7].

4.3. References

[1] **N Gisin**, J P Pellaux and J Von der Weid (1991), "Polarisation Mode Dispersion of short and long single-mode fibers", *J. Lightwave Technol.* **9**(7), pp 821-827

[2] Polarisation Mode Measurement for Single-Mode Optical Fibers by Interferometry, TIA/EIA-455-124-A (FOTP-124A), 2004, Telecommunications Industries Association

[3] **T B Gibbon**, A B Conibear and A W R Leitch (2002.), "PMD Measurements Using a Cross-Correlation Interferometry Technique", *in Proc. Of SATNAC*, KwaZulu-Natal, South Africa

[4] **N Gisin**, R Passy, J C Bishoff and B Perny (1993), "Experimental Investigation of the statistical Properties of Polarisation Mode Dispersion in Single Mode Fibers", *IEEE Photon. Technol. Lett.* **5**(7), pp. 819-821

[5] **F Audet**, "PMD: The Interferometry Method", EXFO FTB 5500 Application Note

[6] **D Derickson** (1998), "Fiber Optic Test and Measurement", Prentice Hall, New Jersey, pp. 508 and 510

[7] **N Cyr** (2004), "Generalized Interferometry PMD Measurement Method: Exact Analysis and Traceable Result for any coupling regime", *J. Lightwave Technol.*, **22**(3), pp. 794-805

[8] **M Brodsky** (2003), ""Long Term" PMD characterization of installed fibers-how much time is adequate?" *in Proc. Of OFC,* Vol. 2, pp 515-517

[9] **N Cyr**, B Ruchet, R Roberge and P Cantin (2003), "Interferometry PMD measurement of an Amplified Link", *in Proc. 29th Eur. Conf. Optical Comm.*, Rimini, Italy, paper Mo3.7.6, pp.68-69

[10] **N Cyr**, R Roberge, J Bradley, G Amice, F Audet and G W Schinn (2004), "Interferometry PMD Measurement of a Transatlantic, 5512-km Fiber Link Including 119 EDFAs", *in Proc. Of OFC*, (MF13)

CHAPTER 5

PMD LITERATURE SURVEY

Accuracy in the measurement of polarization mode dispersion is important for system designers to make an informed decision regarding the state of the fibre optic network. This makes long-term assessment of the PMD for a deployed optical network very important. Section 5.1 focuses on the work reported in literature about the long-term monitoring of PMD. Section 5.2 presents a review of some of the investigations in literature performed with the interferometric techniques.

5.1 Studies on long-term monitoring of PMD

Long-term monitoring of PMD is very important in the determination of the true mean PMD of the fibre. Results for such measurements are presented in Chapter 7 (Section 7.4). Allen *et al.* (2003) [1] and Nellen *et al.* (2004) [2] showed that accurate determination of PMD can help in predictions of the outage probabilities of the network with good accuracy.

Nespola *et al.* (2004) [3] and Cameron *et al.* (1999) [4] have reported on the time evolution of PMD for installed aerial and buried fibre cables. Their studies showed that PMD fluctuates more rapidly for aerial cables than for buried cables. This was in agreement with our studies on buried and aerial cables. The results of our studies are presented in Section 7.4 as mentioned above.

Brodsky *et al.* (2004) [5] performed an investigation with the interferometric technique to determine how much time is required to characterize and measure the true mean PMD of the fibre with a good accuracy. Their studies were conducted on a buried cable with single mode fibres. The results showed that long-term PMD measurements do not necessarily improve the accuracy of the measurements. A short time (about a week) is

required to characterize a fibre that is exposed to environmental changes (such as aerial fibres) while longer time (more than a year) is required to characterize a fibre that is deployed underground and not exposed to many environmental changes. Cyr (2004) [6] showed that a lot of time can be saved if polarization scrambling is applied with the interferometric technique during long-term monitoring. This is in agreement with the results from our studies presented in Chapters 8 and 9.

Allen *et al.* (2003) [1] reported on the study of time and spectral measurements of DGD on a 95 km of buried single mode fibre over a 86 day period to determine the distribution and rate of change of high DGD events. The results showed that DGD does not vary rapidly with time while, on the other hand, it varies rapidly with wavelength.

Nellen *et al.* (2004) [2] reported that long-term PMD measurement results correlate with changes in weather conditions. Measurements also showed that DGDs at a specific wavelength have a Maxwellian distribution. This has also been reported by Curti *et al.* (1990) [7], Poole *et al.* (1991) [8] and Gisin *et al.* (1991) [9].

5.2 PMD studies with the interferometric techniques

The interferometric PMD measurement technique is the main method used in the field for the characterization of PMD of the deployed optical fibres. The interferometric method is tolerant to the movement along the fibre during measurements; and movement changes the details of the interferogram but not the overall shape [10]. Details about this technique are presented in Chapter 4.

Gisin *et al.* (1991) [11] reported on some of the earliest measurements of PMD with the interferometric techniques. PMD measurements were done on short and long single mode fibres at wavelength of 1300 nm. The technique was implemented with interferometer scan range of 0.1 to 80 ps. The study showed at the time that some standard single mode fibres have relatively high PMD due to the accidental birefringence introduced during manufacturing. Furthermore, the study further introduced a statistical model that showed

that in long birefringent fibre PMD increases with the square-root of the fibre length. For short fibres with low mode coupling, however, PMD increases linearly with the fibre length. This was in agreement with the studies by Curti *et al.* (1990) [7] and Poole *et al.* (1988) [12].

Gisin *et al.* (1994) [13] subsequently reported on a study of the comparison between the interferometric and the fixed analyzer techniques. The study showed that the interferometric technique provide the same information as the fixed analyzer technique. The spectral information of the fixed analyzer technique for the high and low mode coupled fibres was collected and Fourier transformed. PMD in the time-domain by the application of the Gaussian fit on the transformed fixed analyzer data agreed very well with the interferometric measurements. The measurements agreed within an accuracy of 0.1 ps when using the same fitting procedure.

Heffner *et al.* (1995) [14] presented a theoretical study which showed that for a fibre with high mode coupling, PMD measured with the interferometric technique depends on the bandwidth and the spectral shape of the light source used. It was further shown that the results from the Jones Matrix Eigeanalysis (JME) and the wavelength scanning methods may be considered to be independent of the optical source spectrum used (see Chapter 3, Section 3.3.1).

De Faria *et al.* (2006) [15] carried out a study on a 924 km long-haul backbone optical ground wire cabled fibre installed in Brazil. PMD measurements were made before and after deployment. The results showed that floor sensitivity of the instrument (0.08 ps) can give incorrect readings of the fibre PMD. Furthermore, it was shown that there was variation in PMD between factory and field measurements. It was mentioned that field measurements are an essential part of the cable qualification. Oberson *et al.* (1997) [16] showed that the floor sensitivity of the technique is the result of the coherence time of the source. Their studies with an interferometric technique improved the sensitivity to about 10 fs for an LED source with bandwidth of about $\Delta\lambda$=100 ps, showing the independence of measurements on the coherence time of the light source used.

The improvement of the interferometric technique was reported by Cyr (2004) [6]. The set-up is called the generalized interferometric technique, and it eliminates all the assumptions made regarding the spectral shape of the source spectrum, interferogram and mode coupling of the fibres under test. This technique was presented in Chapter 4 and it was used in the measurements of some of the results presented in Chapters 7 and 8. The technique is used in combination with polarization scrambling to increase the accuracy of the PMD measurements. Cyr *et al.* (2003) [17] reported PMD measurement results from a 5512 km fibre link including 119 erbium doped amplifiers (EDFAs). The uncertainties of the measurements were in agreement with the theoretical uncertainties predicted by Cyr (2004) [6].

5.3 References

[1] **C T Allen**, P K Kondamuri, D L Richards and D Hague (2003), "Measured Temporal and Spectral PMD Characteristics for Network-Level Mitigation Approaches", *J. Lightwave Technol.*, **21**(1), pp 79-86

[2] **P M Nellen**, R Brönnimann, M Held, and U Sennhauser (2004), "Long-Term Monitoring of Polarization-Mode Dispersion of Aerial Optical Cables With Respect to Line Availability", *J. Lightwave Technol.*, **22**(8), pp. 1848-1855

[3] **A Nespola** and S Abrate (2005), **"**Long-term PMD characterization of installed G.652 fibers in a metropolitan network"**,** *Proc. Optical Fiber Communication Conference*, Aneheim, California, USA, Mar. 2005, **3**, pp. 3

[4] **J Cameron**, L Chen, X Bao and J Stears (1998), "Time evolution of Polarization Mode Dispersion in Optical Fibres", *IEEE Photon. Technol. Lett*. **10**(9), pp. 1265-1267

[5] **M Brodsky**, P Magill and N J Frigo (2004), ""Long-term" PMD characterization of installed fibers-how much time is adequate?", *Proc. Optical Fibre Conference*, Los Angeles, California, USA, Feb. 2004, **2**, pp 515-517

[6] **N Cyr (2004),** "Generalized Interferometric PMD Measurement Method: Exact Analysis and Traceable Result for any coupling regime", *J. Lightwave Technol.*, **22**(3), pp 794-805

[7] **F Curti**, B Daino, G de Marchis and F Matera (1990), "Statistical Treatment of the Evolution of the Principal States of Polarization in Single-Mode Fibers", *IEEE J. Lightwave Technol.*, **8**(8), pp.1162-1166

[8] **C D Poole**, J H winters and J A Nagel (1991), "Dynamical Equation for Polarization Dispersion", *Opt. Lett.*, **16**(6), pp. 372-374

[9] **N Gisin (1991),** "Solutions of the dynamical equation for polarization mode dispersion", Opt. Commun., **86**, pp. 371-373

[10] **D Derickson** and P. Hernday (1998), "Fiber Optic Test and Measurement", Prentice Hall, New Jersey, pp.511

[11] **N Gisin**, J Von der Weid, and J Pellaux (1991), "Polarization Mode Dispersion of Short and Long Single-Mode Fibers", *J. Lightwave Technol.*, **9**(7), pp. 821-827

[12] **C D Poole (1988),** "Statistical treatment of polarization mode dispersion in single mode fiber", *Opt. Lett.*, **13(8)**, pp. 687-689

[13] **G Gisin**, R Passy, and J P Von der Weid (1994), "Definitions and Measurements of Polarization Mode Dispersion: Interferometeric Versus Fixed Analyzer Methods", *IEEE Photon. Technol. Lett.*, **6**(6), pp. 730-732

[14] **B L Heffner (1995),** "Influence of Optical Source Characteristics Upon Measurement of Polarization of Highly Mode-Coupled Fibers", *Opt. Lett.*, 21(2), pp. 113-115

[15] **G V de Faria**, M R Jimenez, and J P von der Weid (2006), "PMD Variations From Factory to Field in OPGW Cabled Fibers", *IEEE Photon. Lett.*, **18**(1), pp. 250-252

[16] **P Oberson**, K Julliard, N Gisin, R Passy, and J P von der Weid (1997), "Interferometric Polarization Mode Dispersion with Femtosecond Sensitivity", *J. Lightwave Technol.*, **15**(10), pp. 1852-1857

[17] **N Cyr**, B Ruchet, R Roberge and P Cantin (2003), "Interferometric PMD–Measurement of an Amplified Link", *Proc. ECOC*, Rimini, Italy (Mo3.7.6), Sept.

CHAPTER 6

EXPERIMENTAL INSTRUMENTATION

In this study, optical fibres were characterized in terms of Chromatic Dispersion (CD) and Polarization Mode Dispersion (PMD). This chapter presents the experimental techniques that were used for field and laboratory characterization of dispersion in optical fibres. The FTB 5500 and 5500B PMD analyzers were used for PMD characterization, and the FTB 5800 was used for CD characterization. In addition, this chapter describes some of the other instruments used with PMD and CD analyzers, such as the light sources, polarization scramblers.

6.1 Interferometric PMD analyzers

The interferometric PMD analyzer systems used for the investigations in Chapters 7 and 8 were the EXFO FTB-5500 (TINTY) and 5500B (GINTY). These techniques comply with PMD standards compiled by the international telecommunication associations [1, 2]. The theory of the mathematical principles on which these systems are based is given in Sections 4.1 and 4.2. The EXFO FTB-5500 and 5500B are each compactly packaged inside a module. The module is inserted into one of the EXFO FTB-400 platform module slots. The EXFO FTB-400 and a typical PMD module are shown in Figure 6.1.

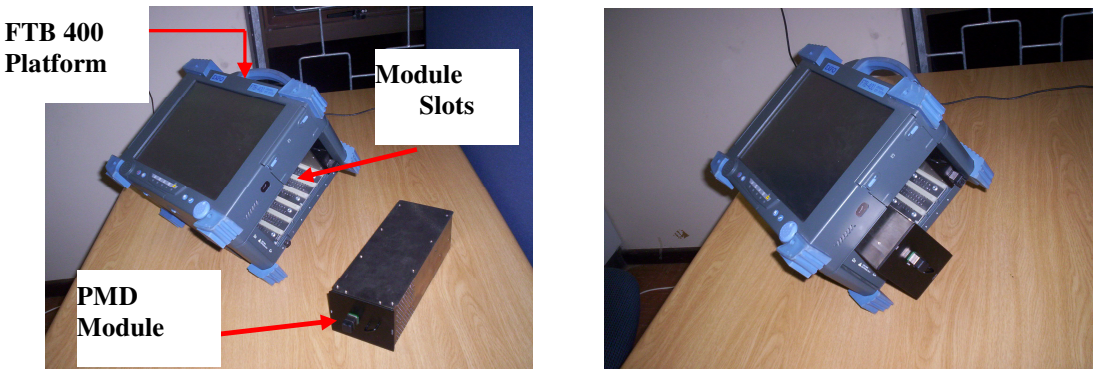

Figure 6.1: FTB 400 Platform and the PMD 5500 analyzer module.

The module comprises a Michelson interferometer, an analyzer and detector(s). The FTB-5500 has one detector, on the other hand, FTB-5500B has two detectors. The FTB 5500B has an additional beam splitter added at the interferometer output for the separation of light into two orthogonal polarizations states, and consequently two interferograms analyzed. Figure 6.2 shows the interior of the FTB 5500B module. The theoretical aspects of interferometery measurement techniques are presented in Chapter 4. Typical set-ups for the application of Generalised Interferometry (GINTY) and Traditional Interferometry (TINTY) is shown and described in Section 8.1.

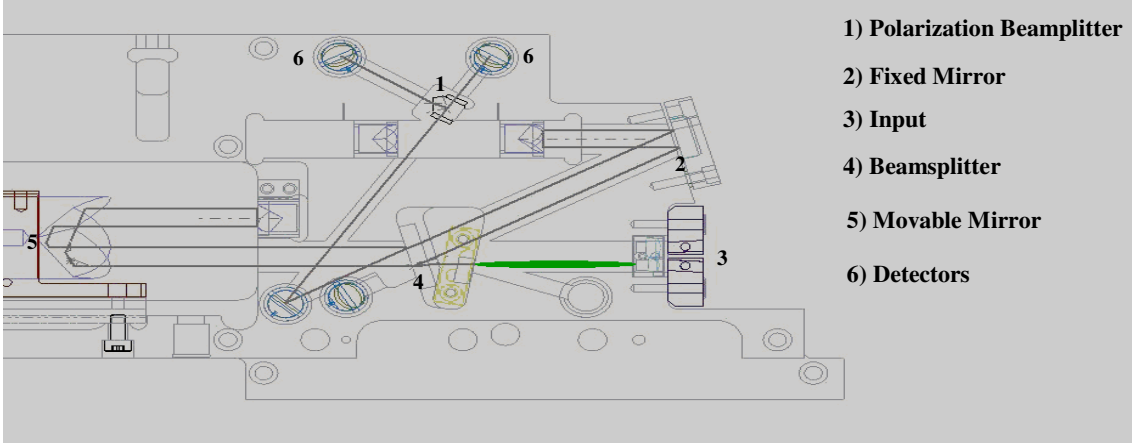

Figure 6.2: The internal structure of the PMD 5500B module with the Michelson interferometer, polarization beamsplitter and two detectors (after EXFO).

6.2 Chromatic Dispersion Analyzer

Characterization of the deployed buried fibres for chromatic dispersion (CD) in Pretoria (see Section 7.2.2) was carried out with the EXFO FTB 5800 CD analyzer module. The module uses the phase-shift technique to measure CD. This is also standardized by the telecommunication association [3]. Typical setup using the phase-shift technique for the measurements of CD is shown in Figure 6.3.

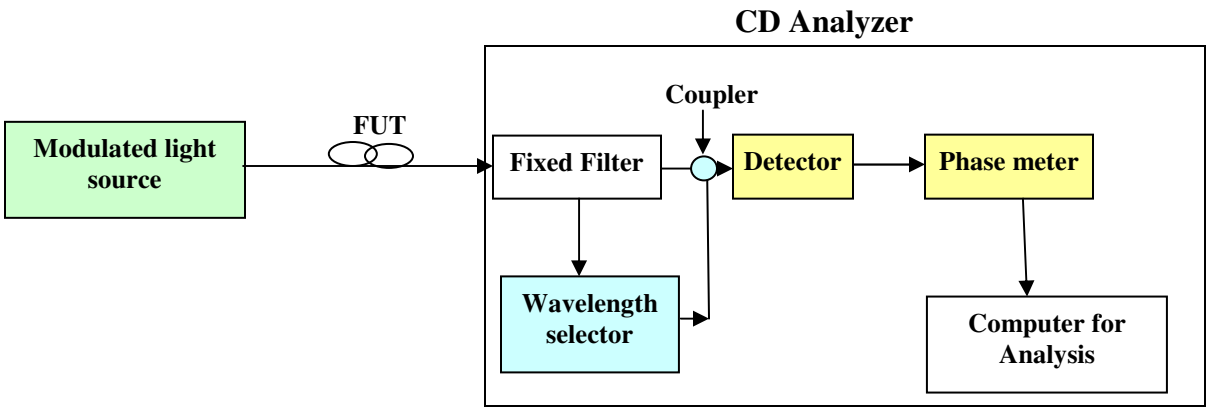

Figure 6.3: A typical setup of the phase-shift method used in the study to measure Chromatic dispersion in the buried deployed fibres.

The fixed filter sets the reference wavelength and the wavelength selector selects a wavelength whose phase is compared to that of the reference wavelength. The phase meter detects the difference in phase between the reference and chosen wavelength. The interval between the selected wavelengths was 2 nm. The phase difference between the wavelengths is translated into relative group delay using the equation below,

$$\tau_g = \frac{\Delta\phi}{f}, \qquad 6.1$$

where τ is the relative group delay between the reference and selected wavelength, $\Delta\phi$ the phase difference and f represents the frequency of modulation of the light source. A graph of group delay versus wavelength is plotted for all the wavelengths within the spectral width of the light source. Equation 6.2 below (the Sellmeire equation) is then fitted to the $\tau_g(\lambda)$ data, and its derivative gives CD in $ps.nm^{-1}$ for the fibre under study. The equation for the relative group delay τ_g is given by,

$$\tau_g = A + B\lambda^{-2} + C\lambda^{2}, \qquad 6.2$$

where A, B, and C are the Sellmeier coefficients determined experimentally, and λ is the wavelength [4].

6.3 Polarization Controllers

Polarization controllers were a necessity for all the investigations reported in Chapter 8. Scan-to-scan polarization scrambling at the input and output of an optical fibre link under test was implemented with the Adaptif A3200 polarization scramblers. This was performed to observe the variation of PMD (measured with INTY) with input and output polarization scrambling described in Section 8.1. A manual scrambling was implemented between the optical fibre links in the study of PMD variation with the change in mode coupling and states of polarization described in Section 8.2. The two types of polarization controlling methods are described in the sections below.

6.3.1 Manual Polarization Scrambler/Controller

For the study described in Chapter 8, manual and automatic polarization scramblers was placed at an intermediate point on the cabled fibre link to change mode coupling of the fibre. A manual polarization scrambler specially designed and built for the investigation of the effect of mode coupling on PMD of the deployed fibres is described as follows: a $10\,\text{cm}\times10\,\text{cm}\times10\,\text{cm}$ cube was made out of perspex with an open top and a fibre wound on a bobbin of 10cm diameter as shown in Figure 6.4. Rotation of the cube changes state of polarization of the light that passes through it and thus mode coupling.

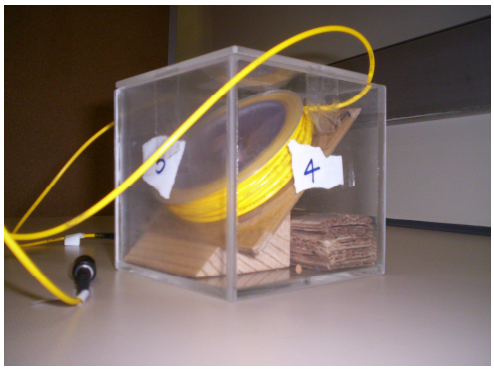

Figure 6.4: The manual scramblers used in the study of the distribution PMD measured with GINTY and TINTY and how the PMD changes with the SOPs of the light signal in the fibre.

Initially, the bobbin is placed parallel to one of the cube faces, for example, a face labelled 2 and the cube at 0º rotation reference line as shown in Figure 6.5. The cube was then rotated clockwise four times without repeating any rotation with face 5 downward and the cube at 0º reference line. Face 4 was then put downward and four clockwise rotations were done without any repetition with the cube at 0º to the rotation reference line. The same procedure above was followed with face 3, 2, 1 and 6 down, and the cube at 0º rotation reference line. In total 24 rotations were made with the fibre loop parallel to face 2 and the cube at 0^0 reference line. Each cube rotation changed the SOP of the output, and measurements were performed for every rotation.

Next, the cube was placed at the 45º reference line and the fibre loop still parallel to face 2. Face 5 was put down and 4 clockwise rotations made with the cube at 45º rotation reference line. This same procedure was followed with face 4, 3, 2, 1 and 6 down and the cube at 45º to the rotation reference line. In total 24 rotations were made with the cube at 45º to the rotation reference line and the fibre loop parallel to the cube.

After exhausting all the possible rotations with the fibre loop parallel to face 2, the orientation of the loop was changed to 45º with respect to face 2. A cube was placed at 0º rotation reference line with face 5 down, and subsequently, 4 rotations without any repetition were made. The same procedure was followed with face 4, 3, 2, 1 and 6 down and the cube at 0º at the rotation reference line. A total of 24 rotations without repetition were made with the cube at 0º to the rotation reference line and the fibre at 45º to face 2.

Finally, the cube was placed at 45º to the rotation reference line with the fibre loop still at 45º to face 2. As before, face 5 was first put down and 4 rotations were made without repetitions. Face 4, 3, 2, 1 and 6 were put down and non repeatable rotations were made. A total of 24 rotations without repetitions were then made. The total number of rotations that a cube allows with the 2 orientations of the fibre and the rotation reference line is 96.

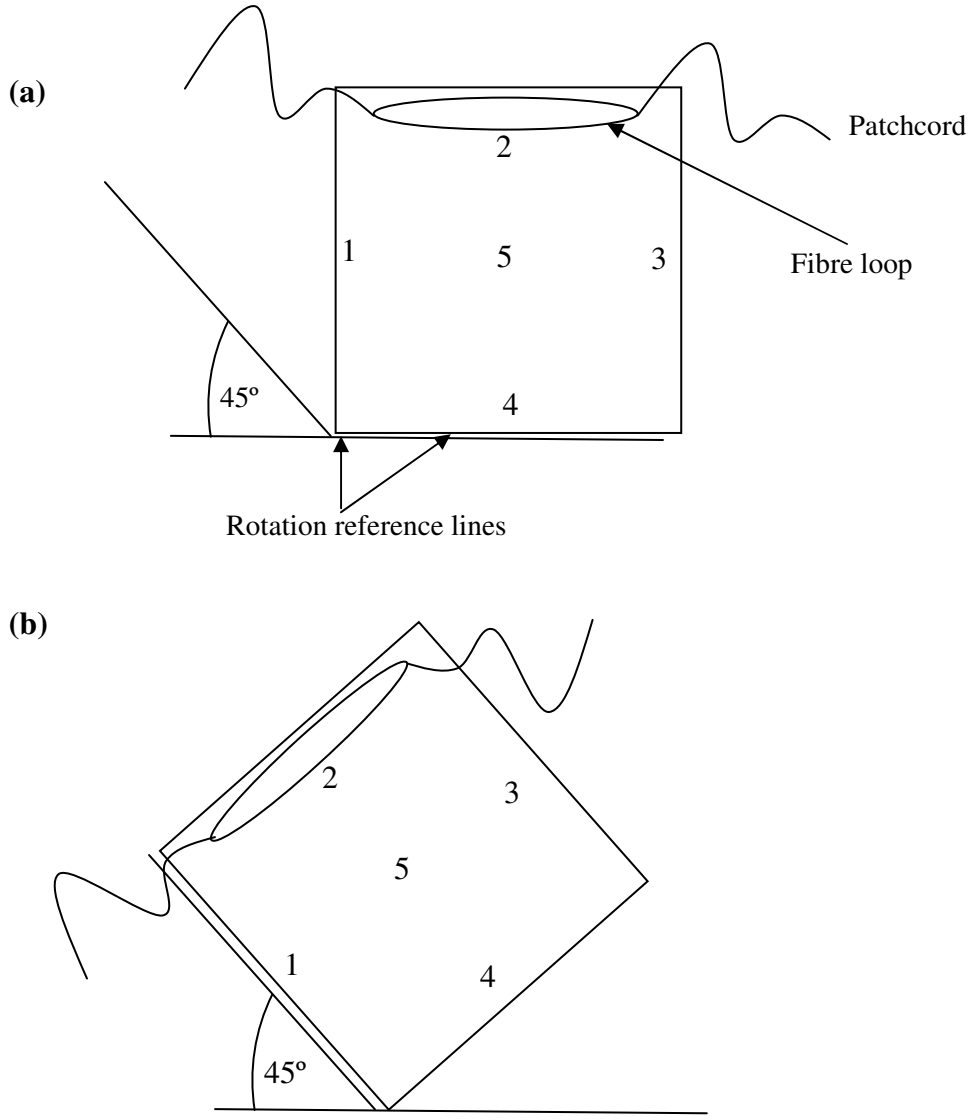

Figure 6.5: a) The top view (through face 6) of the manual polarization controller at the rotation reference line of 0º with the fibre loop parallel to face 2. **b)** The manual polarization controller at the rotation reference line of 45º with the fibre loop parallel to face 2 (Top View-face 6).

6.3.2 Automated Polarization Controller/Scrambler

The Adaptif Photonics A3200 Polarization controllers were used in the study for the results reported in Chapter 8 to change the SOPs of the light signal at the input and output of the fibre under test. The A3200 Polarization controller uses a $LiNbO_3$ crystal to control the SOP of the input light signal. The $LiNbO_3$ crystal works like a series of five endlessly rotatable waveplates as shown in Figure 6.6.

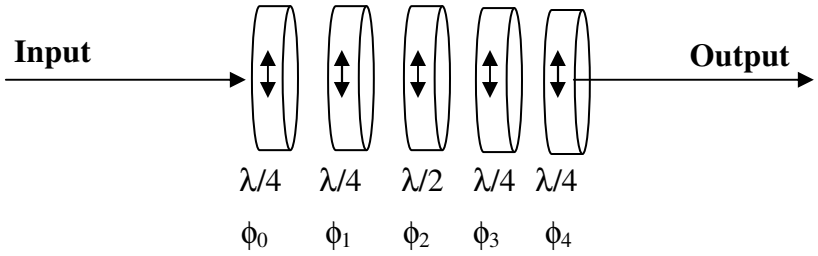

Figure 6.6: A series of waveplates equivalent to a $LiNbO_3$ crystal implemented with the A3200.

In Figure 6.6, the SOP of the light passing through the waveplates is determined by the position of the waveplates expressed in terms of the angles ϕ_0 to ϕ_4. The SOP remains unchanged for the rotation through 2π. The polarization of the input light signal can be changed manually (hence using it as a manual polarization controller), or automatically. Automation is implemented by means of a look up table stored in the memory of the instrument and it can be processed once or repeatedly at different clock rates [5].

In this study, software provided with the instrument was used to control the polarization state automatically. The section below discusses the broadband light sources that were used with the PMD analyzers and polarization controllers discussed above.

6.4 Optical Spectrum Analyzer

The Agilent 86140B series optical spectrum analyzer (OSA) was used to measure the spectrum of the light sources. The power (in dBm) of the light source producing the spectrum is measured as a function of wavelength (in nm). Figure 6.9 shows the Agilent 86140B series OSA used in the research.

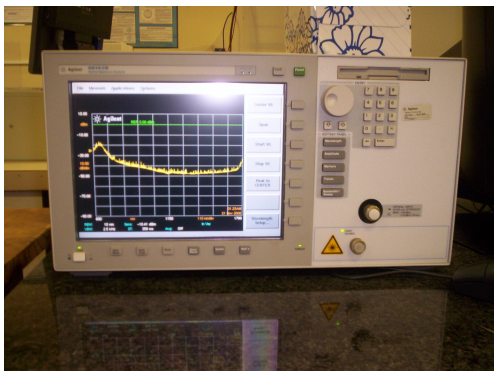

Figure 6.8: The Agilent 86140B series optical spectrum analyzer.

Measurements of the optical spectrum are done by connecting the output of the light source with the input of the OSA. Consequently, the spectrum obtained would be that of the light source; this is displayed on the screen of the OSA. The noise on the traces was smoothed out with the OSA's averaging over the spectral traces.

6.4 Light Sources

This study made use of two light sources, namely, EXFO FLS-5800 and M2100. Field measurements reported in Section 7.2 were conducted with the use of the EXFO M2100 broadband light source and TINTY. The light source has a variable power output and peak wavelength at 1545 nm. Figure 6.9 shows the M2100 source spectrum.

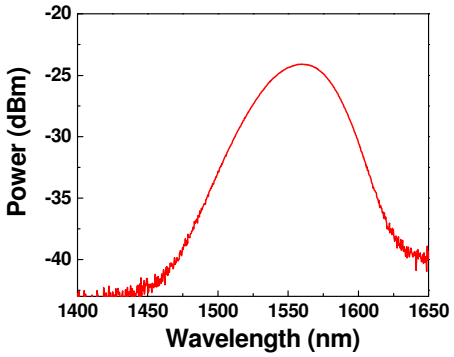

Figure 6.9: The EXFO M2100 light source with peak wavelength at around 1545 nm.

The EXFO FLS-5800 is equipped with the different wavelength bands, namely, C (1530-1565 nm), L (1565-1625 nm) and C+L (1530-1625 nm). In this study, the C+L band was used with GINTY, TINTY and FTB 5800 for the experiments performed in the field on deployed optical fibres. The results of the investigations are presented in Section 7.2 and Chapter 8. For the investigations in the Fibre Optics Laboratory at the Nelson Mandela Metropolitan University (NMMU), the C and C+L bands of the FLS 5800 light source were used. Figure 6.10 depicts the FLS 5800 light source and the spectra of the wavelength bands mentioned above. This source has 4 dBm power output and is invariable in all the wavelength bands.

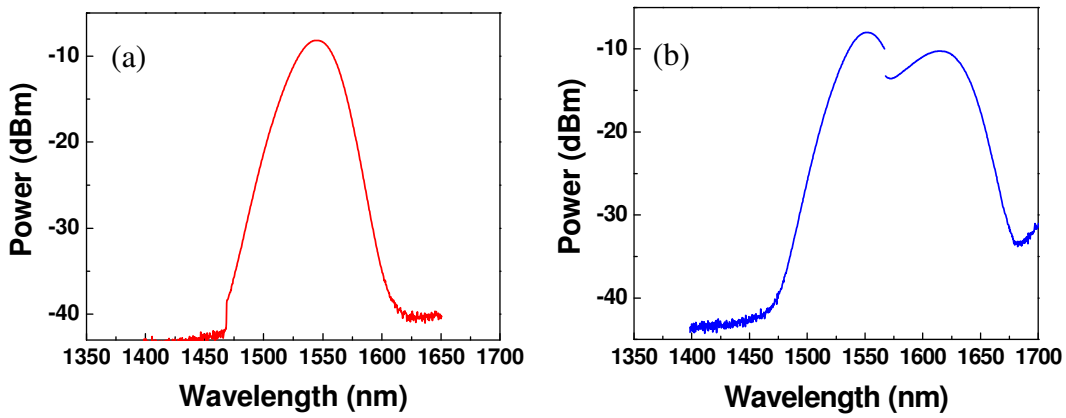

Figure 6.9: The spectra of the FLS-5800 light source that was used in the study: (a) C and (b) C+L band spectra.

6.5 References

[1] Polarisation Mode Measurement for Single-Mode Optical Fibers by Interferometry, TIA/EIA-455-124-A (FOTP-124A), 2004, Telecommunications Industries Association

[2] Definitions and test methods for statistical and non-linear related attributes of single-mode fibre and cable, ITU-T standards G.650.2 (2005), International Telecommunications Union

[3] Chromatic Dispersion of single mode optical fibers by the phase-shift method, TIA/EIA Standard FOTP-169,(1992), Telecommunications Industries Association

[4] **B Costa**, D Mazzoni, M Puleo and E Vezzoni (1982), "Phase shift technique for the measurement of chromatic dispersion in optical fibers using LED's", *IEEE J. of Quan. Electr.*, **18**(10), pp. 1509-1514

[5] Adaptif Photonic User Guide Rev. 1.3 for A1XXX/A2XXX/A3XXX, Adaptif Photonics GmbH, pp. 14-25

CHAPTER 7

UPGRADEABILITY OF DEPLOYED OPTICAL FIBRE NETWORKS IN SOUTH AFRICA

Polarization mode dispersion (PMD) and chromatic dispersion (CD) are major obstacles for high bit rate transmission systems. Characterization of optical fibres for PMD and CD in the field is a very important step towards an upgrade and maintenance of telecommunication networks to ensure that they are suitable for higher transmission speeds. Characterization of optical fibres for PMD is a particular challenge as it varies statistically with time. CD, on the other hand, is relatively easy to characterize as it does not vary statistically with time.

In this Chapter, PMD and CD measurements were conducted on two deployed optical fibre networks in order to determine the upgradeability from 2.5 to 10 $Gb.s^{-1}$. Interferometric techniques and the phase-shift methods were used to characterize the deployed fibres mentioned above for PMD and CD, respectively.

PMD and CD results from the investigations on a metropolitan telecommunication link in Gauteng, Pretoria, are presented. Furthermore, the results for the characterization of aerial fibres in the Northern and Eastern Cape are presented in Sections 7.2 and 7.3. Long-term monitoring of PMD on buried and aerial fibres are discussed in Section 7.4, in order to give an indication of the timescales over which PMD changes for the various deployment configurations.

7.1 Issues relating to PMD and upgradeability of optical networks

Telkom, the South African national operator, use a Time Division Multiplexing (TDM) system to transmit data, and it is transmitted as pulses in a series of 1's and 0's (binary system). The detector detects these pulses by comparing the detector voltage to some threshold voltage. Dispersion in the fibre causes a spreading of the pulses, which might lead to inter-symbol interference and the detector subsequently not being able to differentiate between the different pulses. Consequently, the bit-error-rate (BER) would be high in the system. BER is the ratio of the bits received in error to the total number of bits received.

At low bit-rates the bit periods are large, so high PMD values do not affect the BER so much as at high bit-rates where the bit period is short. In the design of a telecommunication system, standards were set so that the acceptable limit in the system must be 10 % of the bit period [1]. Table 7.1 shows the limit on the amount of PMD acceptable for a few transmission rates, and assuming a transmission length of 400 km.

Table 7.1: Transmission speeds and the maximum PMD limits for 400 km span.

Bit rates ($Gb.s^{-1}$)	**Bit Period (ps)**	**Max. PMD (ps)**	**PMD Coeffecient ($ps.km^{-1/2}$)**
2.5	400	40.0	2.00
10	100	10.0	0.50
40	25	2.5	0.125

Before an upgrade can be carried out, the PMD of the existing fibres must be measured to find out if they can be used at the envisaged higher bit-rates. Sections 7.2 and 7.3 give tests for upgradeability of the buried metropolitan and aerial cables, respectively.

7.2 Upgradeability of the Pretoria Network[1]

A metropolitan ring network in Pretoria, Gauteng, was earmarked by Telkom for an upgrade from 2.5 to 10 $Gb.s^{-1}$. PMD on this link was measured using GINTY, the technique described in Chapter 4. The schematic of the network is shown in Figure 7.1. For the tests, the network ring consisting of underground loose tube cables was divided into five sections. The division was necessary because the light signal was not intense enough to travel through the entire loop network. On each of the sections on the link (Figure 7.1), four fibres were available for testing, and in total, 20 fibres on the network were tested. The labels in the ellipses are used by Telkom to identify their transmission centres. The total length of the network ring was 51.524 km.

EXFO FLS 5800 C+L (1530 to 1625 nm) broadband polarized light source was used with GINTY for these tests. Note that these tests were conducted without polarization scrambling the input or output states of polarization (SOPs). It has been shown that polarization scrambling of the input and output SOP is essential, especially for the interferometric techniques since measurements of PMD with interferometric techniques depend on the SOPs of the light signal [2].

Polarization scrambling is time consuming to implement, compared with simply taking an average of a few measurements. It also adds a further level of complexity to the experiment. In this case the objective was a quick overview, and since the necessary equipment was not readily available, no scrambling was carried out. Chapter 4 discusses polarization scrambling in more detail. This will be illustrated experimentally in Section 8.1. In this instance, no polarization scrambling will imply a larger uncertainty in the measured PMD value.

[1] The author would like to thank **Mr Chris Nel** of Lambda Test and Equipment c.c for his guidance and assistance during the tests.

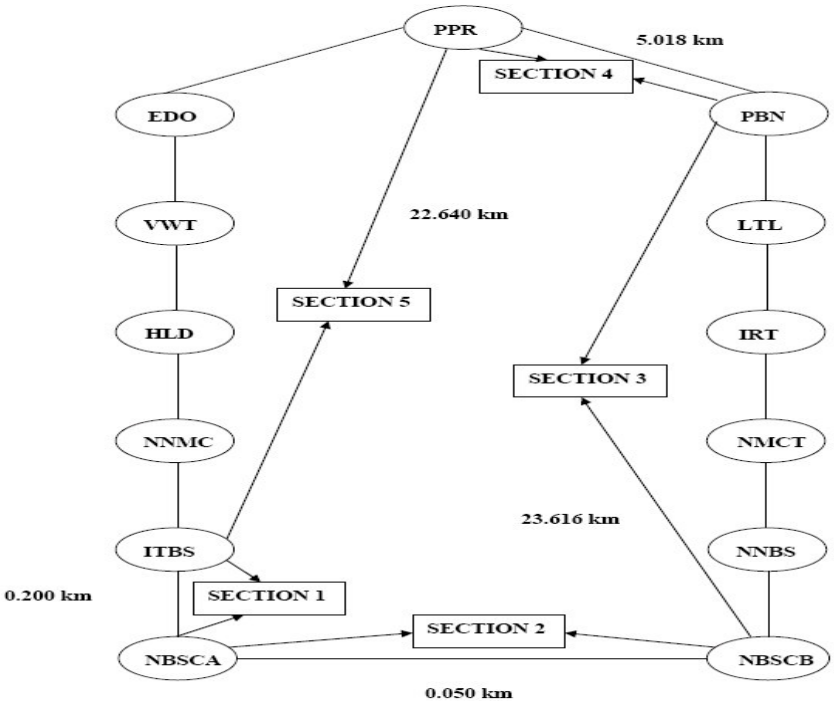

Figure 7.1: Schematic of the Telkom Metropolitan Network in Pretoria on which PMD tests were conducted. The different sections and their respective lengths are also shown (not to scale).

7.2.1 PMD measurements

Ten consecutive PMD measurements were taken. PMD of the fibre was then recorded as the mean of the 10 measurements. The results for each cable section are shown in Table 7.2(a). Calculations and discussion of the uncertainty ranges were presented in Section 4.2.4. All fibres in the individual sections were in the same cable. Section 1 had the shortest length and lowest PMD values. Section 3, on the other hand, is the longest and has the highest PMD values. This observation is consistent with the study by *Gisin et al* (1991) [3] which showed that PMD accumulates with the transmission distance. Total PMD of the concatenated fibres in the network is given by,

$$PMD_{total} = \sqrt{\sum_{i}^{5} PMD_i^{\,2}}\ , \qquad 7.1$$

where PMD_i is PMD of the ith section of the network [2]. Table 7.2(b) gives the total PMD for the entire ring network.

Table 7.2(a): Summary of the mean PMD values measured using GINTY for the five sections of the metropolitan ring network in Pretoria.

Fibre No.	**PMD_{mean} (ps)**				
	Section 1 (0.200km)	*Section 2 (0.050km)*	*Section 3 (23.616km)*	*Section 4 (5.018km)*	*Section 5 (22.640km)*
1	0.030 ± 0.083	0.057 ± 0.022	5.230 ± 0.371	0.151 ± 0.051	2.045 ± 0.232
2	0.049 ± 0.110	0.065 ± 0.024	5.280 ± 0.373	0.216 ± 0.067	2.053 ± 0.232
3	0.079 ± 0.030	0.131 ± 0.045	6.497 ± 0.414	0.227 ± 0.069	3.182 ±0.289
4	0.109 ± 0.039	0.167 ± 0.017	7.771 ± 0.453	2.851 ± 0.274	4.428 ± 0.336

Table 7.2(b): Total PMD of the network

Fibre No.	**Total PMD (ps)**	**PMD Coefficient ($ps.km^{-1/2}$)**
1	5.618 ± 0.439	0.783
2	5.670 ± 0.446	0.790
3	7.230 ± 0.513	1.007
4	9.380 ± 0.467	1.307

The mean PMD coefficients for each of the fibres tested in the network are shown in Figure 7.2. For the design of optical fibre systems, the PMD of the fibre must be 10% of the bit period, and the PMD must be less than the tolerable PMD specified in the telecommunication standards, as was mentioned in Section 7.1 [1]. The threshold PMD coefficients in Table 7.1 were used as the reference to determine the upgradeability of fibres in the network.

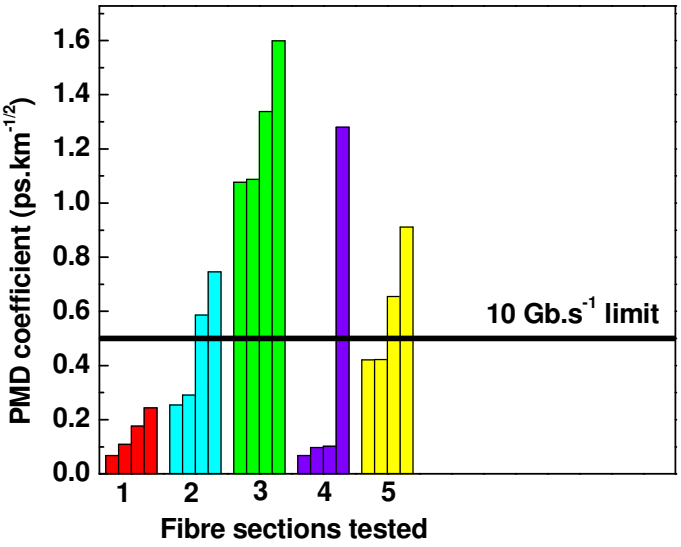

Figure 7.2: The average PMD from 10 consecutive measurements of the four fibre links and the limit for 10 Gb.s^{-1} data transmission rate.

It can be observed on the figure above that all the fibres in section 1 are upgradeable to 10 Gb.s^{-1}. In section 3, however, no fibre can be upgraded to 10 Gb.s^{-1}. The number of fibres upgradeable to 10 Gb.s^{1} in section 2, 4 and 5 of the network are 2, 3 and 2, respectively. Section 3 is the dominant contributor to the overall PMD of the network. In Table 7.2(b) it can be observed that none of the cable loops measured would be suitable for 10 Gb.s^{-1} transmission speeds, since the PMD coefficients all exceed the maximum allowed for transmission at 10 Gb.s^{-1}.

There are several solutions that Telkom can consider in order to transmit their signal successfully at 10 Gb.s^{-1}. In the case of the network that was tested, one of the solutions would be to test all the fibres in the cable and find out if other fibres in the same cable have PMD lower than the maximum tolerable PMD (some of the fibres in the cables were not tested because they were carrying data traffic). If all the fibres in the cable have PMD greater than the tolerable maximum PMD (as in section 3 of the link) then the cable should be replaced. Another method that may be considered is the regeneration of the optical signal at a point on the link where the PMD approach an intolerable level. Polarization mode dispersion compensators can also be applied at the detector. Another

method that may be considered is the error-correction-codes which reduce the data payload in exchange for a marginal gain in PMD [4].

7.2.2 Chromatic dispersion measurements

The phase-shift technique (described in Chapter 6) was used to measure the chromatic dispersion (CD) in the Pretoria metropolitan optical fibre network (see Figure 7.1). The apparatus used in the tests were the EXFO FLS 5800 light source, 1530 to 1625 nm, at one end of a cable section, and an EXFO FTB 5800 chromatic dispersion analyzer at the opposite end of the cable section. In total 20 fibres were tested on the loop, and for each section, four fibres were tested.

The phase-shift method measures the phase difference between the reference wavelength and the selected wavelength, and converts it to a relative group delay (RGD). The points for RGD of the wavelengths in the C+L band are then plotted. The Sellmeier equation, expressing delay dependence on wavelength, is fitted to the points and its differential gives the fibre CD [5]. The RGD in this study were measured at 2 nm wavelength intervals. A typical result for the RGD, fitted RGD and resulting dispersion is shown in Figure 7.3.

It can be observed on the plot that the RGD increases with wavelength. Furthermore, since the Sellmeier equation is quadratic, its derivative (CD), is linear; CD is higher at longer wavelengths than at the shorter wavelengths. This is the case because, for the standard single mode fibres, the wavelengths around the 1550 nm transmission window are in the positive dispersion region; and the region is characterized by longer wavelengths travelling slower than the shorter wavelengths.

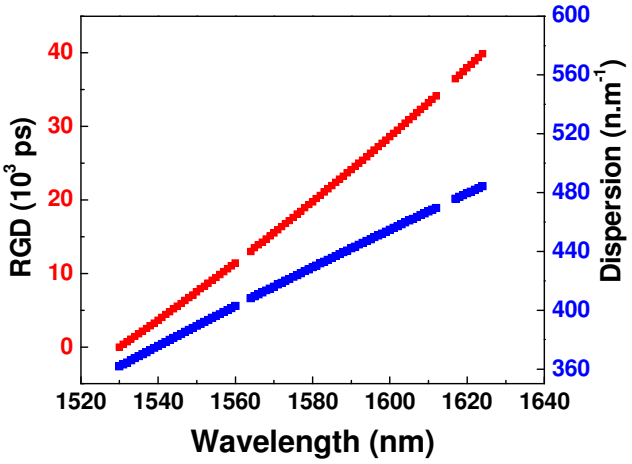

Figure 7.3: Relative group delay, fitted relative group delay and dispersion for a section of a metropolitan link in Pretoria (Section 3 of the link).

A summary of CD results for the fibres in the loop at transmission wavelengths of 1550 and 1620 nm are presented in Tables 7.3. This wavelength range was selected since future wavelength division multiplexing (WDM) systems considered for implementation will be within this range.

Table 7.3: Summary of chromatic dispersion measured in the metropolitan ring network in Pretoria, for the transmission wavelengths at1550nm and 1620nm.

Link Details		**Chromatic Dispersion (ps.nm^{-1})**	
Ring sections	*Length (km)*	*1550 nm*	*1620 nm*
1	0.200	3.6	468.8
2	0.050	0.6	0.8
3	23.616	392.1	482.9
4	5.018	81.0	99.7
5	22.640	381.0	468.8
RING TOTAL	**51.524**	**858.3**	**1056.7**

In Table 7.3, it can be observed that CD increases with the fibre length, as expected. The highest CD measured during the test was in section 3, and the lowest CD measured was in

section 2. CD affects the bandwidth capacity of the single mode fibres, hence the maximum acceptable levels of CD are specified for a given transmission rate. For a 1dB power penalty, the maximum dispersion and link lengths are as indicated in Table 7.4. The maximum distance is calculated for a dispersion coefficient of 17 ps.(nm.km)$^{-1}$, a nominal value applicable to 1550 nm transmission, for standard single mode fibre [6].

Table 7.4: Chromatic dispersion and link length limits for a 1 dB power penalty.

Bit rates (Gb.s^{-1})	2.5	10	40
Max. Dispersion (ps.nm^{-1})	16000	1000	63
Max. link length (km)	941	59	4

The maximum tolerable dispersion is higher at 2.5 Gb.s^{-1} transmission rates, and this implies longer maximum transmission distance of 941 km. At 10 Gb.s^{-1} transmission speed, however, the maximum dispersion is 1000 ps.nm^{-1}, and the maximum transmission distance is 59 km. At 1550 nm the total ring dispersion is less than the 10 Gb.s^{-1} limits, and thus the upgrade will not encounter dispersion limitations at this wavelength. The addition however, of a span of only 10 km would have consequences for the bit error rate because of CD. It is clear, nevertheless, that the link will be CD limited at operating wavelengths beyond 1620 nm for 10 Gb.s^{-1}.

7.3 Upgradeability of the Northern Cape Network[2]

PMD measurements were also conducted in the Northern Cape (see Figure 7.4) on an aerial cable link between the towns of Ritchie and Three-Sisters. The aerial link comprised five sections. The tests were conducted to investigate the PMD state of the fibres and also the suitability of the fibres for data transmission at 10 Gb.s^{-1}. At the time of the tests, TINTY was the only interferometric technique available in our research group for conducting the investigation. It was used in conjunction with an EXFO M2100 C-band light source. The spectrum of the source and the experimental setup are presented

[2] The author would like to thank **Mr Johan Visser** (former Telkom Pty (Ltd) technician) for his assistance during the tests.

in Chapter 6. No input and output scrambling of the SOPs was implemented during the tests. Aerial cables are exposed to the changes in environmental conditions, and the changes introduce unintentional polarization scrambling of the light signal and mode coupling in the fibre. In this section, the summary of the PMD results from all the different sections of the link, the variability over time and the distribution of PMD are presented.

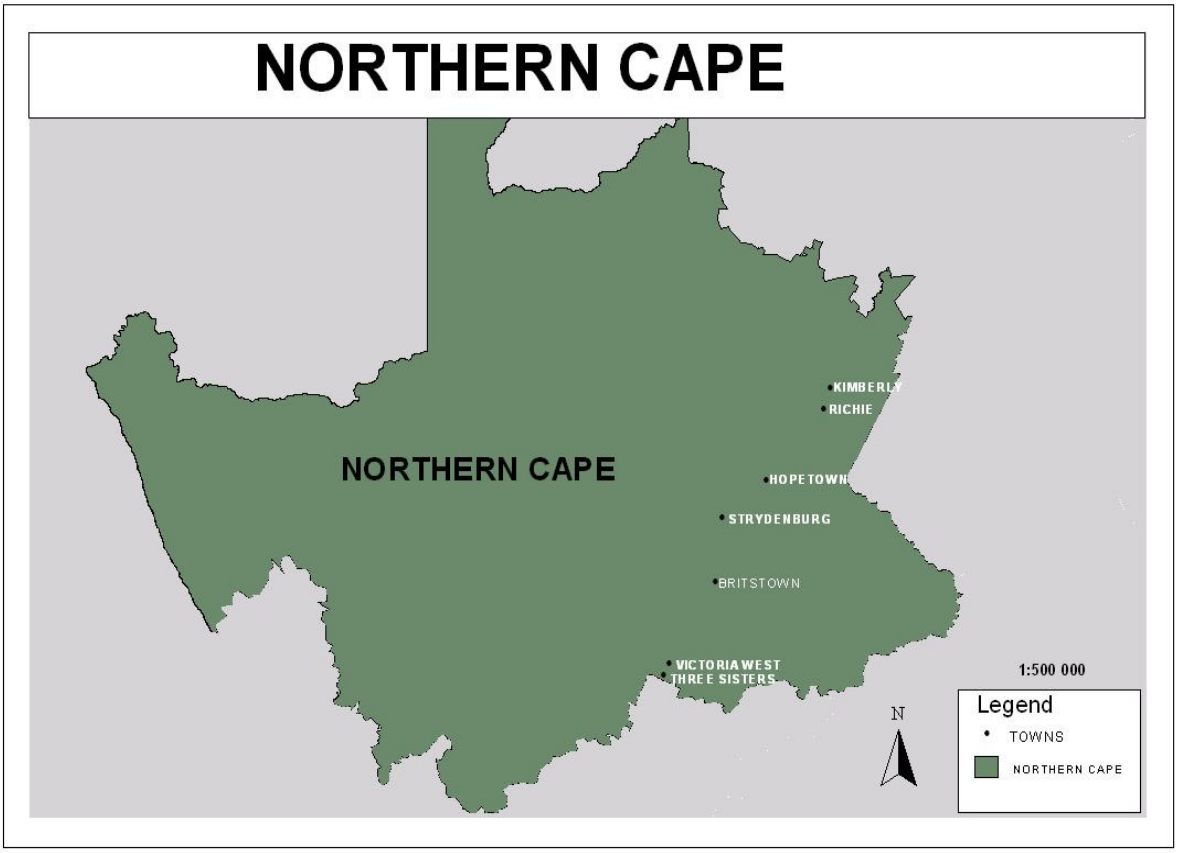

Figure 7.4: A map of the Northern Cape showing the locations of the sites where PMD studies were conducted.

7.3.1 PMD Measurements

A total of 22 fibres were tested, and a different number of fibres were available on each cable section for tests. On each fibre, five PMD measurements were taken without polarization scrambling using the same procedure mentioned in Section 7.2.1 above. The summary of PMD values for different fibre sections is shown in Figure 7.5 and a

summary of the results is presented in Tables 7.5(a) to (f). The link consisted of two types of cables, namely, a tight buffer and loose tube cables. The tight buffer cable connects Ritchie and Hopetown and loose tube cable was deployed for all the other sections. The cables on the link were deployed at different time scales. The "old" cables were deployed before the year 1993, and the "new" cables deployed between the years 1998 and 2000.

Table 7.5(a): Summary of results for a link between Ritchie and Hopetown (Section 1-87.891 km)

Fibre No.	**PMD_{mean} (ps)**
1 (Old)	16.819 ± 0.497

Table 7.5(b): Summary of the results for a link between Hopetown, Strydenburg and Britstown (Section 3-135.234 km)

Fibre No.	**PMD_{mean} (ps)**
1 (Old)	4.779 ± 0.265
2 (New)	14.955 ± 0.469
3 (New)	20.139 ± 0.544

Table 7.5(c): Summary of the results for a link between Hopetown and Strydenburg (Section 2 -56.300 km)

Fibre No.	**PMD_{mean} (ps)**
1 (Old)	1.149 ± 0.130
2 (Old)	1.422 ± 0.144
3 (New)	13.137 ± 0.440
4 (New)	20.441 ± 0.548

Table 7.5(d): Summary of the results for a link between Strydenburg and Britstown (Section 4-78.033 km)

Fibre No.	PMD_{mean} (ps)
1 (Old)	4.359 ± 0.253
2 (New)	3.374 ± 0.223
3 (New)	6.353 ± 0.306

Table 7.5(e): Summary of the results for a link between Britstown and Victoria West (Section 5-112.757 km)

Fibre No.	PMD_{mean} (ps)
1 (Old)	4.452 ± 0.256
2 (Old)	3.864 ± 0.238
3 (New)	10.698 ± 0.397
4 (New)	13.103 ± 0.439
5 (New)	16.513 ± 0.493
6 (New)	17.247 ± 0.504
7 (New)	22.313 ± 0.573

Table 7.5(f): Summary of results for a link between Victoria West and Three-Sisters (Section 6-63.510 km)

Fibre No.	PMD_{mean} (ps)
1 (New)	0.520 ± 0.080
2 (Old)	2.981 ± 0.209
3 (New)	5.941 ± 0.296
4 (New)	8.293 ± 0.349

In section 1, Table 7.5 (a) (Ritchie to Hopetown), only one fibre was available for the tests, which had a relatively high PMD of 16.819 ps. The fibre PMD was over the limit

for data transmission at 10 Gb.s^{-1}, and just under the limit for 2.5 Gb.s^{-1} data transmission.

In sections 2 to 6, two types of cables were tested, namely the so called “new” and “old” cables. The PMD results from these cables are presented in Tables 7.5(b) to 7.3(f). In Figure 7.5, PMD results of the fibres in the “old” and “new” cables are identified by hatched and non- hatched bars, respectively.

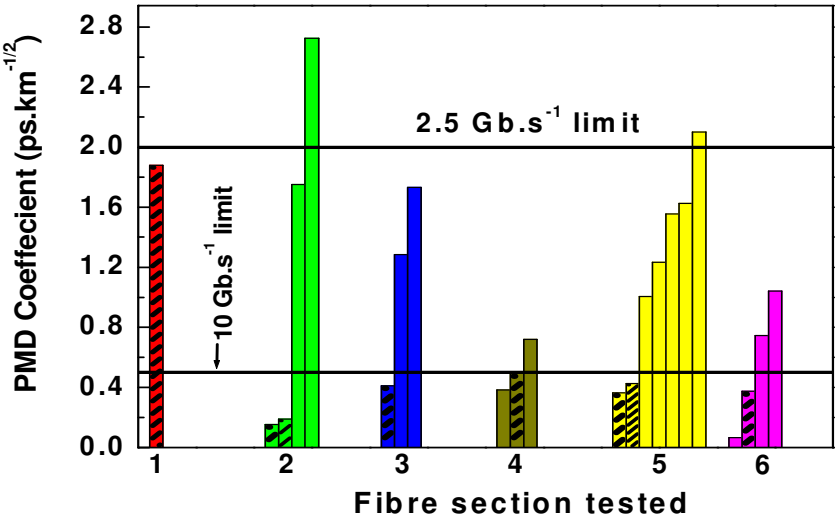

Figure 7.5: The PMD coefficients for the fibres tested on the six sections of the link and the lines for 2.5 and 10 Gb.s^{-1} data transmission limits (2.0 and 0.5 ps.km$^{-1/2}$). The hatched bars show the coefficients of the “old” cables.

In section 2 (Table 7.5 (b), Hopetown to Strydenburg), 2 fibres were tested on each cable- “old” and “new”; Both of the fibres in the “old” cable were suitable for data transmission at 2.5 and 10 Gb.s^{-1}. On the other hand, both fibres in the “new” cable were not suitable for data transmission at 10 Gb.s^{-1}. Furthermore, only 1 of the 2 fibres in the “new” cable was suitable for transmission at 2.5 Gb.s^{-1}. Generally, it can be observed in Figure 7.5 that in the “new” cables had higher PMD than fibres in the “old” cables.

Telecommunication network operators have a big concern about PMD in the old cables since the fibres were manufactured, cabled and deployed at a time when the PMD was not considered as transmission was done at lower bit rates. De Lignie *et al.* [7] showed

that older fibres can have large noncircular cores, and loose tube cables may have long mode coupling lengths resulting in high PMD. In our study, however, it was observed that fibres in the new cables have a higher PMD values than fibres in the old cables, and this is opposite to what was expected since newer cables or fibres are manufactured carefully to ensure that they have a low PMD.

The high PMD measured in the fibres in the "new" cables might have been caused by cable deployment method, and low PMD in "old" may have been caused by an increase in mode coupling due to long-term exposure to environmental fluctuations. Measuring the cable for PMD before and after deployment would have determined whether mechanical stresses introduced during deployment had any effect on PMD of these fibres [5].

7.4 Long-term monitoring of PMD on deployed fibres

The sections below present results for the long-term monitoring of PMD in buried and aerial fibres, respectively. PMD of the deployed fibres vary with mechanical and thermal fluctuations. Aerial cables are affected more by these fluctuations than buried cables [2]. The fluctuations imply that the mean PMD of the fibre varies with time. If PMD of the fibres is monitored over a longer period of time, the mean PMD will give a better estimate of the true PMD of the fibre.

For buried fibres, however, a more accurate estimate of the true PMD of the fibre can be achieved with the change of the states of polarization during the measurements, and averaging PMD measured from the individual scans each with different state of polarization. In making decisions about the PMD in the network, mean PMD from long-term monitoring will ensure that system designers measure outage-probabilities of the network with a good accuracy.

7.4.1 Long-term monitoring of PMD on buried cables on metropolitan network in Pretoria

PMD of a fibre is known to vary statistically with time and the environment [9]. To observe the variation of PMD with time, long-term measurements were performed on fibres 4 and 5 in Section 5 (see Figure 7.1). The fibres were monitored for 13 and 15 hours, respectively, on different days. Variations of PMD with time for these fibres are shown in Figure 7.6.

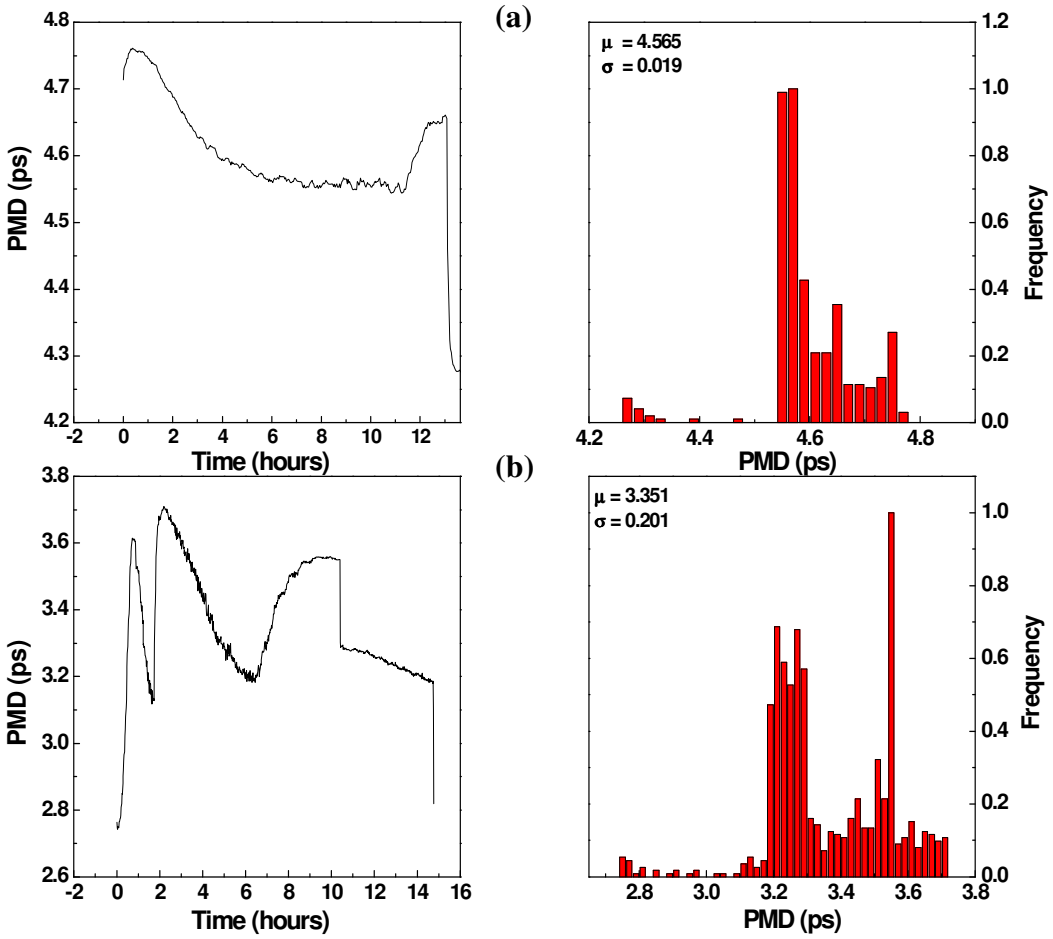

Figure 7.6: The distribution and variation of PMD with time for a 23.616 km (Section 5) in the Pretoria metropolitan network: **(a)** fibre 4 and **(b)** fibre 5.

PMD of fibre 5 in section 4, Figure 7.6 (a), increases at the beginning of the data collection for about 0.5 hours, and then decreases steadily. The PMD then remains

relatively stable for about 4 hours, and then increases abruptly during the next 1.5 hours. Subsequently, PMD decreases rapidly after the 13th hour. The tests were conducted without changing the state of polarization of the input and output light signal. The abrupt changes at the beginning and the end of monitoring (see Figure 7.6 (a)) are believed to have been caused by the movement of the patchcord between the light source and the fibre input, or fibre output and the PMD analyzer. Movement of a patchcord changes the state of polarization of the light signal in the fibre, and the measured PMD depends on the fibre input and output SOPs [7, 8]. In general the variation of PMD in this fibre is not "wild", but relatively stable, in stark contrast with the results for aerial cable which we shall present in Figure 7.7. Figure 7.6 (a) also depicts the distribution of PMD of fibre 4 in section 5 of the network (see Figure 7.1). Most of the PMD values measured for this fibre lie in the range, 4.500 to 4.800 ps. Other PMD values were sporadically distributed in the range, 4.300 to 4.500 ps. PMD measured on this fibre is 4.567 ± 0.664 ps, and discussions for the determination of the measurement uncertainty was presented in Section 4.2.4.

For fibre 5, variation of PMD with time and the distribution of PMD were also observed. In Figure 7.6 (b), PMD of the fibre increases sharply for an interval of about 1 hour, decreases sharply within a period of 1 hour, increases abruptly for half an hour, decrease steadily over a period of about 4 hours. At about 10 hours after start of monitoring, a sudden discontinuity is observed.

The distribution of the PMD is concentrated in the range 3.100 to 3.700 ps (see Figure 7.6 (b)). The other PMD values with a rare occurrence are in the range 2.750 to 3.100 ps. PMD from this overall distribution is then given by 3.350 ± 0.201 ps. In general, it can be observed from Figures 7.6(a) and (b) that PMD measurements with the interferometric techniques are polarization sensitive.

Normally, the network operator would want accurate measurements of PMD in a short period of time. If one input state of polarization is applied with the interferometric technique on a buried cable, many measurements will have to be performed over a long

period of time to get a significant variation of PMD due to the change in the input state of polarization. If input state of polarization is varied, however, PMD of the fibre would be measured from different input SOPs and this would increase the accuracy of measuring the true PMD of the fibre.

7.4.2 Long-term monitoring of PMD in aerial cables in the Northern Cape

Long-term monitoring was carried out on the aerial cables in the Northen Cape (see Figure 7.4), namely, Ritchie to Hopetown (section 1), Hopetown to Strydenburg (section 2), Britstown to Victoria West (section 5) and Victoria West to Three-Sisters (section 6) for up to 18 hours. As it was explained previously, the aerial cables are exposed to extreme changes in the environmental conditions like wind and temperature. Therefore, the time evolution of PMD is very important for consideration as its change due to environment makes PMD compensation difficult [2, 7].

Figures 7.7(a)-(d) show the long-term evolution of PMD with time for various aerial cable sections mentioned above, the distributions of PMD are also shown on the figure. The frequency of PMD occurrences in the distributions were normalized by the highest number of occurrences. It can be observed that PMD varies rapidly with time. The results of the measurements are summarized in Table 7.5 below. It can be seen that the measurement uncertainties for the 5 scans (Section 7.2.1) is higher than that for the long-term monitoring. Details about the calculations of the measurement uncertainties are given in Section 4.2.4.

Table 7.5: Comparison of PMD averaged from 5 scans and implementation of long-term monitoring.

Section No.	**No. of Scans monitoring**	**PMD_{mean}(ps)**	
		Long-term monitoring	*5 measurements*
1	259	17.602 ± 0.064	16.819 ± 0.444
4	353	4.781 ± 0.028	4.779 ± 0.238
5	349	4.250 ± 0.026	4.581 ± 0.232
6	247	0.498 ± 0.010	0.520 ± 0.078

In Figures 7.7(a)-(d), unlike in the case of buried cables, PMD data for the aerial cables show that they are severely affected by environmental fluctuations. These fluctuations change the state of polarizations of the light signal propagating in the fibre under test. Since the interferometric techniques are polarization sensitive, mean PMD measured would be close to the true mean PMD of the fibre. Nevertheless, polarization scrambling can still be applied for the measurements on the aerial fibre, and this is essential for network operators to make decisions about the PMD conditions of the fibre in a short time. Our studies are in agreement with studies by Nespola *et al.* (2005) [9], Cameron *et al.* (1998) [2] and Brodsky *et al.* (2004) [10] which showed that PMD fluctuate more rapidly for aerial cables than for buried cables. These studies were reviewed in Chapter 5.

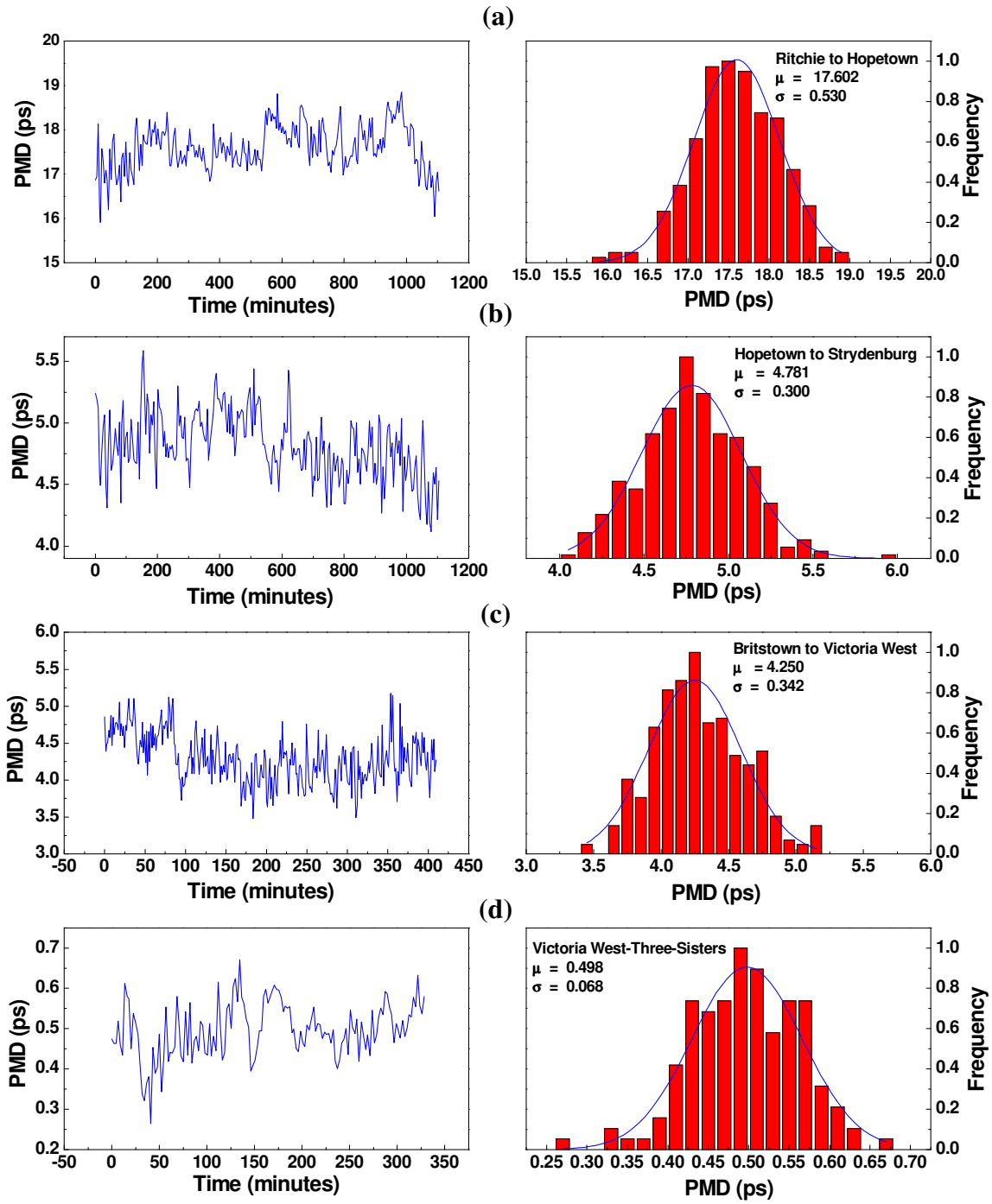

Figure 7.7: The distribution and variation of PMD with time for the link Sections: (a) Section 1 (Ritchie to Hopetown), (b) Section 2 (Hopetown to strydenburg), (c) Section 5 (Britstown to Victoria West) and (d) Section 6 (Victoria West to Three-Sisters).

7.5 Summary

On the buried metropolitan network cables in Gauteng, it was found out that 11 of the 20 fibres tested were suitable for an upgrade to 10 $Gb.s^{-1}$ data transmission rate. For the aerial cable link in the Northern Cape, 9 of the 22 fibres tested were suitable for upgrade to 10 $Gb.s^{-1}$ data transmission rate. Several solutions can be proposed to the network operator to make transmission at higher bit-rates feasible. One of the solutions is to test all the fibres inside the individual cables. This would enable the designer to make an informed decisions about the state of PMD on each cable section. After all the measurements were finished, cable sections with PMD higher than the tolerable level may be removed. Other alternative solutions include putting a PMD compensator at the receiver end of the fibre to reverse the effect of PMD, and another solution would be to regenerate the light signal at the point on the link where the PMD approach the intolerable level.

The chromatic dispersion results for the metropolitan ring network cable in Pretoria showed that CD increases linearly with distance. It was observed that at wavelengths around the low loss wavelength, 1550 nm, CD will not hamper an upgrade of the fibres to 10 $Gb.s^{-1}$. On the contrary, at the wavelengths beyond 1620 nm, CD can cause problems for an upgrade, this can be addressed by an implementation of a CD compensator at the receiver end of the fibre.

Our studies on the buried cables showed that PMD of the fibres does not vary rapidly with time. It was also observed that measurements with interferometric techniques are polarization sensitive. This implies that many states of polarization are required to measure PMD of the buried fibres with a good accuracy. Applying the interferometric technique to measure PMD of the buried fibres with one state of polarization as it is done by many network technicians incurs high uncertainties in the measurements. Furthermore, long-term monitoring with a single input state of polarization does not seem to be the solution unless it is performed over many months, and this is not feasible for network operators.

Long-term PMD monitoring on the aerial cables showed that there is a change in the output states of polarization due to environmental fluctuations. This implies that there is unintentional polarization scrambling of light in the fibre, and PMD consequently the measured varies for different output states of polarization. The sensitivity of the interferometric techniques to polarization improves the accuracy of the measurements since PMD measured is an average of individual measurements with different SOP. Polarization scrambling can still be applied with measurements on the aerial cables to reduce the scan time, and this would be favourable for the network operator.

7.6 References

[1] Guideline to the statistical specification of Polarization Mode Dispersion on Optical Fiber Cables, TIA/EIA TSB 107, Telecommunications Industries Association

[2] **J Cameron**, L Chen, X Bao and J Stears (1998), "Time evolution of Polarization Mode Dispersion in Optical Fibres", *IEEE Photon. Technol. Lett*. **10**(9), pp 1265-1267

[3] **N Gisin**, J Von der Weid, and J Pellaux (1991), "Polarization Mode Dispersion of Short and Long Single-Mode Fibers", *J. Lightwave Technol.*, **9**(7), pp. 821-827

[4] **C T Allen**, P K Kondamuri, D L Richards and D Hague (2003), "Measured Temporal and Spectral PMD Characteristics for Network-Level Mitigation Approaches", *J. Lightwave Technol.*, **21**(1), pp 79-86

[5] **B Costa**, D Mazzoni, M Puleo and E Vezzoni (1982), "Phase shift technique for the measurement of chromatic dispersion in optical fibers using LED's", *IEEE J. Quan. Electron*., **18**(10), pp 1509-1514

[6] **R M Jopson (2000)**, "Measurement Issues for Dispersion Compensation", Symposium on Optical Fiber Measurements, pp 177-180.

[7] **M C De Lignie**, H G J Nagel, and M O van Deventer (1994), "Large Polarization Mode Dispersion in Fiber Optic Cables", *J Lightwave Technol.*, **12**(8), pp 1325-1329

[8] **L Wu**, L Viljoen, M C Mankga, T B Gibbon, A B Conibear and A W R Leitch (2006), "Interpreting PMD data in a deployed fibre network: influence of polarization scrambling", *Presented at the Second conference on Information and Communication Technology in Africa (ICTe Africa 2006)*, Nairobi, Kenya

[9] **A Nespola** and S Abrate (2005), **"**Long-term PMD characterization of installed G.652 fibers in a metropolitan network"**,** *Proc. Optical Fiber Communication Conference*, Aneheim, Carlifonia, USA, Mar. 2005, **3**, pp 3

[10] **M Brodsky**, P Magill and N J Frigo (2004), ""Long-term" PMD characterization of installed fibers-how much time is adequate?", *Proc. Optical Fibre Conference*, Los Angels, Carlifonia, USA, Feb. 2004, **2**, pp 515-517

CHAPTER 8

FIELD AND LABORATORY MEASUREMENTS OF PMD

Input and output polarization scrambling is required for any PMD measurement instruments that do not control the input and output states of polarization (SOP), in order to characterize all the SOP changes that a light signal can undergo in a fibre. In this chapter, however, in-depth comparisons between GINTY and TINTY PMD measurements with input and output scan-to-scan polarization scrambling are presented, the theoretical aspects of which were discussed in Chapter 4. Section 8.1 compares GINTY and TINTY in the field on different fibre configurations with the implementation of scan-to-scan polarization scrambling. Furthermore, perturbation is done on the fibre configurations and the effect of the change in mode coupling on the links is also investigated. Section 8.2 discusses the accuracy of GINTY and TINTY on a fibre with a 'low' PMD. Moreover, the traceability of GINTY measurements is also investigated with the Jones Matrix Eigenalysis (JME) as the reference test method [7].

8.1 Comparison of GINTY and TINTY measurements on deployed fibres[3]

The investigations were conducted to study the performance of GINTY and TINTY before and after a change in mode coupling on deployed buried cabled fibres. Due to the sensitivity of the techniques to polarization, long-term monitoring was implemented with scan-to-scan polarization scrambling at the input and output of the fibre under test before the node perturbation experiments. The distributions of PMD from long-term monitoring were used to calculate the accuracy of the measurements. Section 8.1.2 presents the findings from the investigations.

[3] The author would like to thank **Dr Lorinda Wu, Mr Archie Pelaelo and Mr Eric Mudau** for their assistance during the tests.

Controlled node perturbation was performed to observe PMD variations due to a change in mode coupling at an intermediate point in the fibre optic cable. This study is the simulation of the changes that may occur on PMD of the fibre over a long period of time. Brodsky *et al.* (2004) [6] reported that the state of buried fibres may change a little in over a year's time scale. The study is also important in investigating the effect of maintenance on PMD of the fibre. Controlled perturbation was performed with the rotation of a manual scrambler. The findings from this study are presented in Section 8.1.3.

8.1.1 Description of the test set-up

The investigations were conducted on Telkom's underground loose tube cable connecting Sidwell and Linton Grange transmission exchange centres in Port Elizabeth (Eastern Cape). Two Adaptif automated polarization scramblers (described in Chapter 6) were placed separately at the input and output of the deployed buried fibre under test. The schematic of the set-up used in the investigations is shown in Figure 8.1. A 3-dB beam-splitter (1×2) was connected to the scrambler at the output end of the fibre, and was used to separate and send the output light signal to GINTY and TINTY. Thus, the beam-splitter was used to ensure that both instruments take measurements on the same fibre, under the same conditions and at the same time.

The polarization scramblers were set to scramble the polarized light signal every 5 seconds. A manual polarization scrambler was placed at an intermediate point on the link to cause a controlled perturbation and consequently introduce mode coupling. The manual scrambler used in the tests was placed in 96 different orientations to sample random points on the Poincaré sphere. The procedure used in changing the orientations of the manual scrambler is presented in Section 6.3.

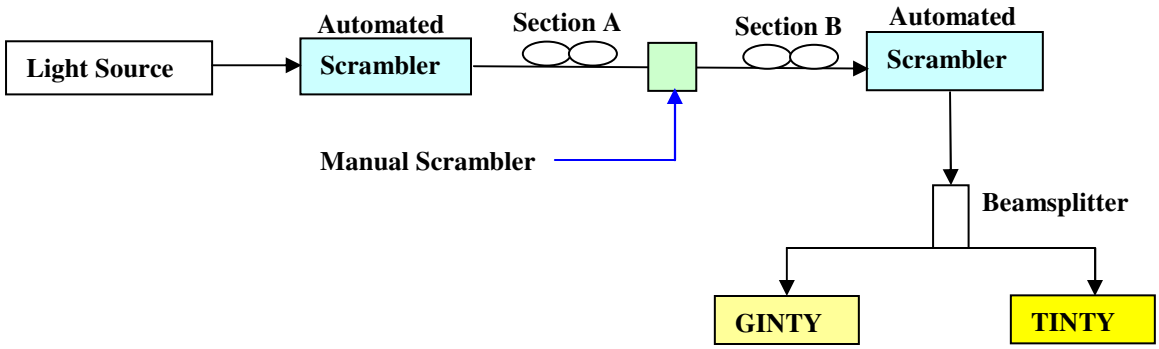

Figure 8.1: Schematic of the set-up implemented in the investigation of the effect of node perturbation on the scan-to-scan PMD distribution and measurement uncertainty of GINTY and TINTY.

This section presents the single scan PMD distribution or variations of PMD for different fibre configurations listed in Tables 8.1.1 and 8.1.2. Before the tests were conducted, quick PMD scans were done performed to check the "ballpark" PMD of the fibres. This gives an idea of the true PMD of the fibre. The configurations were chosen because optical fibres are most likely to have some of the properties highlighted and measurements represent extremes in possible PMD combinations. The subscripts in the tables below indicate the number of the fibre tested. For example, short low PMD_1 ($SLPMD_1$) indicates a short fibre 1 with low PMD, and short low PMD_2 ($SLPMD_2$) indicates fibre 2 of a short length and low PMD. The uncertainty reported in the Table 8.1.1 is for single scan measurements, and this is discussed in Section 8.1.2.

Table 8.1.1: Properties and types of fibre links used in the study.

Fibre Type	Abbreviation	Length (km)	PMD (ps)
Short low PMD_1	$SLPMD_1$	28.800	3.209 ± 0.291
Short low PMD_2	$SLPMD_2$	28.800	2.669 ± 0.265
Short high PMD_1	$SHPMD_1$	28.800	10.075 ± 0.515
Short high PMD_2	$SHPMD_2$	28.800	7.644 ± 0.449
Long high PMD_1	LHPMD	57.600	12.259 ± 0.569
Long low PMD_1	LLPMD	57.600	4.184 ± 0.332

Table 8.1.2: Combination of fibre links used in the study.

Configuration No.	*Combinations*
1	$SHPMD_1$ + LLPMD
2	$SHPMD_1$ + $SHPMD_2$ (LHPMD)
3	$SLPMD_2$ + LHPMD
4	$SLPMD_1$ + $SLPMD_2$ (LLPMD)

8.1.2 Measurements of PMD with automated scan-to-scan polarization scrambling

Prior to the implementation of manual perturbation, the PMD of the configurations mentioned above was measured using scan-to-scan polarization scrambling. Findings in this section are for the study of single scan PMD frequency distributions in buried fibres with input and output scan-to-scan polarization scrambling; the set-up is as shown in Figure 8.1, excluding the manual polarization scrambler. As was mentioned in Chapter 4, GINTY's interferometer has a faster scan speed than TINTY. A GINTY scan on average takes about 5 seconds to complete whereas a TINTY scan, usually takes 150 seconds to complete. The intervals between measurements were set in such way that measurements with GINTY and TINTY were taken at a similar time. The interval between GINTY scans during the long term monitoring was set at 175 seconds and for TINTY it was set at 30 seconds.

Normalized single scan PMD frequency distributions obtained from the long-term monitoring on the fibre configurations in Table 8.1.2 are presented in Figure 8.2. Frequency of occurrences was normalized by the number of scans implemented on each configuration. All the distributions are seen to be Gaussian. Since the PMD is defined as the DGD_{rms} by GINTY and TINTY (an average for all DGDs corresponding to the wavelengths in the spectral width of the light source spectrum) then the single scan PMD values plotted in Figure 8.2 are the distributions of averages. Consequently, the PMD distribution obeys the Central Limit Theorem.

The Central Limit Theorem states that for a large number of independent states that are identically distributed random variables, say, X_1, X_2, . . ., X_n, with a finite variance, the average $\overline{X}_n$ (where n is an integer) has a normal distribution no matter what the distribution of X_i is [1]. It is seen that, all the single scan PMD distributions are consistent with this theorem. According to this theorem the mean PMD would be a good representation of the true PMD of the fibre tested.

In all configurations, the GINTY distributions are broader than TINTY distributions. This indicates that GINTY samples a larger ensemble of states of the mean PMD, whereas TINTY samples only certain states of the mean PMD of the fibre. The bias with TINTY measurements may have been brought about by some of the limitations relating to the assumptions made with mode coupling, shape of the interferograms, coherence time of the light source and the width of the cross-correlation envelope. All the assumptions lead to TINTY assuming a Gaussian interferogram. However it is not known by how much the PMD measurements are affected if the interferogram deviates from this shape. GINTY, on the other hand, eliminates the effects of the source shape or bias by subtraction of the square autocorrelation rms width σ_0^2 in the calculation of PMD [2].

Configuration 2 (LHPMD) as shown in Figure 8.2(b) has the distributions with standard deviation of 0.405 and 0.216 ps for GINTY and TINTY, respectively. Configuration 3 is a combination of configuration 2 (LHPMD) with $SLPMD_2$, and the distribution from the single scan PMD values for this combination is broader than that of configuration 2. Configuration 4 (LLPMD) has a narrower distribution than that of configuration 2 and 3. Configuration 1 (see Figure 8.2(a)) is a combination of configuration 4 (LLPMD) and $SHPMD_1$, and the distribution in this case is narrower than the distribution of Configuration 4. The observations in Figure 8.2 indicate that the broadness of the distributions depends on PMD of the fibre, i.e., the higher the PMD the greater the degree of variability. The discrepancy in configuration 1 with respect to configuration 4 (LLPMD) may have been brought about by the number of scans performed. Only 234 and 373 scans were done with GINTY and TINTY, respectively.

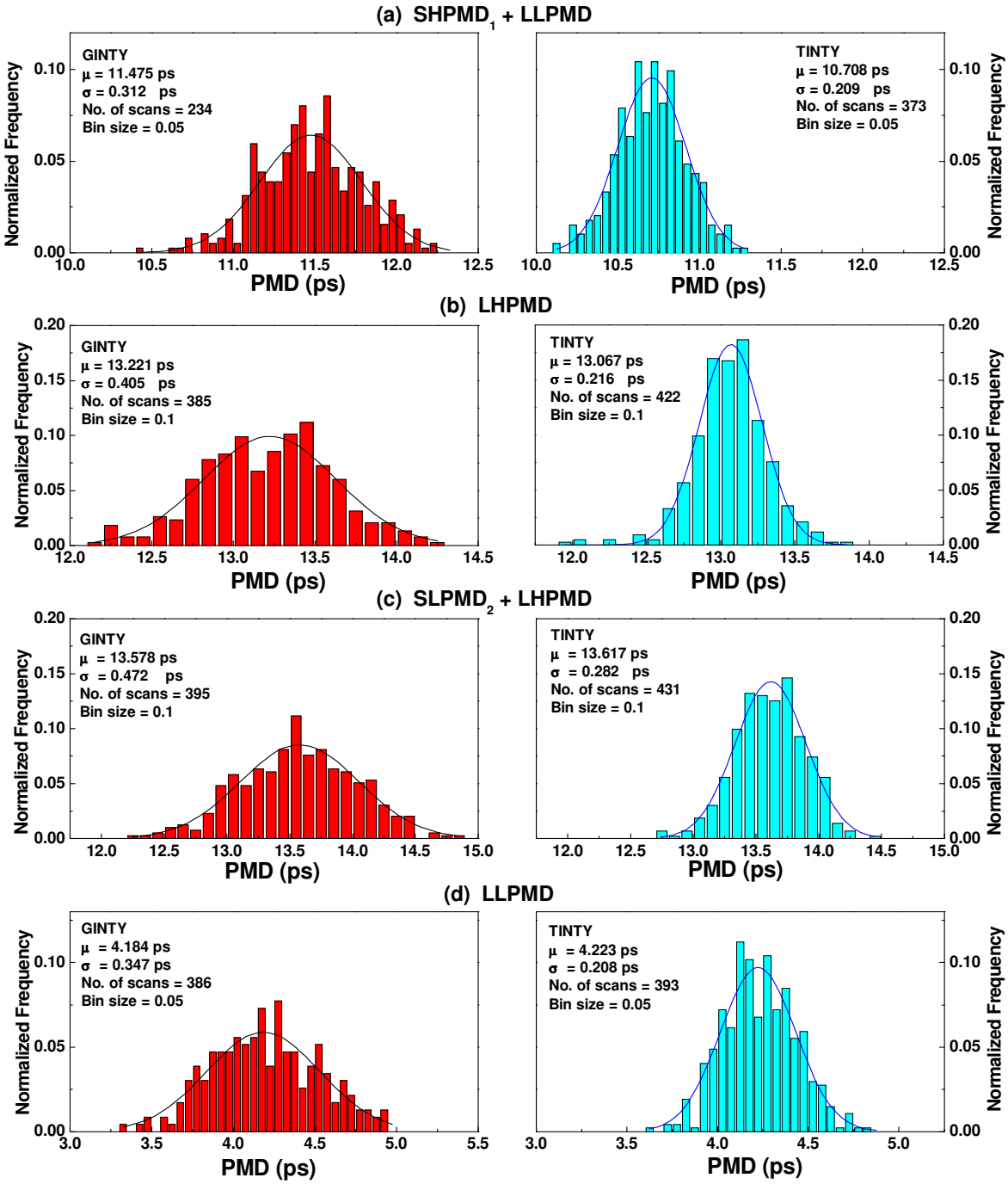

Figure 8.2: The distributions of single scan PMD measured with GINTY and TINTY prior to node perturbation for the following configurations: (a) $SHPMD_1$ + LLPMD fibres, (b) $SHPMD_1$ + $SHPMD_2$ fibres, (c) SHPMD + $LPMD_2$ fibres, and (d) $SLPMD_1$ + $SLPMD_2$.

Table 8.2: Summary of PMD measured for the fibre configurations used in the test

PMD (ps)		*Diff. in PMD values (%)*	*Configurations*
GINTY	*TINTY*		
11.475 ± 0.032	10.708 ± 0.021	6.7	$SHPMD_1$ + LLPMD
13.221 ± 0.042	13.067 ± 0.022	1.2	LHPMD
13.578 ± 0.048	13.617 ± 0.027	0.3	$SLPMD_2$ +LHPMD
4.184 ± 0.046	4.223 ± 0.020	3.9	LLPMD

Table 8.2 gives the summary of PMD values measured with GINTY and TINTY for the configurations in Table 8.1.2. The uncertainty margins reported in the table above were calculated as follows: given that the estimated single scan uncertainty, σ, is the standard deviation of the distribution of PMD values, by the Central Limit Theorem, uncertainty in the measurements is given by $\sigma/\sqrt{N}$, where N represents the number of scans or the sample size during monitoring. This is applied if polarization scrambling is implemented in the set-up. For the 95.5% confidence level, the uncertainty is taken as $2\sigma/\sqrt{N}$ [1, 2].

The relatively large measurement uncertainty, 1.1 %, was measured with GINTY on configuration 4 (LLPMD). For the other configurations measured using GINTY, low uncertainty of at most 0.4 % was measured. For TINTY, on the other hand, uncertainties in all configurations were less than 0.5 %, and relatively large uncertainty was measured for configuration 4 (LLPMD). It can be seen in Table 8.2 that the difference between PMD values between GINTY and TINTY is at most 6.7 %, for the combination of $LLPMD_1$ and $SHPMD_2$.

The single scan uncertainty, σ, measured from the single scan PMD distributions can also be predicted theoretically (σ_{single}). This was discussed in Chapter 4 and it can be calculated from Equation 4.17 below,

$$\sigma_{\text{single scan}} = \sqrt{(1-\frac{8}{3\pi})\frac{1}{\sqrt{1+\frac{1}{4}(\frac{\text{PMD}_{\text{mean}}}{\sigma_A})^2}}}. \qquad (4.17)$$

For the light source used in the study (1467 to 1682 nm), the rms width or auto-correlation width of the source is $\sigma_A = 0.038$ ps, assuming a rectangular spectrum. Table 8.3(a) and (b) give the comparison of the theoretical single scan uncertainty and its estimate from the experimental single scan PMD distributions in Figure 8.2.

Table 8.3 (a): The single scan uncertainties in the measurements

GINTY		**TINTY**		**Fibre Configurations**
σ_{single} (Theoretical)	**σ (Experimental)**	**σ_{single} (Theoretical)**	**σ (Experimental)**	
0.359	0.312	0.347	0.209	$SHPMD_1$ + LLPMD
0.387	0.405	0.388	0.216	LHPMD
0.392	0.472	0.393	0.282	$SLPMD_2$ + LHPMD
0.226	0.347	0.221	0.208	LLPMD

The percentage difference between the measured and theoretical single scan uncertainties are shown in Table 8.3(b). For the first three configurations GINTY gives a "better" estimate of the single scan uncertainty than TINTY. In configuration 4 (LLPMD), however, TINTY gives a "better" estimate of the single scan uncertainty than GINTY. The accuracy in the calculation of the theoretical single scan uncertainty is determined by the accurate determination of the σ_A of the light source.

Table 8.3(b): Comparison of the measured and theoretical single scan uncertainties

GINTY	*TINTY*	*Fibre Configurations*
% difference	% difference	
13.1	39.8	$SHPMD_1$ + LLPMD
4.7	44.3	LHPMD
20.0	28.0	$SLPMD_2$ +LHPMD
53.0	5.8	LLPMD

8.1.3 The effect of change in mode coupling on PMD of the deployed optical fibres

The tests were performed to observe PMD variations due to a controlled change in mode coupling at an intermediate point on the buried optical fibre cable. This type of change can occur unintentionally on fibre cables during maintenance or repairs. Controlled mode coupling was introduced by the rotation of a cubic manual polarization scrambler at an intermediate point on the fibre link. For every rotation of the manual polarization scrambler, scans were taken with GINTY and TINTY for that orientation. Only 96 rotation are possible with a cubic manual polarization scrambler. Details about the rotation of the manual polarization scramblers are given in Chapter 6. The set-up in Figure 8.1 was used for the investigations in this section.

Since mode coupling influences the PMD, each manual polarization scrambler rotation will affect PMD of the fibre. The single scan PMD distributions for the configurations listed in Table 8.1.2 with implementation of controlled perturbation are shown in Figure 8.3. The distributions do not all approach a Gaussian shape as was observed in the previous section. The shapes of the distributions can be attributed to the change in PMD with each rotation of the manual polarization scrambler. This implies that measurements were not taken for the same ensemble of states of the mean PMD. In section 8.1.2 (scan-to-scan polarization scrambling without perturbation) single scan PMD measurement were done in the same ensemble of states of mean PMD of each fibre configurations, and hence a Gaussian shape was observed in accordance with the Central Limit Theorem.

In Figure 8.3, it can be observed that there is no discernable trend regarding the widths of the distributions. For configurations 2 (SHPMD) and 4 (LLPMD), GINTY gives a broader distribution width than TINTY, while the opposite is true for the other configurations. Calculation of the measurement uncertainties in this case will require long-term monitoring with polarization scrambling and collection of single scan PMD values for each of the 96 orientations.

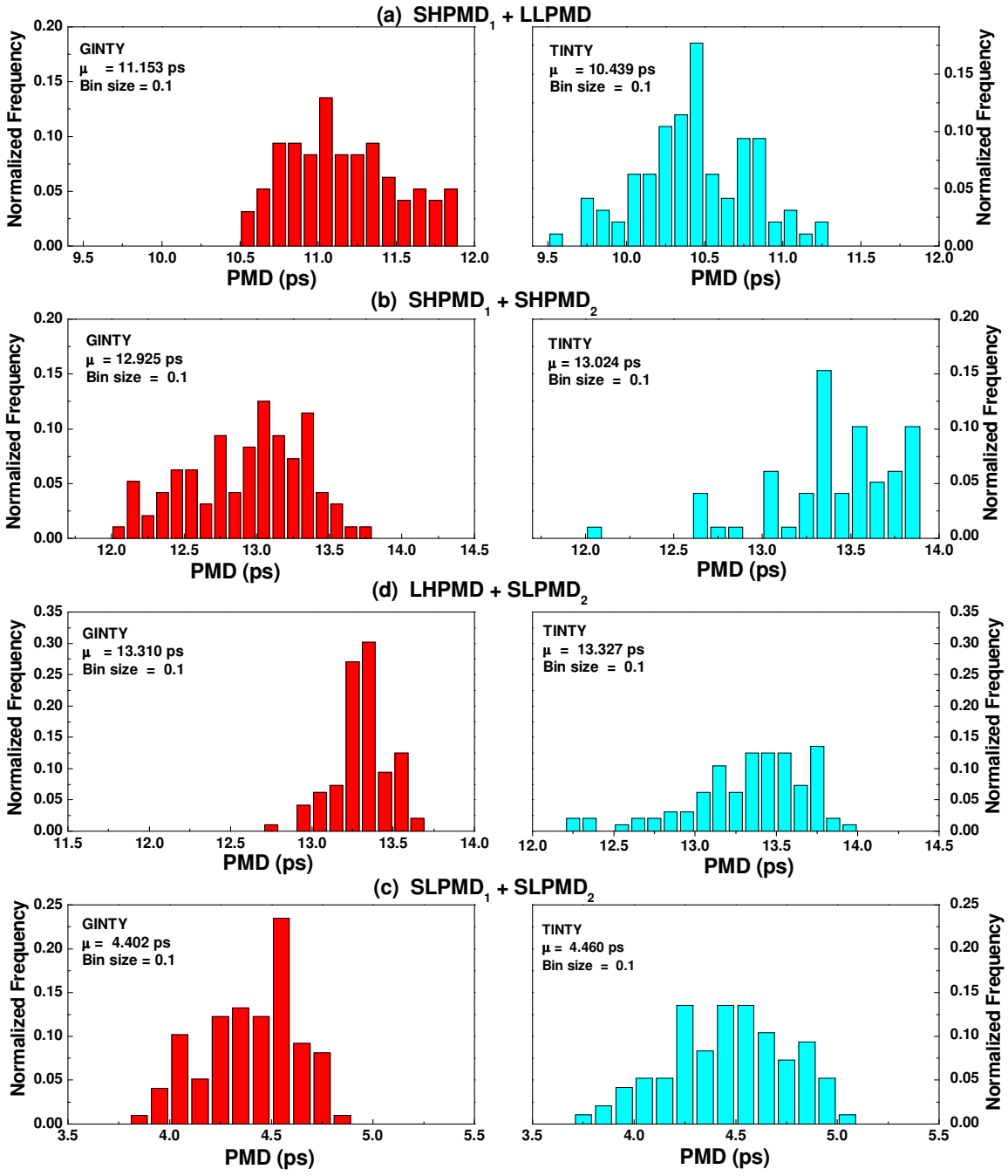

Figure 8.3: The single PMD distributions the following configurations with the effect of change mode coupling: (a) $SHPMD_1$ + $LLPMD_1$, (b) SHPMD +$SHPMD_2$, (c) $SLPMD_2$ + LHPMD and (d) $SLPMD_1$ + $SLPMD_2$.

The Central Limit Theorem would then be applied to each of the 96 distributions to measure the individual measurement uncertainty, and the overall measurement uncertainty will be the average uncertainty of the 96 distributions. Tables 8.4.1(a) and (b) give a comparison of PMD values measured before and after node perturbation with GINTY and TINTY, respectively. PMD values measured before the node perturbation were previously presented in Table 8.2.

Table 8.4.1(a): Difference of PMD values measured with GINTY after the node perturbation

GINTY		
PMD (ps) after Perturbation	*Diff. of PMD after node Perturbation (%)*	*Type of fibre Configuration*
11.153	-2.8	$SHPMD_1 + LLPMD_1$
12.925	-2.3	$SHPMD_1 + SHPMD_2$
13.310	-2.0	$SLPMD_2 + LHPMD_1$
4.402	+5.2	$SLPMD_1 + SLPMD_2$

Table 8.4.1(b): Difference of PMD values measured with TINTY after node perturbation

TINTY		
PMD (ps) after Perturbation	*Diff. in PMD after node Perturbation (%)*	*Type of fibre Configuration*
10.439	-2.5	$SHPMD_1 + LLPMD_1$
13.024	-0.3	$SHPMD_1 + SHPMD_2$
13.327	-1.9	$SLPMD_2 + LHPMD_1$
4.460	+5.6	$SLPMD_1 + SLPMD_2$

The percentage difference in PMD after the node perturbation was calculated with reference to the mean PMD measured before perturbation (Table 8.2). The signs in the percentage difference column indicate PMD decrease (-) or increase (+) after the perturbation. There is a decrease in PMD in all configurations but 4 (LLPMD). PMD decreased by at most 2.8 %. The decrease was caused by the change in mode coupling in

the fibres. This was in agreement with studies by Chen *et al.* (2002) [3] and Massar *et al.* (2006) [8]. The anomaly in the configuration 4 cannot be explained, which should be investigated. The experiment would be repeated on configuration 4 and the results compared to the ones obtained in this study. In general, the results show that over a period of time PMD of the deployed fibres will most likely decrease due to mode coupling.

For future work, this experiment can be performed in the laboratory to find out if the same observation can be made on the cabled or spooled fibres in the laboratory environment.

8. 1.4 Summary

Various configurations of cabled buried single mode fibres were measured for PMD with the implementation of scan-to-scan polarization scrambling. The tests were initially performed without node perturbation. The distribution of PMD from the single scan PMD measurements resulted in a Gaussian shape in accordance with the Central Limit Theorem. For all the configurations, GINTY gave a broader PMD distribution than TINTY. This indicated that GINTY measurements cover a larger ensemble of states of the mean fibre PMD. It would also imply the caution that TINTY measurements may underestimate the standard deviation of the PMD. The discrepancy in TINTY is attributed to the assumption made concerning the shape of the scan interferograms. However, PMD values measured with GINTY and TINTY compare very well. The highest and least differences were 6.7 and 3.9%, respectively. It was further observed that the degree of variability of PMD with polarization changes depends on the PMD of the fibre. The fibres with high PMD have the highest variability.

Fibre configurations mentioned above were then characterized after mode coupling was introduced with a manual polarization scrambler. The distributions of PMD for all configurations did not all approach a Gaussian shape. This was attributed to a change in mode coupling for every rotation of the manual scrambler and consequently measuring a

different fibre PMD with each rotation. In general, it was observed that operation or maintenance on deployed fibres can introduce mode coupling which result in a slight decrease in fibre PMD.

8.2 Laboratory measurements of Polarization Mode Dispersion

This section presents a comparison of GINTY and TINTY PMD measurements on the optical fibres at the NMMU Fibre Optics Laboratory. Measurements were conducted, as described in Section 8.2.1, with the implementation of the scan-to-scan polarization scrambling. Findings from the measurements of PMD (with GINTY) from the averaged square auto-correlation and cross-correlation envelopes are presented. Furthermore, tests were also conducted on an emulator to investigate the traceability of PMD values measured with GINTY. The Jones Matrix Eigenalysis (JME) method, as described in Section 3.3.1, was used as a reference method in the investigation of the traceability of PMD values measured with GINTY.

8.2.1 Investigations on a cabled fibre

The study was conducted on a 6 km fibre within a loose tube cable wound on a 1.8m diameter drum. A fibre with PMD lower than the low PMD fibre discussed in Section 8.1 was selected. EXFO C+L band source (FLS 5800), two automated polarization scramblers (one placed at the input and the other at the output of the fibre), GINTY and TINTY were used. The set-up for this investigation was similar to that shown in Figure 8.1, but without the manual polarization scrambler.

8.2.1.1 Repeatability of the generalizaed interferometric technique (GINTY)

The tests were performed to investigate the repeatability of the GINTY measurements on a fibre under stable conditions (not exposed to fluctuations in environmental conditions or under stress). The cable in our laboratory under relatively constant environmental conditions was used for the tests. This implies that PMD of the fibres in the cable was relatively constant. The tests were performed with scan-to-scan polarization scrambling at the fibre output and input. GINTY was set to average 96 square auto-and cross-correlation envelopes from the scan with different states of polarization; The averaging of the 96 square envelopes was repeated 96 times. A typical interferogram for the 96 scans is shown in Figure 8.4. PMD measured for the square auto-and cross-correlation envelopes of the 96 scans mentioned above is 0.085 ± 0.006 ps.

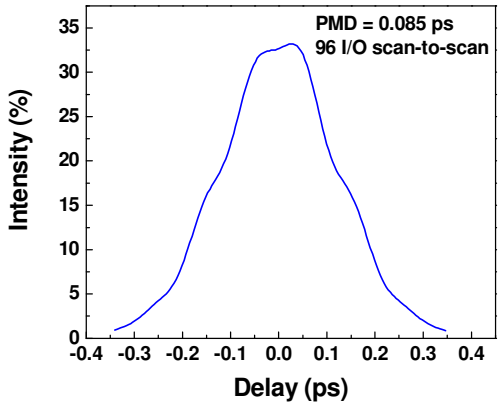

Figure 8.4: Averaged mean square envelope for 96 GINTY scans and states of polarization change.

Figure 8.5 shows the variation of PMD with number of 96 averaged input and output scans for the cabled fibre mentioned above. The mean PMD of the averaged scans is 0.082 ± 1.000×10^{-4} ps. It was observed that out of 56 measurements, each with 96 averaged square envelopes, only 2 measurements were outside the 2σ uncertainty margin (95.5 % confidence level). These findings indicate a good repeatability of GINTY in measuring PMD under the stable environment.

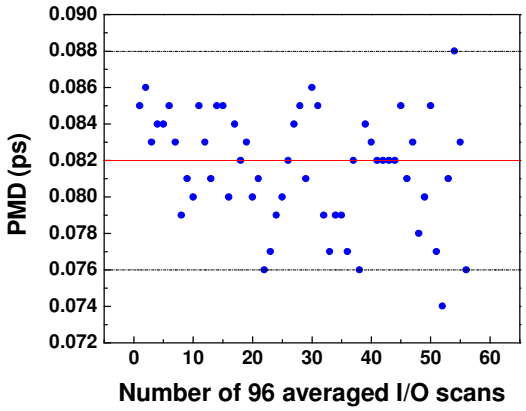

Figure 8.5: Variability of PMD with the number of scans. Solid line indicates the mean PMD and dashed lines the uncertainty range of the measurements for 2σ.

8.2.1.2 Effect of polarization scrambling on the accuracy of GINTY and TINTY measurements

Long-term monitoring with input and output scan-to-scan polarization scrambling was conducted on the cabled fibre mentioned above in order to further compare PMD measured with GINTY and TINTY. As it was found in Section 8.1.1, GINTY had a broader scan-to-scan distribution than TINTY. The distribution further illustrates that GINTY covers a greater ensemble of states to determine the mean PMD whilst TINTY covers only a limited number of states to determine the mean PMD of the fibre.

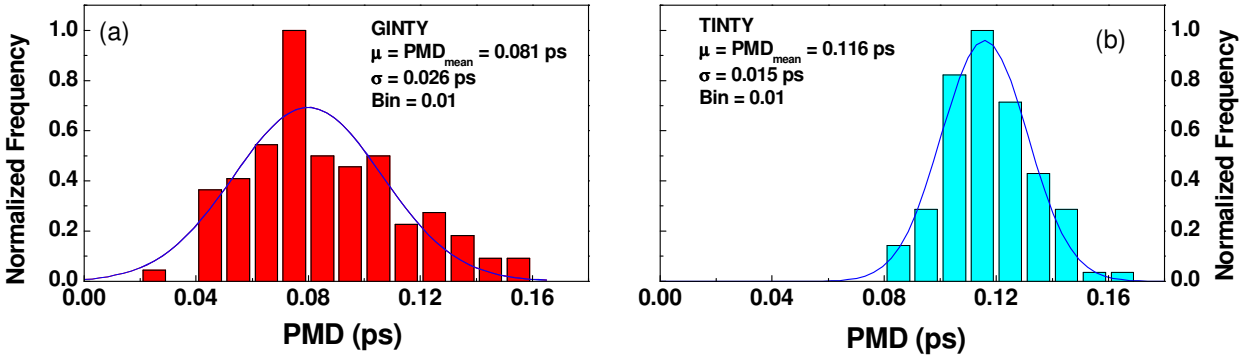

Figure 8.6: Scan-to-scan distribution of PMD for a cabled fibre on a drum before deployment, measured using (a) GINTY; and (b) TINTY.

GINTY PMD values were found to range from 0.02 to 0.16 ps whereas TINTY values ranged from 0.08 to 0.16 ps. The difference in ranges can be attributed to the floor

sensitivity of TINTY [4, 5]. This occurs when the rms width of the auto-correlation peak or coherence of the source is of the same magnitude or greater than the PMD of the fibre under test. The estimate rms width of the source is measured from the width of the auto-correlation peak or central peak of the interferogram (red curve) in Figure 8.7, while the black curve in figure is the TINTY interferogram for the fibre under test.

Unlike TINTY, GINTY eliminates the effect of the source by subtraction of the square rms width of the square auto-correlation envelope. It can be observed in Figure 8.6(a) that GINTY is not affected by the coherence time of the light source: it also measures PMD below the coherence time or rms width of the light source [2]. It is thus important not to use TINTY when very low PMD values are being measured, the GINTY technique is preferable, as demonstrated by the results above.

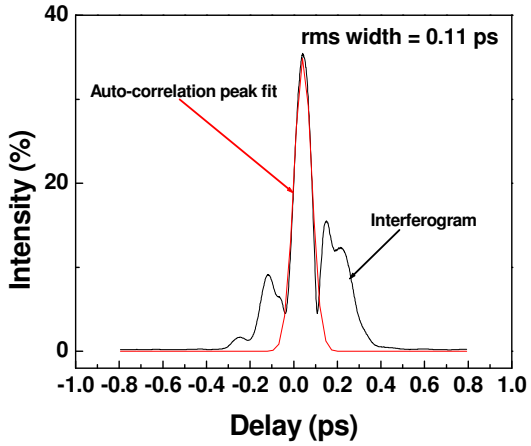

Figure 8.7: The width of red curve give an estimate rms width of the C+L band light source used in the study. The rms width determines the floor sensitivity in TINTY.

Single scan measurements were also taken to investigate the accuracy of GINTY and TINTY when polarization scrambling is not applied. The number of measurements that were performed with TINTY and GINTY were 712 and 634, respectively. The tests were carried out on the same 6 km cabled fibre used for the results reported above. Figure 8.8 shows the single scan PMD distribution from GINTY and TINTY scans. The single scan PMD distributions are concentrated in a small region of the PMD distribution of the fibre

PMD (see Figure 8.8). TINTY PMD values are around 0.09 ps, close to its (TINTY) floor sensitivity; this indicates bias in the measurements as it was explained above.

When polarization scrambling is applied, GINTY gives extreme range of 0.140 ps, but with no polarization scrambling only a range of 0.026 ps is covered. For TINTY in the presence of polarization scrambling a width of 0.09 ps is populated but for no scrambling, however, only a small region of 0.029 ps is covered.

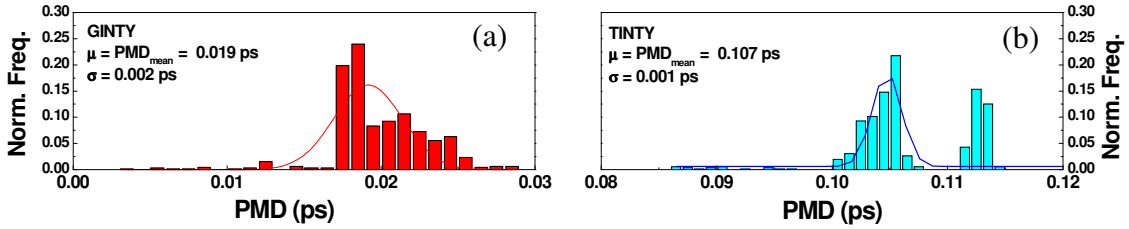

Figure 8.8: Distribution of single scan PMD values of the 6km cabled fibre on a 1.8 m drum, without polarization scrambling: (a) using GINTY; and (b) using TINTY.

PMD of the fibre is 0.019 ± 0.004 ps and 0.107 ± 0.002 ps from GINTY and TINTY scans, respectively. The theoretical uncertainties (equation 4.17) are given by ± 0.014 and ± 0.076 ps for GINTY and TINTY (for a spectral width 95 nm (1530–1625 nm)), respectively. The accuracy of the measurements is determined by the closeness of the measured single scan uncertainties to the theoretical uncertainties. For GINTY the difference is 52 %, and 69 % for TINTY. The results indicate that PMD of the fibre cannot be measured with good accuracy if polarization scrambling is not implemented. The results also show that long-term monitoring of PMD does not necessarily improve the accuracy of measurements unless polarization scrambling is implemented in good agreement with Ref.[6].

8.2.2 Comparison of the GINTY and the Jones Matrix Eigenanalysis (JME)

In Chapter 4, it was mentioned that the traditional analysis of PMD has basic limitations which restrict its application to interferograms that do not deviate from a Gaussian shape. These limitations lead to TINTY not having any reference method against which it can be

tested. GINTY, however, overcomes all the limitations and it can be used in all the PMD regimes and with a light source of any spectral shape. Cyr [2] proved theoretically that PMD measured with GINTY (equation 4.10) is related to the PMD (DGD_{rms}) measured within a selected wavelength band by,

$$DGD^2_{rms} = \frac{\int DGD^2(\nu) w_0^{\,2}(\nu) d\nu}{\int w_0^{\,2}(\nu) d\nu}, \qquad 8.1$$

where $w_0(\nu)$ and DGD (ν) are the optical spectrum and the frequency dependent DGD at the output of the fibre under test. This equation is valid for all mode coupling regimes and interferogram shapes.

This theoretical basis for GINTY is tested in our laboratory as follows:

The test device was an emulator consisting of a concatenation of 10 random short lengths of polarization maintaining fibres with single mode fibres in between each segment. The fibres making the emulator were spliced randomly and not at any specific angle. The light source used with GINTY was in the wavelength range 1467-1610 nm, and had a Gaussian spectrum with rms width of σ_a=0.198 ps (EXFO C-band FLS 5800). The spectrum of the source and its Fourier transform (auto-correlation) curve are shown in Figure 8.9.

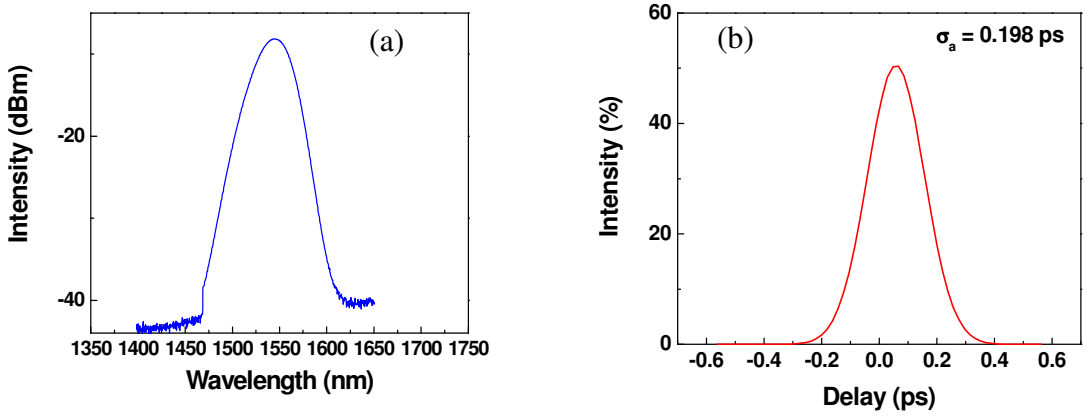

Figure 8.9: (a) Spectrum of the light source used with GINTY. (b) The auto-correlation function or Fourier transform of the light source used with GINTY.

GINTY PMD scans with averaging of 96 square envelopes were taken; their mean square envelope is shown in Figure 8.10 (a). PMD measured from this envelope is 4.030 ± 0.098 ps (that is, ± 2.4 %). Uncertainty calculations were done using the procedure described in Section 8.1.2. The laser source used with JME in the wavelength range 1519-1575 nm. JME scans were performed with wavelength steps of 0.021 nm. The DGD curves are shown in Figure 8.10(b).

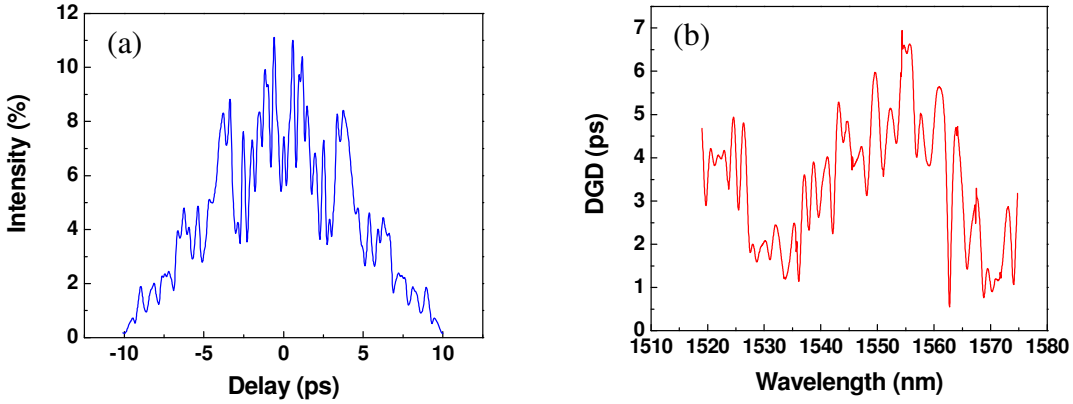

Figure 8.10: a) Mean square envelope for 96 input and output scan-to-scan polarization scrambling on an emulator. b) DGD spectrum from JME scans on an emulator.

The DGD curve obtained from the JME method and source spectrum in Figure 8.9 were used in equation 8.1 to calculate the expected PMD, resulting in 3.700 ps. This gives a difference in PMD of 0.330 ps (8.1 %) which lies slightly outside the GINTY uncertainty margin (2σ-95.5 %) by about 8.1 % (see Table 8.5). By comparison, Cyr [2] reported an uncertainty of 0.8 % for an emulator with PMD of 1.000 ps.

Table 8.5: Comparison of PMD measured with GINTY and JME.

Method	*PMD (DGD_{rms}) (ps)*
GINTY (1467-1616 nm)	4.030
JME (1519-1575 nm)	3.409
Calculation from 8.1	3.700

The difference in PMD may have been caused by the wavelength range of the broadband light source used with GINTY. The light source is in the wavelength range 1467-1616

nm, while the laser source used with JME is in the range 1519-1575 nm. When the investigations were conducted, we did not have a broadband light source that could be used with GINTY and having wavelength range corresponding or within the scanning range of the laser source used with JME. Furthermore, a slight movement of the emulator may have changed the orientation of the principal state of polarization of the sections of the fibre at the splices. This may have subsequently changed PMD of the fibre.

8.2.3 Summary

A study was performed with GINTY on a 6 km long cabled fibre having low PMD, wound on a 1.8 m drum in the Fibre Optic Laboratory at NMMU. Repeatability of PMD measurements on this fibre was investigated. Findings indicated that at least 96.4 % of the measurements were within the 2σ uncertainty margin; and this showed repeatability of the GINTY measurements of a fibre with a relatively constant PMD.

Comparison of PMD measurements with GINTY and TINTY was further performed in the laboratory on the cabled fibre mentioned above. Distributions of PMD from the long-term monitoring with scan-to-scan scrambling showed (as in section 8.1) that GINTY covers most of the ensemble of states of the mean PMD of the fibre. The discrepancy in TINTY indicated bias in the distribution and this was attributed to the assumptions its algorithm makes in the measurement of PMD. It was also observed that if polarization scrambling is not applied, few polarization states contributing to the mean PMD are covered.

Traceability of PMD values measured with GINTY and JME was investigated. Measurements with GINTY were different to JME measurements by about 8.1 %, and this difference was attributed to the wavelength range of the light sources used in the study.

8.3 References

[1] **M Dekking**, F M Dekking, C Kraaikamp, H P Lopuhaä, L E Meester (2005), "A modern introduction to Probability and Statistics: Understanding why and how", Springer, London, pp. 195-199

[2] **N Cyr** (2004), "Generalized Interferometric PMD Measurement Method: Exact Analysis and Traceable Result for any coupling regime", *J. Lightwave Technol.* **22**(3), pp. 794-805

[3] **X Chen**, M Li, and D A Nolan (2002), "Scaling properties of polarization mode dispersion of spun fibers in the presence of random mode coupling", *Opt. Lett.,* **27**(18), pp. 1595-1597

[4] **G V de Faria**, M R Jimenez, and J P Von der Weid (2006), "PMD Variations from factory to Field in OPGW Cabled Fibres", *IEEE Photon. Technol. Lett*., **18**(1), pp. 250–252

[5] **B L Heffner** (1996), "Influence of Optical Source Characteristics Upon Measurement of Polarization-Mode Dispersion of Highly Mode-Coupled Fibre", *Opt. Lett*., **21**(2), pp. 113-115

[6] **L Wu,** L Viljoen, M C Mankga, T B Gibbon, A B Conibear and A W R Leitch (2006), "Interpreting PMD data in a deployed fibre network: influence of polarization scrambling", *Presented at the Second conference on Information and Communication Technology in Africa (ICTe Africa 2006)*, Nairobi, Kenya (17 – 21 May 2006).

[7] Fibre optic communication subsystem test procedures – Part 4-4: Cable plants and links - Polarization mode dispersion measurement for installed links (2005), *IEC 61280-4-4 Ed. 1.0*, International Electrotechnical Commission

[8] **S Massar** and S Popescu (2006), "Reducing Polarization Mode Dispersion With Controlled Polarization Rotations", *http://arxiv.org/abs/physics/0606028*, *e-print:* oai:arXiv.org:physics/0606028

CHAPTER 9

CONCLUDING REMARKS

The focus of this work was twofold, firstly studying the upgradeability of some of the deployed fibre network in South Africa, and secondly exploring issues impacting reliable field measurements of PMD, with particular emphasis on the traditional and generalized interferometric methods (TINTY and GINTY).

Polarization mode dispersion (PMD) and chromatic dispersion (CD) measurements were performed in the Pretoria metropolitan network to determine the upgradeability to 10 $Gb.s^{-1}$ of the buried optical fibres on a metropolitan network. It was found out that just over a half of the fibres in various sections tested were upgradeable to 10 $Gb.s^{-1}$. However, the combined cabled fibre loops in the network will result in high PMD, and consequently none of the fibres tested would be upgradeable to 10 $Gb.s^{-1}$ transmission rates. One of the cable sections was the main contributor to the high PMD of the cable loop.

As far as the CD is concerned, all the fibres tested in this metropolitan loop were within the limits for 10 $Gb.s^{-1}$ transmissions at 1550 nm. Nevertheless, it was observed that the network would be CD limited at longer wavelengths beyond 1620 nm, and this may pose a problem for wavelength division multiplexing (WDM) systems, as such systems use multiple wavelengths to transmit signals in optical fibres.

Another series of field tests was conducted in the Northern Cape on a long-haul aerial cable. Only 41 % of the fibres were found to be upgradeable to 10 $Gb.s^{-1}$ transmissions. In the studies on the aerial cables, it was observed that newer cables generally had a higher PMD than older cables. Consequently, most of the new cables are not upgradeable to higher bit-rates. This observation was attributed to the change in mode coupling of the

aerial fibres. Changes in mode coupling due environmental fluctuations may have reduced PMD of the older fibres over the years.

A number of possible solutions are recommended for the upgrade of the networks to be feasible. The fibres in the same cable on the loop section contributing to the high PMD of the whole network should be replaced. An alternative solution is the regeneration of the optical signal at the point on the network where PMD approaches an intolerable level. The other possible solution is the application of a PMD compensator at the receiver end of the network.

Studies on the long-term PMD monitoring on buried cables showed that PMD of the fibres does not vary rapidly with time. This was attributed to the cables not being exposed to many environmental fluctuations which can introduce mode coupling in the fibres. Aerial fibres, however, are exposed to more extreme environmental fluctuations and their PMD varies rapidly. Long-term monitoring on the buried and aerial fibres showed that the interferometric PMD measurements are polarization sensitive; such measurements of PMD without polarization scrambling do not necessarily improve the accuracy of the measurements. This is because measurements are performed for a single state of polarization, and the mean PMD is calculated from many scans with the same state of polarization and not from an average of many polarization states.

The measurements on aerial fibres, on the other hand, showed that in these instances, PMD is measured for different states of polarization; the mean PMD statistically represents the most accurate value closest to the true PMD of the fibre. PMD of the buried fibres can therefore be measured more accurately if polarization scrambling is implemented with interferometric techniques. This method can also be applied to interferometric techniques on aerial fibres if measurements are required in a short period of time, which would be of great interest for the network operators.

A study on the effect of mode coupling on the PMD of a link was investigated. Different configurations of buried cables were linked together from fibres with different PMD

values. Prior to the introduction of mode coupling in between links, GINTY and TINTY measurements were performed with the implementation of scan-to-scan polarization scrambling at the input and output of the fibre. It was observed that GINTY results in a broader single scan PMD distribution than TINTY. The narrower distribution of PMD given by the single scan TINTY PMD values was attributed to the assumptions TINTY makes in the calculation of PMD. This implies that measurements uncertainties of the interferometric techniques are underestimated if the single scan TINTY distributions are considered. Nonetheless, the mean PMD measured from the distribution were comparable. It was further observed with the distribution of single scan PMD values that fibres with high PMD have a broader distribution than fibres with low PMD.

As was mentioned above, a study on the effect of mode coupling on the PMD of a link was investigated. Mode coupling was introduced with a specially designed manual polarization scrambler at an intermediary point on the fibre links. It was observed that the introduction of mode coupling on the fibre links decreases the PMD.

Comparison between GINTY and the Jones Matrix Eigenanalysis PMD method was performed at the NMMU Fibre Optic Laboratory, and it was observed that the PMD measurements agreed well. This study further increased our confidence in measurements of PMD with GINTY.

Our studies showed that for future comprehensive evaluation of the deployed fibres for upgrade to higher bit-rates with the interferometric techniques, polarization scrambling is very important. It will save the network operators time and also ensure that PMD measurements are performed with good accuracy. GINTY seems to be the most reliable technique and must be the preferred instrument in the measurements.

For some of the future work, measurements of the effect of mode coupling can be repeated with fibres with different PMD values to find out if the results are consistent with our findings. It would be instructive to compare the JME and GINTY techniques as

we did in this study, but this time using a light source spectrum matching the wavelength scanning range of the laser source used with the JME method.

We have carried out field measurements to determine the suitability of the South African fibre network to higher data transmission rates. It is clear that many fibres are not upgradeable, and this emphasises the need for careful PMD characterization before taking the decision to upgrade. The results of this study show some of the factors that are most important in the making of these measurements.

APPENDIX

RESEARCH OUTPUT

Publications in conference Proceedings

L Wu, L Viljoen, M C Mankga, T B Gibbon, A B Conibear and A W R Leitch (2006), "Interpreting PMD data in a deployed fibre network: influence of polarization scrambling", *Presented at the Second conference on Information and Communication Technology in Africa (ICTe Africa 2006)*, Nairobi, Kenya (17 – 21 May 2006)

Poster Presentations

"Measurements of Chromatic dispersion in a metropolitan network", M C Mankga, A B Conibear and A W R Leitch, *SAIP 50th Annual Conference 2004*

"An investigation of scrambling effects on buried optical cables", V Musara, M C Mankga, M Mathuthu and A W R Leitch, *SATNAC 2006*